

**SLAB BEHAVIOUR IN COMPOSITE BEAMS
AT WEB OPENINGS**

by

SOON HO CHO

Department of Civil Engineering and Applied Mechanics

McGill University

Montreal, Canada

June 1990

**A thesis submitted to the Faculty of Graduate Studies
and Research in partial fulfillment of the requirements
for the degree of Doctor of Philosophy**

© S. H. Cho 1990

ABSTRACT

An explanation is provided for the slab behaviour in composite beams at web holes where the concrete slab carries heavy vertical shear. This is based on the truss concept, and requires consideration of shear studs in the hole region as vertical tension members. According to this, a structural action between the concrete slab and shear connectors for carrying or transferring vertical shear to the steel beam was clearly identified.

On the basis of the slab behaviour identified, truss idealizations capable of determining the slab shear carrying capacity in a rational manner were developed. Then, the ultimate strength for composite beams at web holes was formulated including the truss idealizations. Another ultimate strength analysis accounting for the slab shear carrying capacity in a simple manner, which was also developed during this research project, is given. This provided the fundamental solution procedure for the plastic analysis used.

A series of nine tests was carried out with particular attention being directed to the verification of the proposed truss analogy. The major test parameters included the configurations of the studs in the hole region, the width of the concrete slab and stud detailing near the high moment end of the hole. The ultimate strength predictions were made by the two methods developed, and compared with previous and present test results.

RÉSUMÉ

Une explication sur le comportement des dalles de béton dans les poutres mixtes avec ouvertures dans l'âme est donnée lorsque celles-ci sont soumises aux efforts tranchants. Ceci est basé sur le concept du treillis qui inclut la présence des goujons au-dessus de l'ouverture comme membres verticaux. Le comportement structural de la dalle et des goujons pour transférer l'effort tranchant à la poutre en acier est clairement identifié.

Un concept de treillis capable de déterminer la résistance de la dalle aux efforts tranchants a été formulé. La résistance ultime des poutres mixtes avec ouvertures a été révisée pour inclure le concept du treillis formulé auparavant. Aussi, une autre méthode simple pour le calcul de la résistance ultime lorsque la résistance au cisaillement de la dalle en béton est incluse fut proposée. Ceci fut la méthode fondamentale utilisée lors de la solution d'une analyse plastique.

Une série de neuf expériences en laboratoire fut faite avec une attention spéciale dirigée sur la vérification des concepts proposés. Les paramètres d'expérimentation furent le détail des connecteurs dans la région de l'ouverture la largeur de la dalle de béton et le détail des goujons du côté de l'ouverture soumis à de forts moments fléchissants. Les prédictions de la résistance ultime des deux méthodes proposées furent comparées avec les tests et les résultats de d'autres auteurs.

ACKNOWLEDGEMENTS

The author would like to express his sincere thanks to Professor R. G. Redwood for his knowledgeable and skillful guidance, his continual encouragement and his patience throughout this research programme.

In addition the writer wishes to express his gratitude to Professor Denis Mitchell, who made invaluable criticism at a preliminary stage of this research project.

Donation of shear studs by Nelson Stud Welding Company, and the arrangement for a local welder by Mr. Camille Paquette are very much appreciated. Steel Decking and the W sections by Les Acier Canam Inc. with the arrangement of Mr. R. Vincent is also very much appreciated.

The experimental research was carried out in the Jamieson Structures Laboratory in the Department of Civil Engineering and Applied Mechanics at McGill University. The technical assistance given by the laboratory technicians Mr. Brian Cockayne, Mr. Ron Sheppard, and Mr. Marek Przykowski are very much appreciated. The assistance of Mr. V. S. Channagiri throughout the whole period of testing, and Mr. Feng Lu on attaching strain gauges are also very much appreciated.

The financial assistance provided by the Natural Science & Engineering Research Council of Canada, Grant A-3366, and John Bonsall Porter Scholarship and Summer Bursary awarded by the Graduate Faculty of McGill University is gratefully acknowledged. The partial exemptions on tuition fees given by Quebec and the Republic of Korea Governments are also gratefully acknowledged.

Thanks are also extended to Dr. William D. Cook, who managed and set up the excellent computing facilities in the Department of Civil Engineering and Applied Mechanics, McGill University.

The French translation of the abstract, and the help during pouring concrete by Mr. Claude Pilette should be mentioned. Colleagues in Room 498, McDonald Engi-

neering Building, McGill University, their encouragement and humor should be also mentioned.

In addition the author wishes to express his special thanks to Professor Li-Hyung Lee in the Department of Architectural Engineering, Hanyang University, Seoul, Korea for his continual encouragement.

Finally, the author wishes to express special thanks to his wife Hyun-Sook, for her encouragement, patience and loving support, and also to his children Min-Jae and Anna for sharing joy and sorrow during the course of studying at McGill University.

TABLE OF CONTENTS

ABSTRACT	i
RÉSUMÉ	ii
ACKNOWLEDGEMENTS	iii
TABLE OF CONTENTS	v
LIST OF FIGURES	viii
LIST OF TABLES	x
LIST OF SYMBOLS	xi
1 INTRODUCTION	1
1.1 Problem Definition	1
1.2 Previous Research	3
1.3 Objectives	10
2 FUNDAMENTAL ANALYTICAL PROCEDURE	
FOR ULTIMATE STRENGTH	14
2.1 Introduction	14
2.2 Formulation of Member Capacity	15
2.3 Limitations on Shear Connector Resistance	19
2.4 Concrete Slab Shear Consideration	21
3 TRUSS ANALOGY FOR SLAB BEHAVIOUR	28
3.1 Introduction	28
3.2 Ultimate Strength	29
3.2.1 Behaviour	30
3.2.1.1 Solid Slabs	30
3.2.1.2 Ribbed Slabs	32
3.2.2 Truss Idealization	34
3.2.3 Formulation of Member Capacity	37
3.2.3.1 Bearing Studs at L.M.-Solution I	38
3.2.3.2 Bearing Studs Beyond L.M.-Solution II	42
3.2.3.3 No Studs Within Hole Length- Solution III	43
3.3 Serviceability	45
4 COMPARISON WITH PREVIOUS TESTS	60
4.1 Introduction	60
4.2 Simplified Slab Shear Model	61

TABLE OF CONTENTS (Continued)

4.3	Truss Model	62
4.4	Discussion	65
5	EXPERIMENTAL PROGRAMME	75
5.1	Introduction	75
5.2	Details of Test Specimens	76
5.2.1	Hole 1	77
5.2.2	Holes 2 and 3	77
5.2.3	Holes 4 and 7	78
5.2.4	Holes 5 and 8	79
5.2.5	Holes 6 and 9	80
5.3	Material Properties	80
5.3.1	Concrete	80
5.3.2	Steel	81
5.3.3	Shear Connection	81
5.4	Instrumentation and Test Procedure-Beam Tests	83
6	EXPERIMENTAL RESULTS	96
6.1	Introduction	96
6.2	Overall Behaviour	96
6.3	Slab Behaviour	99
6.3.1	Stud Configurations	100
6.3.2	Slab Width	103
6.3.3	Stud Details	104
6.4	Predictions	105
6.4.1	Ultimate Strength	105
6.4.2	Elastic Deflections	107
7	CONCLUSIONS AND DESIGN RECOMMENDATIONS	140
7.1	Conclusions	140
7.2	Design Recommendations	142

TABLE OF CONTENTS (*Continued*)

STATEMENT OF ORIGINALITY	144
REFERENCES	145
APPENDIX A – EXAMPLE CALCULATIONS	
FOR ULTIMATE STRENGTH USING TRUSS ANALOGY	148
A.1 Solid Slab	148
A.2 Ribbed Slab	152
APPENDIX B – PREDICTION OF DEFLECTIONS	155
B.1 Comments on Analytical Procedure	155
B.2 Analysis Results	157
APPENDIX C – SUMMARY OF PREVIOUS TESTS	160

LIST OF FIGURES

1.1	Web Openings in a Typical Floor of Steel Framed Buildings	11
1.2	Reinforcement of Openings	12
1.3	Contribution of Concrete Slab at a Web Opening	12
1.4	Slab Forces Proposed by Redwood and Poubouras	13
1.5	Shear Area in Concrete Slab	13
2.1	Moment-to-Shear Interaction Diagram	24
2.2	Cross Sectional Details	24
2.3	Assumed Stress Distributions	25
2.4	Force System in Concrete Slab	25
2.5	Graphical Representation of Solution	26
2.6	Graphical Representation of Slab Shear Solution	26
3.1	Possible Truss Action in the Slabs of Composite Floor Members	47
3.2	Typical Slab Failures at Web Holes	49
3.3	A Solid Slab Test at the University of Kansas	50
3.4	A Ribbed Slab Test at McGill University	51
3.5	Truss Idealization for the Slab in a Composite Beam at a Web Hole	52
3.6	Truss Model Providing the Maximum Shear Capacity in the Top Composite Section (β & $\gamma = 0$, and $q_t = q$)	53
3.7	Bearing Studs at the Low Moment end of the Hole	54
3.8	Pull-out Cones of Stud Shear Connection	55
3.9	Bearing Studs Beyond the Low Moment end of the Hole	56
3.10	No Studs Within the Hole Length	57
3.11	Graphical Representation for the Slab Shear Capacity	58
3.12	Measured Deflections Between Hole Ends	58
3.13	Analytical Models for Serviceability Analysis	59
4.1	Non-dimensionalized Interaction Diagram	67
4.2	Transference of Horizontal Connector Forces in Solid Slabs	67
5.1	Test Beams	85
5.2	Details of Beam 1	86
5.3	Details of Beams 2 and 3 (Holes 2 and 3)	86
5.4	Details of Beam 4 (Holes 4 and 7)	87
5.5	Details of Beam 5 (Holes 5 and 8)	87
5.6	Stud Detailing for Holes 5 and 8	88
5.7	Details of Beam 6 (Holes 6 and 9)	89

5.8	Concrete Strength During Testing Period	89
5.9	Deck Profile	90
5.10	Test Setup for Push-out Specimens	90
5.11	Failure Modes for Push-out Tests	91
5.12	Shear Load Versus Slip on Push-out Tests	92
5.13	Loading System	93
6.1	Relative Deflections Between Hole Ends ($M/V=0$)	109
6.2	Relative Deflections Between Hole Ends ($M/V=950$)	109
6.3	Relative Deflections Between Hole Ends ($M/V=1050$)	110
6.4	Longitudinal Strains Around Web Holes	111
6.5	Shear Strains Around Web Holes	114
6.6	Slips Along Length of Beam	117
6.7	Schematic Representation of Crack Development	119
6.8	Failure of Hole 1	120
6.9	Failure of Hole 2	121
6.10	Stud Strains Around Hole 1	122
6.11	Stud Strains Around Hole 2	123
6.12	Failure of Hole 4	124
6.13	Failure of Hole 7	125
6.14	Close-up View of Slab After Removing Cracked Concrete	126
6.15	Failure of Hole 6	127
6.16	Failure of Hole 9	128
6.17	Close-up View of Slab Cracking on the Soffit	129
6.18	Failure of Hole 3	130
6.19	Stud Strains Around Hole 3	131
6.20	Failure of Hole 5	132
6.21	Failure of Hole 8	133
6.22	Stud Strains Around Holes 5 and 8	134
6.23	Moment-to-Shear Interaction Diagrams	135
6.24	Load Versus Deflection Response up to 60% of P_{ult}	136
A.1	Truss Model Used for Prediction of Ultimate Strength on Solid Slab	151
A.2	Truss Model Used for Prediction of Ultimate Strength on Ribbed Slab	154

LIST OF TABLES

2.1	Limiting Values of Shear Connector Resistance	27
4.1	Theoretical Values Defining Interaction Diagrams	68
4.2	Experimental and Predicted Failure Loads	69
4.3	Non-Dimensional Parameters of Test Beams	70
4.4	Various Connector Resistance Related to Each Solution Procedure	71
4.5	Calculated Shearing Forces for Test Beams	72
4.6	Experimental and Predicted Failure Loads	73
4.7	Horizontal and Vertical Resistance of Shear Connection	74
5.1	Geometric Properties of Test Specimens	94
5.2	Summary of Concrete Strengths	95
5.3	Material Properties of Steel Sections	95
5.4	Summary of Push-out Test Results	95
6.1	Summary of Test Results	137
6.2	Theoretical Values Defining Interaction Diagrams	138
6.3	Comparison Between Actual and Predicted Failure Loads	139
6.4	Horizontal and Vertical Load Carried by Shear Connection	139
B.1	Comparisons of Measured and Predicted Deflections at 30% of Ultimate Load	158
B.2	Comparisons of Measured and Predicted Deflections at 60% of Ultimate Load	159
C.1	Geometric Properties for Previous Tests	161
C.2	Material Properties for Previous Tests	162

LIST OF SYMBOLS

a	half length of web opening
A_c	pull-out cone surface area
b	width of flange
b_e	effective width of composite beam slab
C_i	compressive forces in concrete slab ($i = 0, 1, 2$)
D_h	diameter of stud head
d	overall depth of steel beam
$F_{yf,yw}$	tensile yield stress of steel beam flange, web
F_u	ultimate tensile stress of steel beam flange or web
f'_c	compressive strength of concrete (from a standard cylinder test)
h_r	rib height in ribbed slab
H	half height of web opening
H_s	height of stud after welding
$k_{h,v}$	horizontal, vertical stiffnesses of shear connection
k_i	factors defining points of stress reversal ($i = 1, \dots, 6$)
L_e	length of stud under head
l_{s0}	longitudinal spacing of shear connectors
l_{si}	longitudinal distances between nearest studs and hole ends ($i = 1, 2$)
M_0	pure bending resistance of composite beam without hole and with 100% shear connection
M_{0h}, M'_{0h}	pure bending resistance at hole with 100% shear connection, and for partial shear connection
N_v	number of vertical members in compression or tension within hole length
n	number of shear connectors between high moment end of opening and the nearest point of zero bending moment
n_h	number of shear connectors within length of opening
n_t	number of shear connectors consisting of a vertical member in compression or tension
$P_{wt,wb}$	maximum normal force on web above, and below the opening, taking account of shearing force
P_{yf}	normal force in flange at yield
q	horizontal shear force carried by one shear connector
q_e	horizontal shear force carried by one shear connector to ensure stress reversals within steel flanges

LIST OF SYMBOLS (Continued)

q_i	horizontal shear forces carried by one shear connector corresponding to vertical compression or tension members ($i = 0, \dots, 3$)
q_r	horizontal shear resistance of one shear connector
Q_i	stress resultants at tee section above and below hole ($i = 1, \dots, 4$)
$s_{t,b}$	depth of steel tee web above, below opening
T	vertical tensile (or compressive) force carried by one shear connector
T_0	yield load of net steel beam section
T_i	vertical tensile (or compressive) forces carried by one shear connector corresponding to vertical members ($i = 1, \dots, 3$)
T_r	pull-out tension capacity of one shear connector
T_s	overall slab thickness
t	steel beam flange thickness
t_s	cover slab thickness in ribbed slab
V_0	pure shear capacity of steel beam web without hole
V_c	shearing force carried by concrete
$V_{t1,b1}$	shearing force carried above, below hole corresponding to point 1 on the interaction diagram
$V_{st, sb}$	shearing force carried by steel above, below hole
V_{cu}	ultimate shear strength of concrete slab
$V_{pt, pb}$	pure shear resistance of steel tee web above, below hole
w	web thickness
$w_{r1, r2, r}$	top, bottom, and average rib width
\bar{y}_i	distances defining position of stress reversal ($i = 1, \dots, 4$)
$\alpha, \beta, \delta, \gamma$	factors defining portion of vertical forces transferred from concrete slab to steel beam
ϵ_y	yield strain of steel beam flange or web
τ_y	shear yield stress of steel beam web
θ	inclination of diagonal strut through thickness of slab
θ'	inclination of diagonal strut across width of slab
L.M.	low moment end of hole
H.M.	high moment end of hole
COV	coefficient of variation

CHAPTER 1

INTRODUCTION

1.1 Problem Definition

Placing large holes in steel beam webs for the unimpeded passage of utility ducts and pipes is a common engineering approach to eliminate the excessive plenum depth between the floor and the ceiling of building structures (see Fig. 1.1), thereby reducing the overall construction depth. However, the presence of such web penetrations in regions where shear is high causes a significant reduction in the ultimate load carrying capacity of the beam, and may result in the need for reinforcement around openings to restore the strength lost due to the introduction of holes. To do this, a number of detailing methods associated with reinforcement around openings exist (see Fig. 1.2), but it is generally recognized that opening reinforcement involves high costs in fabrication, resulting in a high proportion of the total structural cost.

Under this situation, the establishment of standardized detailing methods capable of optimizing opening reinforcement may be necessary. However, a more desirable situation is to create web openings that do not require any reinforcement, while maintaining the same resistance as that given in the same beam without holes. This can often be accomplished by considering composite action between concrete slab and steel beam, and this consideration is the starting point of several research projects concerned with composite beams containing large web cut-outs.

Figure 1.3 illustrates the increased shear strength due to the presence of the concrete slab at a web opening as measured in previous tests. For this demonstration, the strengths of non-composite sections having the same hole geometries were calculated from well-established methods given elsewhere¹.

Despite their inherent low resistance to shear, the slabs in the regions of web openings display considerable ability in carrying vertical shear forces; a potential 40%~420% increase over the steel section alone for solid slab beams and 30%~260% increase for ribbed slab beams. A similar 20%~160% enhancement over the steel section alone has also been demonstrated in recent tests of composite thin webbed plate girders carried out by Porter and Cherif². As a result, the need for opening reinforcement can be eliminated if the slab shear carrying capacity is properly accounted for

Further, from Fig. 1.3, previous tests for composite beams with web holes indicated that the contribution of the concrete slab in carrying vertical shear was more pronounced when a higher number of shear connectors (n_h) were provided within the opening length, and when the slab depth (t_s) was increased relative to the steel beam depth (d). Such aspects of the slab behaviour are illustrating the structural action of the slab and shear connection in the region of a web penetration where the slab carries a lot of shear, and should be clearly identified for an appropriate evaluation of the slab shear carrying capacity.

In this research project an attempt is made to clarify the slab shear phenomenon in the region of a large web hole in a composite beam. Use is made of a truss concept in which shear connectors are considered as vertical reinforcement, in the same way that act in reinforced concrete beams.

The fundamental solution procedure for the prediction of the ultimate strength, which was originally developed by Redwood and Pombouras³ for ribbed slab beams and has been extended during this project to deal with solid slab beams⁴, is firstly dealt with (Chapter 2). This will also give a general description of the overall behavioural

aspects on composite beams at web openings.

Using the truss analogy, an explanation of the previously observed slab failure in the opening region is established, and on the basis of this physical understanding, truss idealizations capable of predicting ultimate strength and serviceability load level performance in the opening region are also developed, which are the principal subjects of this project (Chapter 3). The reliability of the truss models proposed is evaluated by means of predicting the ultimate strength and elastic deflections for all appropriate tests previously reported in the literature (Chapter 4).

In addition, with particular attention being directed to the verification of the proposed truss concept, full scale tests comprising six beams with a total of nine rectangular web holes were carried out, and the results are discussed in Chapters 5 and 6. From test and analysis results, information relevant to design is also given (Chapter 7).

1.2 Previous Research

Considerable work has been made recently on tests and analyses of web openings in composite beams with solid and ribbed slabs since the early two tests of solid slabs conducted by Granade⁵ in 1968.

Todd and Cooper⁶ (1980), in analysing Granade's beams, predicted the ultimate strength at web openings by employing a plastic theory for the steel beam and including the resistance of the slab in compression as a contribution to the moment capacity. However, by ignoring the slab shear carrying capacity in their analysis, a considerable underestimation of the ultimate load carrying capacity of the beam resulted.

Subsequently, Clawson and Darwin^{7,8} (1982) performed six solid slab beam tests and developed a detailed analytical method capable of predicting the ultimate strength at web openings. At this time, the slab shear contribution in the opening region was more clearly demonstrated with their test results, which was also supported in other solid slab tests by Cho⁹ (1982).

Several failure modes, which depended on the moment-to-shear ratio at the opening centerline, were classified from test observations and incorporated in the analytical procedure. In treating the slab contribution to the shear carrying capacity at the opening, a biaxial criterion combining normal and shear stresses was used in the compressive stress block depth over a slab width equal to three times the slab thickness. The compression forces in the slab were calculated based on complete shear connection and were assumed to exist only at the high moment end of the opening.

Comparison of this analysis with test results including Granade's beams indicated that the prediction was greatly improved when compared with the Todd and Cooper method, but still conservative, particularly for Granade's tests. However, the more fundamental problems in their analysis relate to the omission of consideration of partial shear connection, and the considerable amount of computational effort required for the completion of an interaction diagram because all possible stress distributions were included. Although the neglect of the degree of shear connection can be justified for solid slab beams capable of providing a higher number of shear connectors along the whole beam span, its validity for ribbed slab beams is not justified. Further, if the important role of shear connection, in the light of the truss concept proposed in this project, is considered, the Clawson and Darwin method largely obscures the physical significance of shear connection in carrying vertical shear forces even for solid slab beams.

While at this time only solid slab beams were considered in the United States, Redwood and Wong¹⁰ (1982) at McGill University conducted a series of tests comprising metal deck supported slabs. All five beams tested had wide rib profiles and included partial shear connection as one of major test parameters. Although some similar observations to those found in solid slab beams were made in their tests, the observed rib separation represented a different type of slab failure mechanism in the opening region.

To estimate the ultimate strength, they also provided a simplified analytical method based on the four-hinge mechanism failure which represents a typical deformation mode of holes under high shear. A substantial simplicity was achieved by deriving explicit formulas defining the co-ordinates of several points on the interaction diagram. Assuming the slab to be fully cracked at the low moment end of the opening under high shear, the compression force in the slab at the high moment end of the hole was limited to the horizontal resistance of shear connectors provided within the opening length, which might also include a possibility of limited shear connection over the opening length. However, the contribution of the concrete slab to carry shear was not explicitly accounted for so that some caution was necessary in the application of their analysis to solid slab beams.

After comparison with test results, their analysis was found conservative even for ribbed slab beams, and they suggested the inclusion of the additional compression force in the slab at the low moment end of the opening for an improved estimate of the ultimate strength, on the reason that slip can cause the counteracting effects on the low moment end stresses¹¹.

However, in the author's opinion, it is believed that this conservatism resulted from the omission of the slab shear contribution rather than the neglect of the compression force in the slab at the low moment end of the opening. More discussion will be given in Chapter 3.

With the recognition of possible existence of the additional slab force at the low moment end of the opening, Redwood and Poubouras¹² (1983) tested three additional holes with particular attention given to the degree of shear connection within the opening length and the effect of the construction load on the ultimate strength.

Based on test results, they concluded that the absence of shear connectors within the opening length causes a significant reduction in strength, and a construction load up to 60% of the strength of the non-composite section does not significantly affect

the strength. Note that their first conclusion implies the necessity for shear connection within the opening length if the additional slab force is assumed to exist at the low moment end of the opening as well.

As a result, Redwood and Poubouras³ (1984), in proposing an analytical method to estimate the ultimate strength, assumed the compression forces to exist in top and bottom parts of the slab at high and low moment ends of the opening respectively as a high shear situation. Then the magnitudes of these forces were limited by the number of shear connectors provided between the high moment end of the opening and the nearest point of zero moment and within the opening length (see Fig. 1.4). Note that later on, this way of determining the slab forces in the opening region is required to be altered to conform with the use of the truss concept.

On the other hand, in considering the slab shear contribution in their analysis, the total shearing force carried by a composite section above the opening was limited to the pure shear capacity of the steel section alone, although the slab forces used in the analysis assumed that the slab can carry a shearing force. The reason for this limitation was that the proportion of shearing forces carried by the concrete slab is not readily determinable, and so this limit was chosen conservatively. This is the major reason for high conservatism inherent in their analysis when applying to solid slab beams.

More recently, several analytical methods of using the same solution procedure developed by Redwood and Poubouras, but fully accounting for the slab shear carrying capacity have been published (see Fig. 1.5). Such methods can be considered as the generalized approaches of the Redwood and Poubouras theory to deal also with solid slab beams.

The analysis presented by Redwood and Cho^{4,13,14} (1986) includes specific procedures of limiting shear connector resistance to obtain the maximum strength as well as to satisfy equilibrium in view of ensuring assumed stress distributions for various cases of beam geometries. In the treatment of the slab contribution to carry vertical shear, a

similar way of limiting shear connector resistance to that based on the unused portion of the slab between top and bottom compression layers subjected to a pure shear stress was incorporated as shown in Fig 1.5(a).

However, it was realized that this theory does not provide a realistic solution for some beams having a high number of shear connectors between the low moment end of the opening and the support. In those beam conditions, the slab forces calculated based on the corresponding numbers of shear connectors will be significantly higher than the yield capacity of one steel flange. Hence, the shear connector resistance needs to be reduced to maintain stress reversals within the steel flange thicknesses, in the sense of satisfying equilibrium of assumed stress distributions. Thus, the connector forces calculated in this way were found very small compared with their ultimate capacities, resulting in unrealistic interpretation of the performance of shear connection. Full details of this analysis will be given in Chapter 2 as part of this research project.

A similar effort has been also found in a research project involving nine ribbed slab beam tests conducted by Darwin and Donahey^{15,16} at the University of Kansas (1988). In their tests, large steel sections relative to the slab thicknesses were used to investigate the effect of partial shear connection, deck rib orientation and modifications to decks around the opening to accommodate a higher number of shear connectors.

For the prediction of the ultimate strength, they also presented three solutions incorporating the slab shear capacity. This was limited to the value based on the ultimate concrete shear stress acting on an area equal to full slab depth times a width of the slab equal to three times the overall slab thickness as shown in Fig. 1.5(b). This way of consideration does not involve any dependence of the slab shear carrying capacity on the shear connector resistance, which differs from the procedure developed by Redwood and Cho.

A similar problem to that found in the Redwood and Cho method also occurs in Darwin and Donahey's analysis when the compression forces in the slab are limited

by the tensile capacity of one steel flange. This results from yielding of the steel web section in pure shear, or violation of stress reversals within the steel flange thicknesses due to a high number of shear connectors provided between the low moment end of the hole and the support, even though the latter was not noted in their original work. As a result, the connector forces that must be developed to resist the slab forces will correspond to small proportions of their ultimate capacities. Therefore, it is difficult to see how the ultimate stage of the beam can be obtained with such small connector forces in the normal beam configurations allowing for partial shear connection.

Further, concerning the three solutions proposed, it should be noted that unlike the Redwood and Cho method, the first solution does not impose a sufficient condition to satisfy equilibrium, in the sense of maintaining stress reversals within the steel flange thicknesses as assumed. In the other two solutions, the stress distributions assumed in the steel bottom tee do not involve local bending resulting from the elimination of stresses in the steel flange, therefore it is difficult to see how they can lead the shearing force in the bottom tee. In addition, these two solutions did not ensure normal force equilibrium between top and bottom tees, although they provided identical formulas to those originally derived by Redwood and Poubouras in which equilibrium was fully ensured. More discussion on their analyses is given elsewhere¹⁷.

Using the simplified approaches of considering the slab shear contribution in more recent analyses^{4,16}, the prediction of the ultimate strength for solid and ribbed slab beams is possible in a unified manner and with reasonable accuracy. However, there is still lack of justification related to the following two major points.

- i) The slab shear contribution considered does not involve the structural action between the concrete slab and shear connection in a realistic way, resulting in an arbitrary assignment of the shearing forces to the steel section and the concrete slab.
- ii) The way of determining the slab forces based on the numbers of shear connectors

provided both between the high moment end of the opening and the nearest point of zero moment, and within the length of the opening. does not involve realistic connector forces for beam geometries in which the slab forces are required to be limited by the tensile capacity of one steel flange.

1.3 Objectives

The objectives of this research programme are:

- to clarify the slab behaviour and the performance of shear connectors in carrying the vertical shear forces in the region of a web opening.
- to develop analytical methods based on realistic slab and shear connector behaviour for the prediction of the ultimate strength and service performance of composite beams containing large web holes.
- to verify the theoretical background proposed by the experimental investigation.
- to provide design guidance for composite beams with web openings.

Research work described herein is primarily applicable to stockier webbed beams with height to thickness ratio below about 80 and configured with solid or ribbed slabs. However, the truss analogy proposed for the treatment of the slab shear carrying capacity above a web hole can also be used in the slab of composite thin webbed plate girders, composite trusses or possibly in the link beam of eccentrically braced frames, that is, in regions where the slab carries significant proportion of the shearing force.

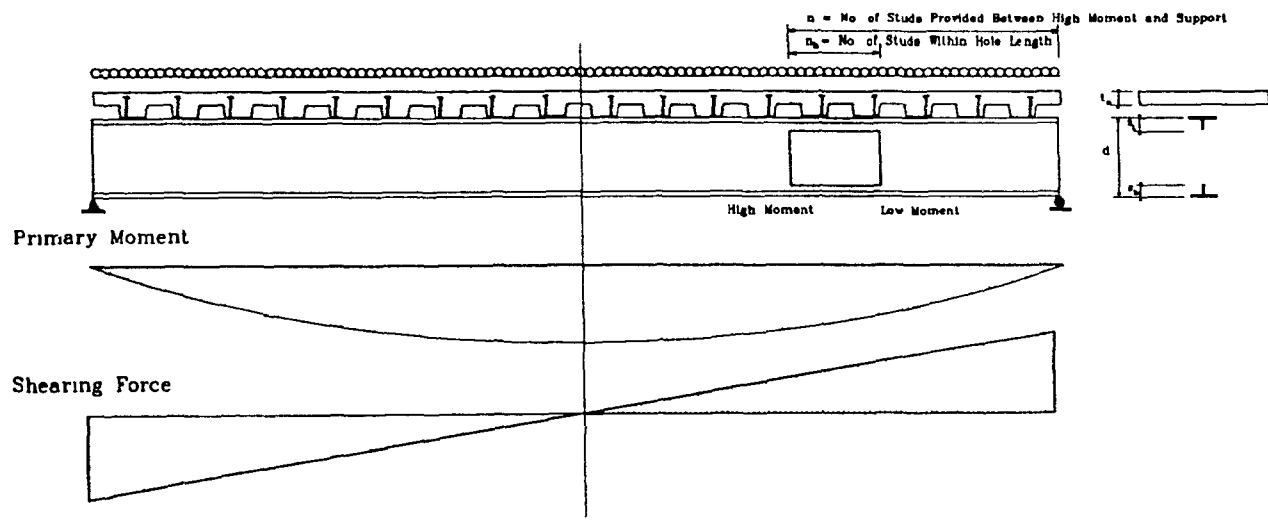
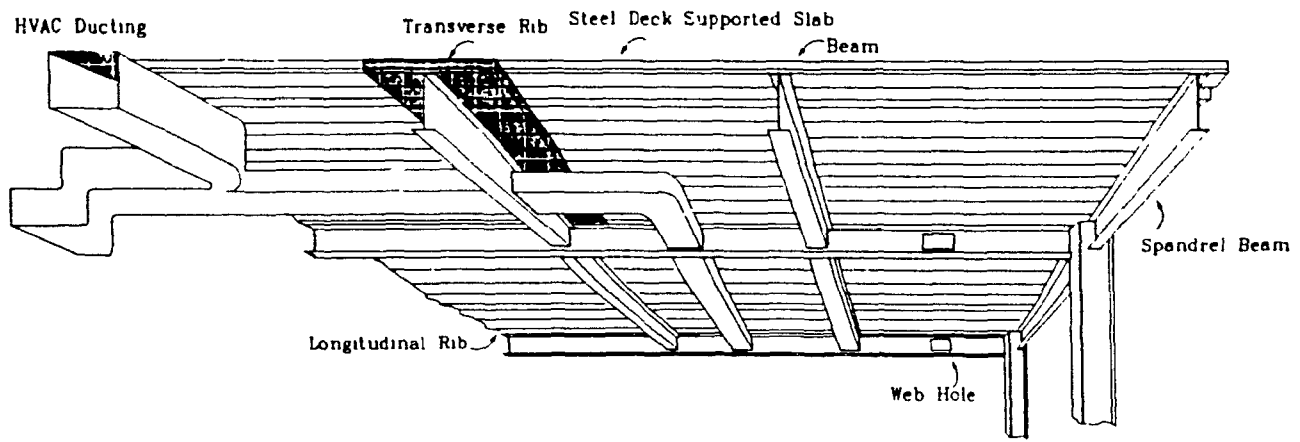


Figure 1.1 Web Openings in a Typical Floor of Steel Framed Buildings

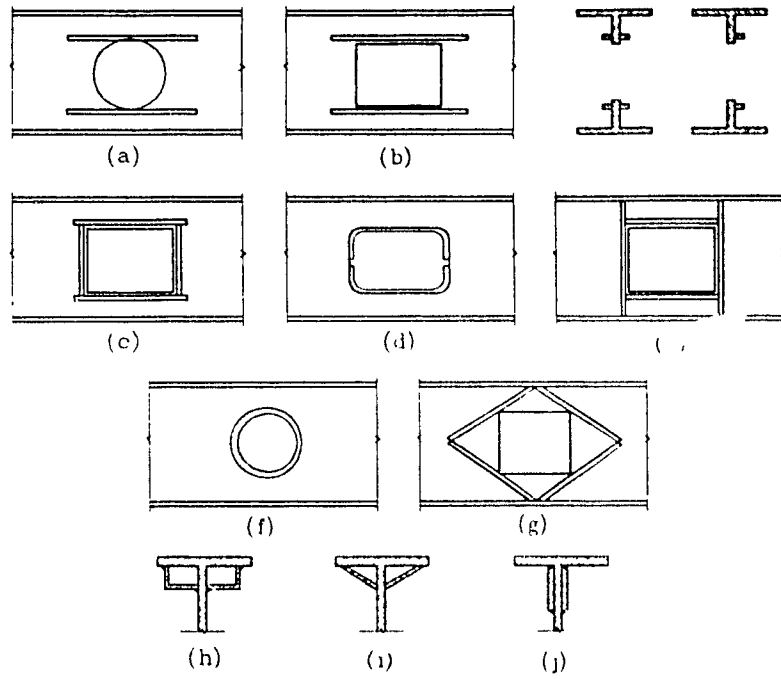


Figure 1.2 Reinforcement of Openings¹.

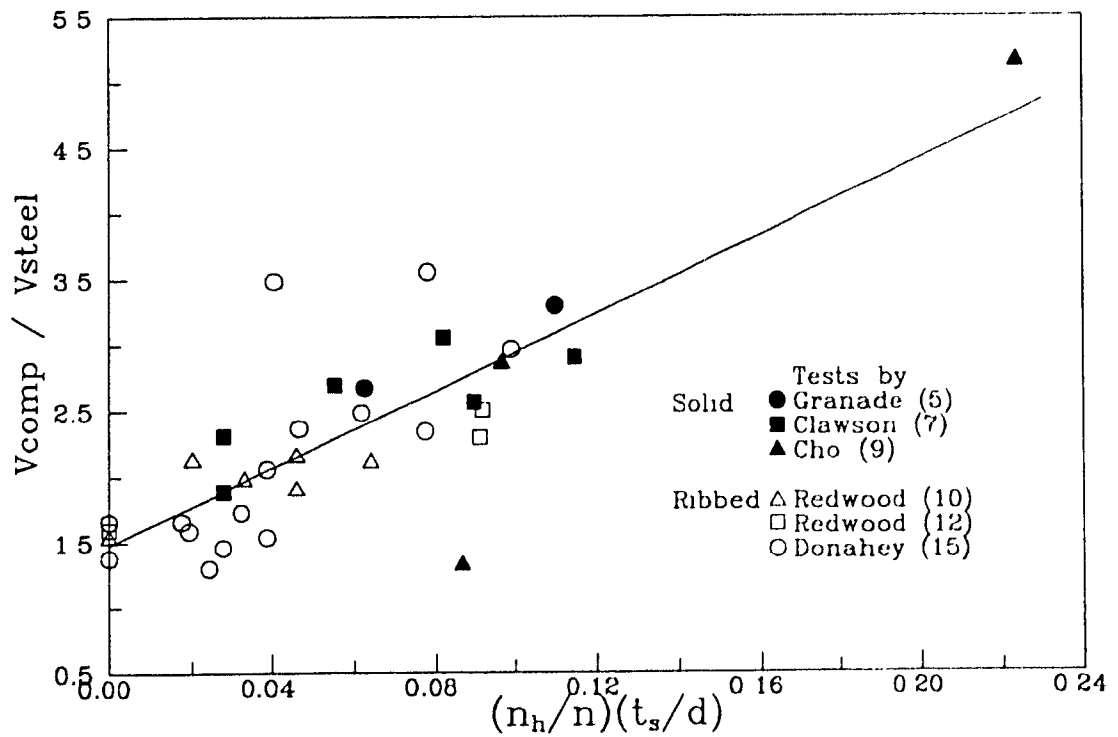


Figure 1.3 Contribution of Concrete Slab at a Web Opening.

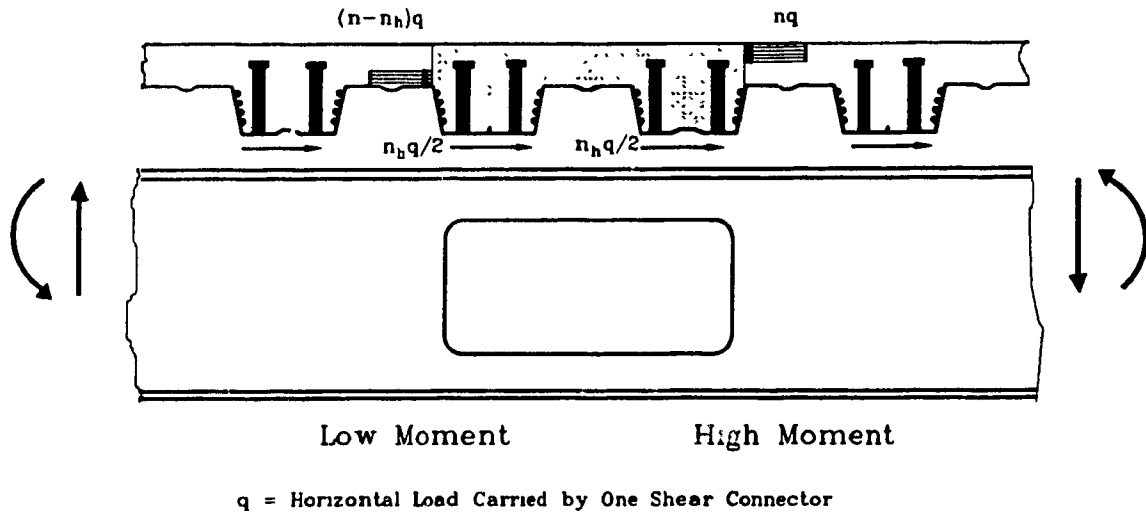


Figure 1.4 Slab Forces Proposed by Redwood and Poubouras³.

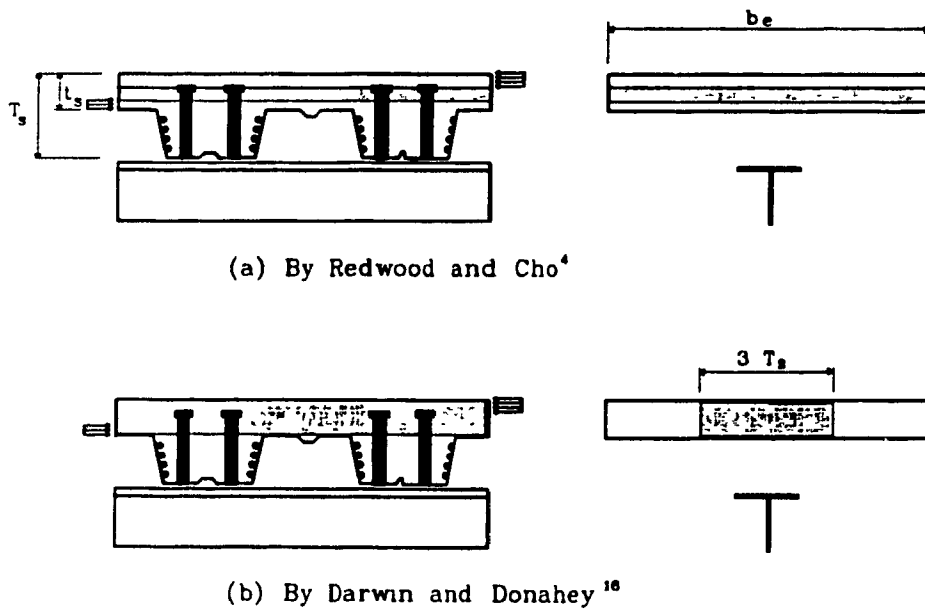


Figure 1.5 Shear Area in Concrete Slab.

CHAPTER 2

FUNDAMENTAL ANALYTICAL PROCEDURE FOR ULTIMATE STRENGTH

2.1 Introduction

A conventional way of estimating the ultimate strength in beams with web holes is to construct the moment-shear interaction diagram which includes member resistance to various load combinations, resulting from different locations of the opening in a beam span. In developing such an interaction curve a higher degree of accuracy in prediction is obtained as more points representing various opening locations are used to define the curve.

However, in normal configurations of composite beams allowing for limited shear connection, this interaction procedure requires another consideration associated with the distribution of the shear connectors along the whole beam span. This arises from the dependence of the strength on shear connector resistance (or distribution of shear connectors). Thus, for the appropriate construction of complete interaction curves in such composite beams, each point on the interaction diagram should be based on the corresponding location of the opening as well as on the distribution of the shear connectors. As a result, the interaction diagram developed in this way can represent only the beam resistance corresponding to a particular location of the opening under

a particular distribution of shear connection. Note that this is a different feature of composite beams compared to steel beams when considering the range of application of a complete interaction diagram. Further, under the situation described above, the possibility of constructing a complete interaction curve that can predict the resistances at different hole locations in a given beam is questionable.

A detailed strength analysis¹⁶ developed at the University of Kansas also fails to include predictions for various opening locations in a given beam since the compression forces assumed in the slab at every opening location were not based on the corresponding distribution of the shear connectors.

With the recognition of this situation, the method of analysis presented herein adopts a simple form of interaction diagram such as that shown in Fig 2.1, consisting of an elliptical curve between points 0 and 1, and a straight line between points 1 and 1' for providing the ultimate resistance of the beam in a specific location of the opening. A detailed procedure to determine the several coordinates which define the interaction diagram will now be described below for the cross sectional details shown in Fig. 2.2. Note that this analysis can also be applied to solid slabs ($t_s = T_s$), or longitudinally ribbed slabs ($T_s = t_s + 0.5h_r$) with appropriately modified slab thickness.

2.2 Formulation of Member Capacity

Point 0 represents the ultimate moment resistance of the net composite cross-section in absence of shearing forces. The value of M_{oh} defining this point can be calculated with the assumption of complete shear connection using the well established ultimate strength method¹⁸. However, in view of the interaction diagram relating only to a specific location of the opening this quantity needs to be modified to the value of M'_{oh} . The moment M'_{oh} defining the point 0' includes the effect of limited shear connection between the hole centerline and the nearest point of zero moment, and could be used in place of M_{oh} in generating the elliptical part of the curve. However,

following the suggestion of Redwood and Pournouras³, a horizontal cut-off at this point is adopted herein.

Point 1' represents the ultimate shearing resistance in the absence of bending moment for a given location of the opening and can be taken equal to the shearing force at the point 1 on the basis of test evidence. Therefore, the remaining part of the analysis relates to the derivation of the ultimate strength values V_1 and M_1 corresponding to point 1, representing the transition of the failure mode of the hole from bending to shear.

In the derivation, failure of steel by yielding and of the concrete by compression or shear is assumed at the beam cross sections coincident with the ends of the hole. Yield of the steel is assumed to be according to Von Mises criterion and the parts of the concrete slab under compression and under shear are treated separately, thus permitting simple failure criteria in pure compression and pure shear. No tension is assumed in the concrete.

For the coordinates of point 1, stress distributions allowing for high shearing forces are assumed as in Fig. 2.3. The factors k_1 to k_6 which all lie between 0 and 1 represent the portion of flange, web or cover slab subjected to tensile or compressive stresses.

Forces acting on the concrete slab over the opening length are assumed as shown in Fig. 2.4 with the maximum eccentricity, $\bar{e} = t_s(1 - 0.5k_5 - 0.5k_6)$ between the top and bottom compressive forces. Later, in developing a truss analogy the magnitudes and locations of these forces will be determined in a rational manner by considering the stud configurations within and beyond the opening length.

Assuming that all studs are identically loaded and each carries the horizontal shear q developed by bending.

$$C_1 = nq \quad (2-1)$$

$$C_2 = (n - n_h)q \quad (2-2)$$

where n is the number of studs between the high moment end of the hole and the nearest point of zero moment, and n_h is the number of studs between the ends of the hole.

The full compressive resistance of the slab C_0 is given by

$$C_0 = 0.85f_c' b_e t_s \quad (2-3)$$

in which b_e is the effective slab width and t_s the cover slab thickness. Thus $k_5 = C_1/C_0 = nq/C_0$ and $k_6 = C_2/C_0 = k_5(1 - n_h/n)$.

Now considering the web of the steel tee section above the hole, we may write, since yield occurs

$$\sigma^2 + 3\tau^2 = F_{yw}^2 \quad (2-4)$$

in which F_{yw} is the web yield stress. Writing $P_{wt} = s_t w \sigma$, $V_{pt} = s_t w F_{yw} / \sqrt{3}$ and $V_{st} = s_t w \tau$, the shear carried by the steel above the opening, then

$$P_{wt} = \sqrt{3V_{pt}^2 - 3V_{st}^2} \quad (2-5)$$

Similar relationships exist for sections below the opening, giving P_{wb} as a function of the shear carried below the opening V_b .

For convenience we may write $\beta_t = P_{wt}/P_{yf}$ and $\beta_b = P_{wb}/P_{yf}$ where $P_{yf} = btF_{yf}$, the yield load of one flange. Integrating the stresses at each of the four failure sections,

$$k_1 = 0.5(\beta_t - \beta_b - \epsilon_1) + k_3 \quad (2-6)$$

$$k_2 = 0.5(\beta_b + \beta_t + \epsilon_2 + 2) - k_3 \quad (2-7)$$

$$k_4 = \beta_b - k_3 + 1 \quad (2-8)$$

in which $\epsilon_1 = C_1/P_{yf}$ and $\epsilon_2 = C_2/P_{yf}$.

The stress resultants at the four sections are denoted Q_i , and their lines of action are defined by \bar{y}_i , as shown in Fig 2.3. We may therefore write

$$Q_1 \bar{y}_1 = P_{yf}[-0.5s_t \beta_t + 2k_1 s_t - s_t + \epsilon_1(s_t + T_s - 0.5k_5 t_s)] \quad (2-9)$$

$$Q_2 \bar{y}_2 = P_{yf}[0.5s_t \beta_t - 2k_2 s_t + s_t + \epsilon_2(s_t + T_s - 0.5k_5 t_s - \bar{e})] \quad (2-10)$$

$$Q_3 \bar{y}_3 = P_{yf}[-0.5s_b \beta_b + 2k_3 s_b - s_b] \quad (2-11)$$

$$Q_4 \bar{y}_4 = P_{yf}[0.5s_b \beta_b - 2k_4 s_b + s_b] \quad (2-12)$$

Equilibrium of the regions above and below the openings and at the opening centerline, requires

$$2aV_t = Q_1 \bar{y}_1 - Q_2 \bar{y}_2 \quad (2-13)$$

$$2aV_b = Q_3 \bar{y}_3 - Q_4 \bar{y}_4 \quad (2-14)$$

where $V_t = V_{st} + V_c$ in which V_c is the shear carried by the concrete and V_{st} is that carried by the steel. Also,

$$M = 0.5H[Q_1 + Q_2 + Q_3 + Q_4] + 0.5[Q_1 \bar{y}_1 + Q_2 \bar{y}_2 + Q_3 \bar{y}_3 + Q_4 \bar{y}_4] \quad (2-15)$$

Using the subscript 1 to denote values corresponding to point 1 of the interaction diagram, and assuming that the steel flange thickness is small compared with the depth of the tee section, substitution from Eqs. (2-6) to (2-12) in Eq. (2-13) leads to two solutions for V_{t1}

$$\frac{V_{t1}}{V_{pt}} = \frac{\mu\gamma + \sqrt{3\gamma^2 - 3\mu^2 + 9}}{(3 + \gamma^2)} \quad \text{for } V_{t1} \leq V_{pt} \text{ (or } \mu \leq \gamma) \quad (2-16)$$

$$\frac{V_{t1}}{V_{pt}} = \frac{\mu}{\gamma} \quad \text{for } V_{t1} > V_{pt} \text{ (or } \mu > \gamma) \quad (2-17)$$

in which $\gamma = 2a/s_t$

and

$$\mu = \frac{C_0}{s_t V_{pt}} [k_5(T_s - 0.5k_5t_s) - k_6(T_s - 0.5k_5t_s - \bar{e})]$$

and also Eq. (2-14) leads to

$$V_{b1} = V_{pb} \sqrt{\frac{\alpha_b}{1 + \alpha_b}} \quad (2-18)$$

where $\alpha_b = 3s_b^2/4a^2$

The total shearing force can be written

$$V_1 = V_{t1} + V_{b1} \quad (2-19)$$

and the maximum moment consistent with this shearing force corresponds to $k_3 = 1$ and is given by Eq. (2-15) as

$$M_1 = dP_{yf}(1 - \beta_b) + 0.5C_0[k_5(T_s - 0.5k_5t_s) + k_6(T_s - 0.5k_5t_s - \bar{e})] \quad (2-20)$$

2.3 Limitations on Shear Connector Resistance

Since the solution procedure is based on the lower bound plastic collapse theorem, it is desirable to choose the maximum value in Eqs. (2-16) or (2-17) subject to equilibrium and yield requirements being satisfied.

In the following, for various beam geometries, a number of additional restrictions to ensure either equilibrium or yield conditions are satisfied as well as to obtain the maximum value of V_{t1} are derived. These are incorporated into the solution by the device of limiting individual shear connector resistance.

The two solutions given by Eqs. (2-16) and (2-17) are illustrated in Figs. 2.5(a) and (b) respectively. They are valid in the range $0 \leq q \leq q_{max}$ where q_{max} is defined as

$$q_{max} = \min\left\{\frac{C_0}{n}, \frac{T_0}{n}\right\} \quad (2-21)$$

This denotes the limiting shear connection corresponding to compression failure of the complete cover slab, or tension yield of the complete net steel section at the hole, where

$$T_0 = 2btF_{yf} + (d - 2t - 2H)wF_{yw} \quad (2-22)$$

The corresponding compression block depth factor k_{5max} is given by

$$k_{5max} = \frac{nq_{max}}{C_0} \quad (2-23)$$

For cases with $\mu \leq \gamma$, a possible range of solution is indicated in Fig. 2.5(a) when V_1 is given by Eq. (2-19), in which V_{t1} is given by Eq. (2-16) and V_{b1} by Eq. (2-18).

The horizontal connector resistance q_0 corresponding to the maximum value of V_{t1} is obtained by maximising V_{t1} in Eq. (2-16), and is given by $q_0 = k_{50}C_0/n$ where

$$k_{50} = \frac{\left[1 - \frac{n_h}{n} + \frac{T_s n_h}{t_s n}\right]}{2\left[1 - \frac{n_h}{n} + \frac{n_h^2}{2n^2}\right]} \quad (2-24)$$

In addition, all stress reversals should be ensured within the steel flange thicknesses, that is with $0 \leq k_i \leq 1$, in order to satisfy equilibrium of assumed stress distributions. Then we may write,

$$q_e = \min\{q_1, q_2\} \quad (2-25)$$

in which

$$q_1 \leq \frac{2P_{yf} - V_{pb} \sqrt{\frac{3}{(1 + \alpha_b)}} + P_{wt}}{n} \quad (k_1 \geq 0) \quad (2-26)$$

and

$$q_2 \leq \frac{2P_{yf} - V_{pb} \sqrt{\frac{3}{(1 + \alpha_b)}} - P_{wt}}{n - n_h} \quad (k_2 \leq 1) \quad (2-27)$$

Note that in cases of $\mu \leq \gamma$ being considered, the values q_1 and q_2 in Eqs. (2-26) and (2-27) must be solved iteratively because of their dependence on P_{wt} , but usually one iterative cycle is sufficient. Similarly, we may write $k_{5e} = nq_e/C_0$.

The solution which corresponds to $\mu > \gamma$ will only normally be feasible over part of the range $0 < q < q_{max}$ defined by q'_a and q'_b , as can be seen in Fig 2 5(b). These values are obtained from $q'_a = k'_5 C_0/n$ etc. where k'_5 are the roots of the following equation derived from $\mu = \gamma$:

$$\left[1 - \frac{n_h}{n} + \frac{n_h^2}{2n^2}\right]k_5'^2 - \left[1 - \frac{n_h}{n} + \frac{T_s n_h}{t_s n}\right]k_5' + \frac{2aV_{pt}}{C_0 t_s} = 0 \quad (2-28)$$

As in the case when $\mu \leq \gamma$, the maximum shearing resistance again occurs when $q_0 = k_{50}C_0/n$ where k_{50} is given by Eq.(2-24), and the Eq. (2-25) should be again considered to ensure stress reversals within the steel flange thicknesses as assumed while q_1 and q_2 are calculated with $P_{wt} = 0$.

2.4 Concrete Slab Shear Consideration

The solution for $\mu > \gamma$ is valid when the steel top tee is fully yielded in shear, and in addition the concrete slab contributes to the shearing resistance.

As a simple model representing the limit of cover slab shear carrying capacity, the ultimate stress distributions shown in Fig. 2.4 are assumed. Top and bottom layers of the cover slab are subjected to the ultimate compressive stress $0.85f'_c$ and the layer

between these two is assumed to carry the ultimate shearing stress⁷ $\lambda\sqrt{f'_c}$ ($\lambda = 0.29$ with f'_c in MPa). The ultimate shearing strength of the slab may therefore be written

$$V_{cu} = \lambda\sqrt{f'_c}b_c t_s(1 - k_5 - k_6) \quad (2-29)$$

For those cases in which the slab shearing resistance must be mobilized, the beam shearing resistance, V_1 , can not exceed $V_{max} = V_{bl} + V_{pt} + V_{cu}$. It may also be noted that $V_{cu} = 0$ when $k_5 + k_6 = 1$, i.e. when

$$k_5 = k_{5c} = \frac{1}{2 - \frac{n_h}{n}} = \frac{nq_c}{C_0} \quad (2-30)$$

The bi-linear upper limit shown in Fig. 2.6 represents V_{max} and the intersection of the two straight lines is located at $q = q_c$.

A solution which intersects the upper limiting line V_{max} , as shown in Fig 2.6, takes place when

$$\frac{\mu}{\gamma}V_{pt} = V_{pt} + V_{cu} \quad (2-31)$$

Solution of this for the corresponding $k_5 (= k_5'')$ gives

$$\left[1 - \frac{n_h}{n} + \frac{n_h^2}{2n^2}\right]k_5''^2 - \left[\left(1 - \frac{n_h}{n}\right)(1 + \Phi) + \Phi + \frac{T_s n_h}{t_s n}\right]k_5'' + \left[\Phi + \frac{2aV_{pt}}{C_0 t_s}\right] = 0 \quad (2-32)$$

where

$$\Phi = \frac{2a\lambda}{0.85\sqrt{f'_c}t_s} \quad \text{and} \quad q'' = \frac{k_5''C_0}{n}$$

The solution for V_{t1} is then obtained by using the lower of q'' and q_t in evaluating μ in Eq.(2-17). and the shearing force carried by the concrete, V_c , may be obtained from

$$V_c = V_t - V_{pt} \quad (2-33)$$

All limiting values of q described so far are summarized below in a tabular format (see Table 2.1).

The full comparison of results given by the theory with previous tests will be given in Chapter 4.

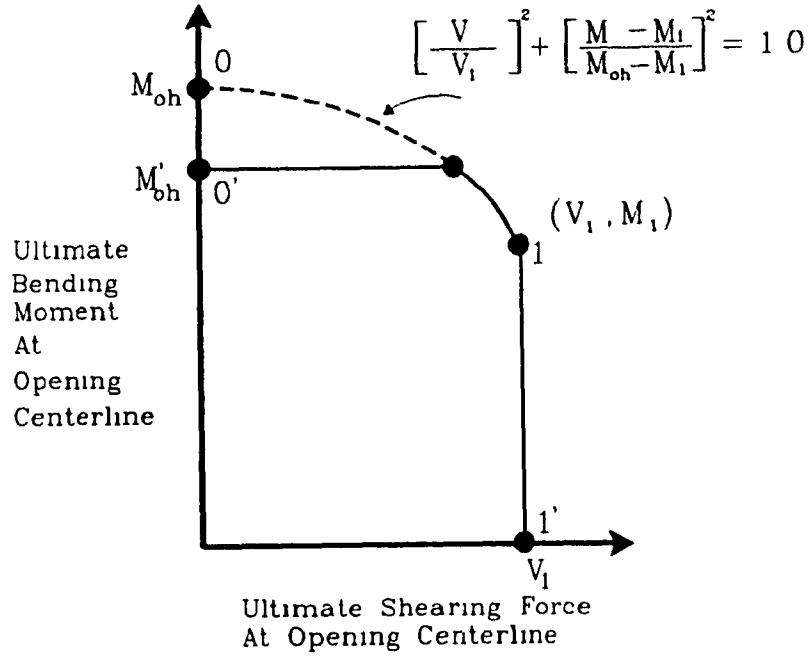


Figure 2.1 Moment-to-Shear Interaction Diagram

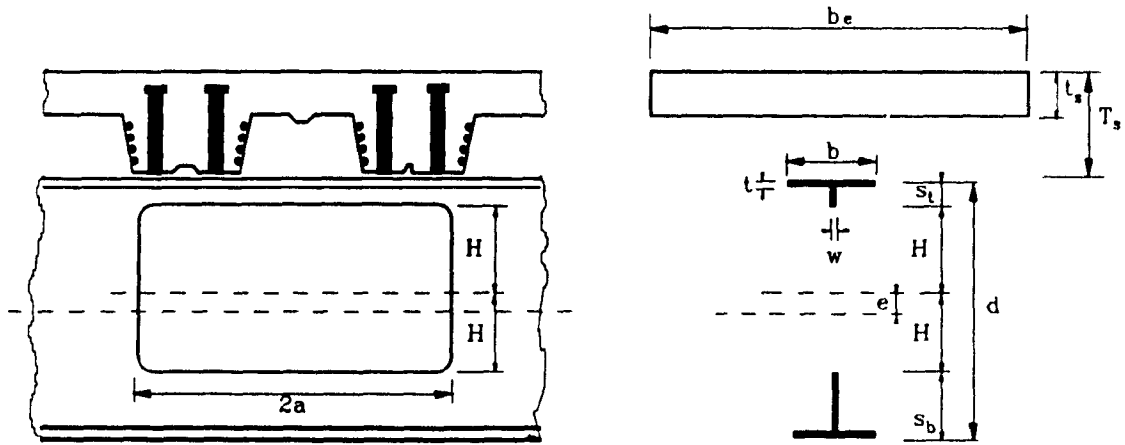


Figure 2.2 Cross Sectional Details

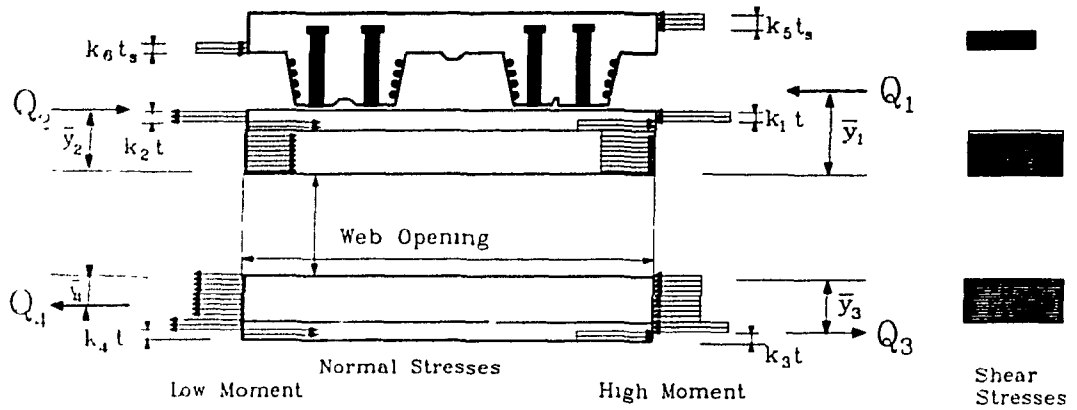


Figure 2.3 Assumed Stress Distributions

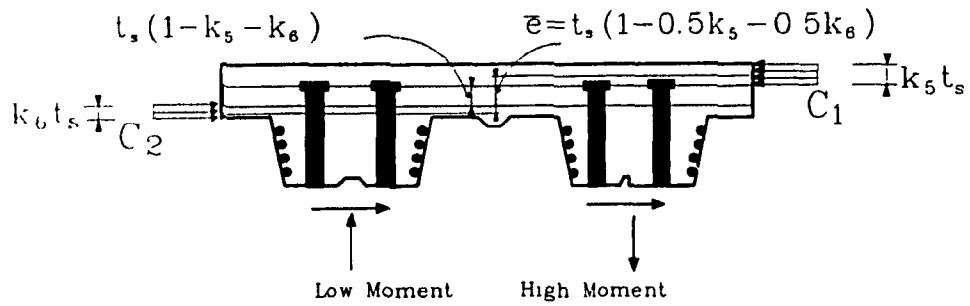


Figure 2.4 Force System in Concrete Slab

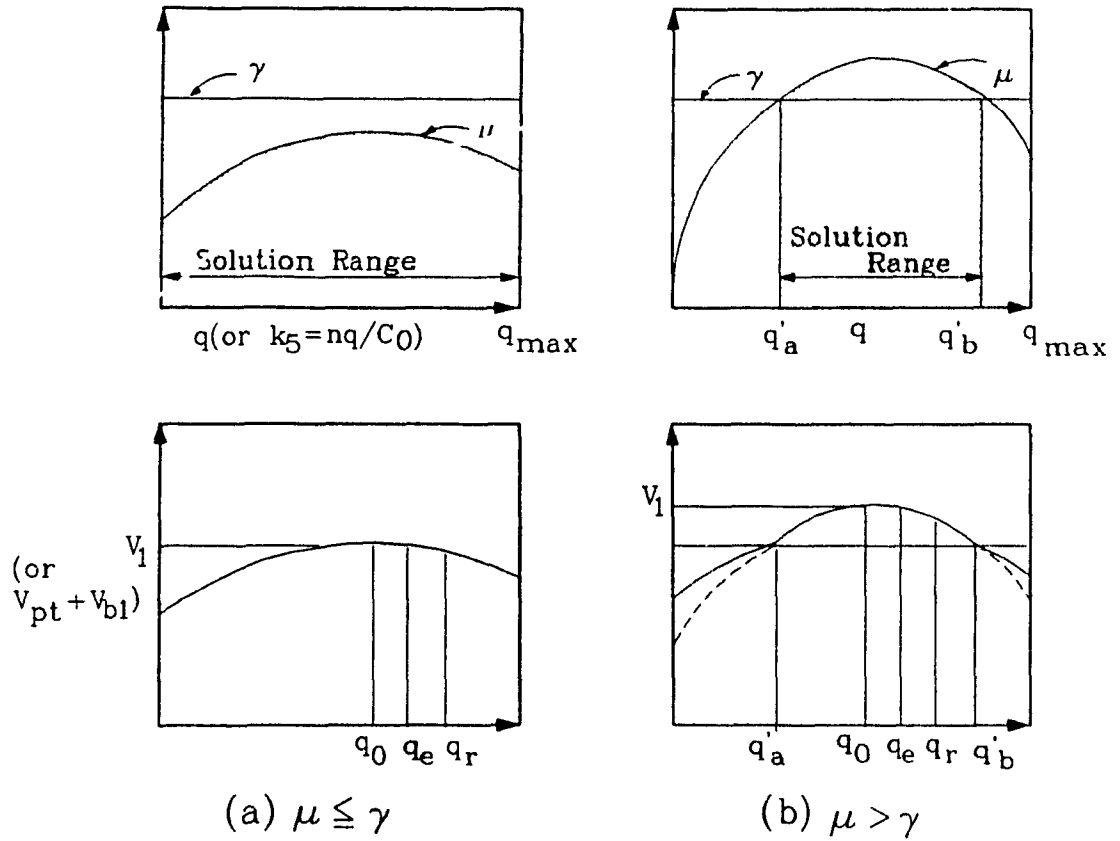


Figure 2.5 Graphical Representation of Solution

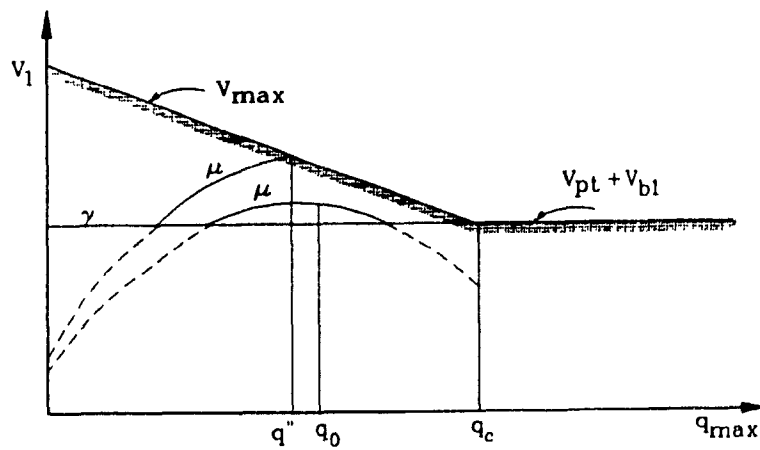


Figure 2.6 Graphical Representation of Slab Shear Solution

Table 2.1 Limiting Values of Shear Connector Resistance

Reasons for Limitations	$\mu \leq \gamma$	$\mu > \gamma$
1 Shear connector ultimate resistance	q_r	same as $\mu \leq \gamma$
2 Optimum value to give maximum beam resistance	$\frac{C_0}{n} \frac{1 - \frac{n_h}{n} + \frac{T_s n_h}{t_s n}}{2[1 - \frac{n_h}{n} + \frac{1}{2} \{ \frac{n_h}{n} \}^2]}$	"
3. Tensile capacity of steel section	$\frac{T_0}{n}$	"
4. Compressive capacity of concrete slab	$\frac{C_0}{n}$	"
5. Full shear resistance of steel and concrete slabs can be developed	NA	q'' (Eq (2-32))
6 To ensure equilibrium of assumed stress distributions is satisfied ($k_1 \geq 0$)	$\frac{2P_{yf} - V_{pb} \sqrt{\frac{3}{(1 + \alpha_b)}} + P_{wt}^*}{n}$	$\frac{2P_{yf} - V_{pb} \sqrt{\frac{3}{(1 + \alpha_b)}}}{n}$
7. To ensure equilibrium of assumed stress distributions is satisfied ($k_2 \leq 1.0$)	$\frac{2P_{yf} - V_{pb} \sqrt{\frac{3}{(1 + \alpha_b)}} - P_{wt}^*}{n - n_h}$	$\frac{2P_{yf} - V_{pb} \sqrt{\frac{3}{(1 + \alpha_b)}}}{n - n_h}$

* The cases indicated must be solved iteratively, but one iterative cycle is usually sufficient

CHAPTER 3

TRUSS ANALOGY

FOR SLAB BEHAVIOUR

3.1 Introduction

The truss analogy¹⁹, in which the internal flow of forces is represented in the form of strut-and-tie models, is today considered as a rational and general basis for shear design of structural concrete. The basic concept of this analogy is that after cracking of concrete, reinforced concrete structures carry loads principally by a set of diagonal compressive stresses in the concrete and tensile stresses in the reinforcement. It can be recognized that by considering the shear connectors as vertical tension members, a similar type of truss action to that found in concrete structures may be possible in the slab of a composite beam, particularly in regions where the slab carries a lot of vertical shear such as in a beam above a web hole, in situations where the steel section is very slender², in composite trusses²⁰, and possibly also in the link beam of eccentrically braced frames²¹ (see Fig. 3.1).

At the present time, no rational procedure to consider any contribution of composite action to strength in vertical shear exists in designing composite structural floor members. This may be because of the small influence of slab shear in normal structural elements or because of the complexity of slab shear problems. However, in those beams

having large web holes, particularly with the ribbed type of slab with limited shear connection, a sound appreciation of the slab and shear connector behaviour in resisting vertical shear is desirable if a full understanding of both ultimate strength and serviceability load level performance is required. For this, a finite element technique capable of predicting the post-cracking behaviour may be useful; but there are serious difficulties in simulating the interface of the concrete and connectors as well as in generating mesh arrangements with the normal element library which describe the connector locations and rib geometries. The truss analogy offers a more promising approach to clarify the structural action of the slab and the studs in the region of a web penetration.

An explanation for the load carrying mechanism in solid and ribbed slabs of composite beams subjected to high shear is presented, and based on this physical understanding, truss idealizations capable of considering the slab shear contribution in a rational manner are developed. With these idealizations, the ultimate resistance of composite beams with web holes representing point 1 on the interaction diagram such as Fig. 2.1 is formulated for three different configurations of the studs in the hole region. A serviceability analysis model that includes the interfacial slip between concrete slab and steel beam as well as truss action identified in the hole region is also proposed.

3.2 Ultimate Strength

Due to the presence of the concrete slab, a surprisingly large increase of the ultimate shear strength has been reported in tests of composite beams with web holes^{7,10} or thin webbed plate girders². In these tests, failure of the slabs was dominated by diagonal tension in solid slab specimens and by rib separation in ribbed slab specimens in the vicinity of web holes (see Fig. 3.2).

As was noted in previous work¹⁰, such slab failures have some relationship to the transference of prying forces between slab and steel beam through shear connection, resulting from the Vierendeel type of action at the opening. However, in discussing this

aspect of shear connection, previous researchers gave more attention to the horizontal shear resistance of the connectors rather than the vertical resistance. While obviously recognizing that the rib separation cracking relates closely to tension action of the studs in the vertical direction, they could not see any practical way of incorporating this specific action of the studs in an analytical procedure because of insufficient understanding of the behavioural aspect of the connectors in their role in carrying "vertical shear".

In the following, the performance of stud connectors in resisting vertical shear is identified and related to the observed slab failures in composite beams with web holes

3.2.1 Behaviour

3.2.1.1 Solid Slabs

In most solid slab tests^{5,7,9} reported, a typical feature which is largely different from ribbed slab tests is that high degrees of shear connection and relatively thick slabs are provided along the whole beam span. Thus, such connectors can be considered as sufficient vertical reinforcement to perform truss action in the slab.

Figure 3.3 shows the stud and opening configurations, and a slab crack pattern around the hole for one of the solid slab beams⁷ tested at the University of Kansas. By applying the truss concept to this slab failure mode, it can be deduced that under high shear, the top compressive stresses in the slab at the high moment end of the opening must be resisted diagonally at bearing formed by the shanks of the studs and the top steel flange near the low moment end of the opening. Considering the occurrence of transverse cracks in top and bottom parts of the slab due to the Vierendeel type of action at the hole, the diagonal strut action described will be more apparent. If there is no tension in the concrete, vertical tension counterbalancing the vertical component of the diagonal compression strut is required in the studs near the high moment end of the opening where stress fields change directions.

At the stage near collapse, it can be further deduced that a diagonal tension crack

shown may be initiated from the local failure of the bearing zone in the bottom of the slab near the low moment end of the opening because only a small size of bearing area may be possible, as a result of the significant propagation of transverse cracks formed in the top of the slab towards the bottom of the slab. However, a more detailed evaluation of the bearing characteristics which would provide clarification of this type of slab failure is not a simple task if the effective slab width and the number of shear connectors participated need to be considered. It may be noted that the stud behaviour can not be clearly observed in tests. To study this, a solid slab beam with a very narrow slab width was included in the parallel experimental programme to examine the slab failure associated with failure of the bearing zone.

Again, from the slab crack pattern shown in Fig. 3.3(a), another important observation associated with the inclination of diagonal compressive stresses in solid slabs can be made: The inclined strut appearing in a test does not necessarily span between the studs within the opening length even though they were placed far enough apart to behave independently in the longitudinal direction. It is, instead, anticipated that diagonal stress fields, as shown, traverse several connectors along the opening length and even those beyond the opening length when there is a lower angle of inclination. Note that this pattern of stress fields may be possible in solid slabs because of the continuous and prismatic nature of the slab geometry, and several different geometrical arrangements of struts and ties are possible for the various stud configurations used for solid slabs. A possible diagonal compression field action for the slab considered herein is shown in Fig. 3.3(b). Several diagonal compressive struts linking the heads of studs and the bases of the nearest studs (or one stud further removed) are incorporated.

In a practical sense, however, the stud placement in solid slabs can be arranged to provide the most favorable configuration to perform truss action as well as to resist vertical shearing forces in an efficient manner.

3.2.1.2 Ribbed Slabs

Unlike solid slab beams, steel deck supported slabs (which are herein termed ribbed slabs), have physical characteristics which limit shear stud placement, and the thin cover slab thickness which is unfavorable in resisting vertical shear forces. Furthermore, features such as partial shear connection and the non-uniform cross section of the slab cause additional problems which are not met with in solid slabs.

The magnitude of forces that one shear connector should resist will be significantly increased when compared with those found in solid slabs at the same load level because of a relatively small number of shear connectors provided along the whole beam span. On the other hand, the horizontal shear and vertical tension capacity of an individual shear connector will be greatly reduced due to the non-uniform slab geometry. As a result, the pull-out failure that causes rib separation cracking was found to dominate in all ribbed slab beams^{10,12} tested at McGill University. The stud and opening configurations, and observed cracks in the slab for a typical test of the McGill beams¹⁰ are shown in Fig. 3.4

If a similar type of load carrying mechanism to that found in solid slabs is assumed to exist, the top compressive stresses in the cover slab near the high moment end of the opening are required to have some inclination to carry vertical shear forces and be anchored at the bottom part of the rib located near the low moment end. With diagonal cracking of the concrete, the studs near the high moment end of the opening must resist tensile forces in the vertical direction caused by diagonal compressive stresses while those near the low moment end provide bearing zones. However, because of insufficient vertical resistance of the studs associated with the cross sectional properties of the ribbed slab, the rib separation cracks are more likely at an earlier stage of loading.

A probable diagonal compression field action for the ribbed slab considered is shown in Fig. 3.4(b). In this, the lower corner regions of the ribs are considered as the bearing zones to anchor diagonal compressive stresses spreading from the heads of the

studs or the top compressive zones in the cover slab. The metal deck supporting the full width of the slab will be helpful in providing wide bearing zones in the narrow ribs, although the loads must be transferred through the thin deck to the weld at the base of the stud. All diagonal compression struts developed may curve, subjected to adequate associated tensile resistance of the concrete, due to the geometrical discontinuities of the slab.

Again, from the slab crack pattern through its thickness shown in Fig. 3.4(a), it can be considered that the rib separation crack appearing in the first rib beyond the high moment end of the opening prevented full development of inclined strut action, such as found in solid slabs. Near collapse, these separation cracks extend towards the load point. This rib separation, which results from the pull-out failure of studs, is not readily avoidable in configurations of ribbed slabs used in practice and this limits the potential strength of the slab. In relation to this, the vertical resistance of the studs for ribbed slabs needs to be enhanced to obtain truss action similar to that found in solid slabs, by preventing the premature failure relating to the pull-out failure of the studs. One possible detailing method to achieve this, in providing horizontal reinforcement welded to the heads of the studs over the opening, will be investigated in the experimental programme.

On the other hand, transverse cracks occurring in the top of the cover slab at the low moment end of the opening will be much more critical than those found in solid slabs due to the small cover slab thickness. Thus, once cracks form in the top of the cover slab, they may penetrate rapidly into the bottom of the slab, resulting in considerable separation of the slab. In this regard, Redwood and Wong¹⁰ assumed stress distributions based on a fully cracked slab section at the low moment end of the opening, but they could not incorporate the slab shear carrying capacity independently.

In these ribbed slab beams transverse cracks also appeared in the cover slab near the end supports^{10,12}. The truss concept implies that at concentrated reactions, the

load is transferred into the supports by fanning of compressive stresses. Therefore, anchoring several struts at the last rib near the support introduces larger horizontal and vertical forces into the studs in that region. As a result, with little compression in the slab near the support, the last rib location is particularly vulnerable to cracking on the top surface of the slab.

3.2.2 Truss Idealization

An idealized truss model capable of representing the slab and stud behaviour described above is shown in Fig 3.5. This model can be considered as a general case for various truss idealizations, and is proposed to apply to solid as well as ribbed slabs.

In order to simulate diagonal anchorage of the top compressive stresses, a strut runs horizontally near the high moment end of the opening and drops to the bottom of the slab near the low moment end of the opening (see Fig. 3.5(a)). Several inclined struts indicating vertical as well as horizontal dispersal of the connector forces at the bases and heads of the studs into the concrete slab are also included to represent complete tension action of the studs in the form of continuous stress fields.

In solid slabs, additional diagonal struts involving lower angles of inclination, such as shown in Fig. 3.3(b), may be necessary for the more realistic representation of the slab behaviour. However, due to the dependence of their magnitudes on the horizontal resistance of shear connection, the inclusion of those additional struts does not involve an increase in the shear carrying capacity of the concrete slab compared with that given by the proposed model. As a result, additional diagonal struts with a lower inclination are not considered. In addition, for the arrangement of the inclined struts in ribbed slabs, the curved diagonal stress fields are idealized as straight lines.

Now, considering a common type of stud configuration in the ribbed slab geometry in which two single studs are placed within the hole length, forces acting on the slab and steel beam can be described as shown in Fig. 3.5. From the force system shown, it is

noted that the slab at sections between AB and CD carries vertical shear, T_1, T_2 or T_3 , depending on vertical load carried by the corresponding shear connection, while in regions beyond those sections all of the vertical shear is assumed to be carried by the steel section alone. Further, in the region between sections AB and CD, the vertical interface forces that can explain "vertical shear transfer" from the concrete slab to the steel beam through the discrete shear connectors exist in the form of compressive or tensile forces. Maximum separation between the slab and the steel beam is observed near the high moment end of the hole, and so the vertical interface forces, δT_2 and γT_3 , are tensile, while those near the low moment end of the hole, αT_1 and βT_1 , are compressive due to the anchorage nature of the top compressive stresses. The factors α to γ define the portion of vertical forces in compression or tension that can be transferred to the steel section from the concrete slab, and all lie between 0 and 1.

Using notation q_i for horizontal load carried by each shear connector and assuming α and γ are equal to 1.0, vertical and horizontal force equilibrium at the corresponding stud locations yields the following expressions about the compression forces in the diagonal struts denoted C_i .

$$C_1 = \frac{T_1}{\sin\theta} = \frac{q_0}{\cos\theta} \quad (3-1)$$

$$C_2 = \frac{T_2}{\sin\theta} = \frac{T_1(1 + \beta)}{\sin\theta} = \frac{q_1}{\cos\theta} \quad (3-2)$$

$$C_3 = \frac{T_3}{\sin\theta} = \frac{T_2(1 - \delta)}{\sin\theta} = \frac{q_2}{\cos\theta} \quad (3-3)$$

In addition, assuming the uniform longitudinal spacing and single action of the studs, the inclination of diagonal struts can be written as

$$\tan\theta = \frac{H_s}{l_{s0}} \quad (3-4)$$

in which H_s is the finished stud length after welding, and l_{s0} is the longitudinal spacing of the studs.

Again, from Eqs.(3-1) to (3-3), vertical and horizontal loads carried by each shear connection can be expressed as follows.

$$T_1 = q_0 \tan \theta \quad (3-5)$$

$$T_2 = T_1(1 + \beta) = q_1 \tan \theta \quad (3-6)$$

$$T_3 = T_2(1 - \delta) = T_1(1 + \beta)(1 - \delta) = q_2 \tan \theta \quad (3-7)$$

and

$$q_1 = q_0(1 + \beta) \quad (3-8)$$

$$q_2 = q_0(1 + \beta)(1 - \delta) \quad (3-9)$$

Note that all equations given above, which define the slab and connector forces in the hole region, can be expressed with three independent variables, β , δ and one of the horizontal loads carried by a shear connector, say q_0 . Therefore, once these three variables are known, a complete set of the slab and connector forces can be obtained by linking the failure criterion of the studs under combined vertical and horizontal loading. Then, with these forces, the shearing force carried by the steel section alone above the opening can be determined following the same procedure used in the previous analysis (Chapter 2).

Now, the values of β and δ are determined by means of varying from 0 to 1 with a small increment (0.1). Then, the value of q_0 corresponding to the situation in which at least, one of the vertical members reaches at its ultimate stage under combined horizontal and vertical loading can be obtained using an iterative calculation procedure with each pair of β and δ values. In doing so, a number of solutions corresponding to various combinations of β and δ are found, however the solution that provides the highest strength will be the appropriate one since the lower bound theory is adopted.

Using the procedure described above, analysis was made for all previous test results and after investigation of the analysis results, it was found that the maximum shear strength of the composite tee section above the hole ($V_{t1} = V_c + V_{st}$) was always obtained when all the connectors considered are equally loaded in the horizontal direction, and the values of β and δ are equal to 0 (see Fig. 3.6). Note that the physical significance of this situation is that "vertical shear transfer" from slab to steel occurs at the nearest location of shear connection to the ends of the hole, not near the centerline of the hole as can be seen in Fig. 3.6(b).

With these added conditions on β, δ and q_1 , a closed form of solution defining the shear carrying capacity of the top composite section can be formulated. In the following, three solutions corresponding to the three practical configurations of the studs transferring vertical compression to the steel section (which will be termed "bearing studs or connectors" hereafter) are presented. Note that these are particular cases of solutions that can be obtained from the truss model being considered

For completeness of the proposed truss concept, truss action across the width of the slab can also be predicted as shown in Figs. 3.5 and 3.6. Note that dispersal of the compression forces at the stud locations to the whole width of the concrete slab generates transverse tension forces in the slab, which may result in longitudinal cracks. In ribbed slabs, steel deck may provide the associated transverse tensile reaction. The inclination of those struts is herein assumed to be $\theta' = \tan^{-1} 1.0$.

3.2.3 Formulation of Member Capacity

With the use of a truss analogy, the slab behaviour observed in tests is clarified, and the corresponding role of shear connectors in resisting vertical tensile (or compressive) forces as well as in transferring those from slab to steel is clearly identified. Such behavioural aspects of the slab and shear connection can be taken into account in an alternative method of prediction of the ultimate strength and even the serviceability

performance in the opening region

For the complete treatment of the truss models given herein, estimation of the actual dimensions of compression struts, their corresponding anchorages and bearing zones, and failure conditions would be necessary. But this is not a simple task because of the impossibility of observation and difficulties in measurement in the interior of the slab. In the following derivation, it is assumed that failure of inclined struts and their corresponding bearing zones does not occur prior to failure of shear connectors. This approach appears to yield safe results when compared with test observations, but full justification is not possible without extensive further study of the interaction of connectors and concrete slabs.

Truss models incorporating three typical configurations of the studs along the opening in either solid or ribbed slabs, and the well-established stress distributions in the steel sections under high shear are shown in Figs. 3.7, 3.9 and 3.10. Three cases of stud configurations which were classified according to the locations of bearing connectors relative to the low moment end of the hole are: i) bearing studs placed exactly at the low moment end of the hole, ii) beyond the low moment end of the hole, and iii) no studs within the hole length. Three solutions corresponding to these stud configuration classifications will now be derived for the determination of the point 1 on the interaction diagram. For other stud configurations, some modifications can be incorporated without changing the fundamental approach considered here.

3.2.3.1 Bearing Studs at L.M.-Solution I

The configuration of the studs considered is shown in Fig. 3.7. By placing studs exactly or sufficiently close to the low moment end of the hole, the top compressive strut which runs horizontally near the high moment end of the hole will be anchored at the stud location corresponding to the low moment end of the hole. It is therefore considered that vertical shear transfer from slab to steel occurs at the low moment end of the hole and at the nearest position of the studs from the high moment end. In this

way, beyond the region where vertical shear transfer occurs, all of the shear forces are assumed to be carried by the steel section alone.

From the force system shown in Fig. 3.7(a), normal force equilibrium at each of the four yield locations gives the following, when the number of vertical members in compression or tension action within the hole length is N_v and the number of shear connectors consisting of each of those vertical members is n_t .

$$k_1 = 0.5(\beta_t - \beta_b - N_v \epsilon_t) + k_3 \quad (3-10)$$

$$k_2 = 0.5(\beta_b + \beta_t + \epsilon_t + 2) - k_3 \quad (3-11)$$

$$k_4 = \beta_b - k_3 + 1 \quad (3-12)$$

in which $\beta_t = P_{wt}/P_{yf}$, $\beta_b = P_{wb}/P_{yf}$ and $\epsilon_t = n_t q/P_{yf}$.

Expressing the distance from the high moment end of the hole to the nearest studs as l_{s1} , moments at the four corner sections above and below the hole

$$Q_1 \bar{y}_1 = [N_v - 1]n_t q [H_s + s_t] + n_t q [l_{s1} \tan \theta + s_t] + P_{yf} [-0.5s_t \beta_t + 2k_1 s_t - s_t] \quad (3-13)$$

$$Q_2 \bar{y}_2 = P_{yf} [0.5s_t \beta_t - 2k_2 s_t + s_t] \quad (3-14)$$

$$Q_3 \bar{y}_3 = P_{yf} [-0.5s_b \beta_b + 2k_3 s_b - s_b] \quad (3-15)$$

$$Q_4 \bar{y}_4 = P_{yf} [0.5s_b \beta_b - 2k_4 s_b + s_b] \quad (3-16)$$

From the truss analogy, the shearing force carried by the concrete slab V_c is obtained as

$$V_c = n_t T = n_t q \tan \theta = n_t q [(N_v - 1)H_s + l_{s1} \tan \theta] / 2a \quad (3-17)$$

where $\theta = \tan^{-1}(H_s/l_{s0})$

Now considering the studs under combined horizontal and vertical forces, a failure criterion has been proposed²² as:

$$\left(\frac{q}{q_r}\right)^{1.67} + \left(\frac{T}{T_r}\right)^{1.67} = 1 \quad (3-18)$$

in which q_r and T_r are respectively the horizontal and vertical resistances of one shear connector. Also, the pull-out capacity of a shear connector, which gives its vertical resistance, can be expressed as follows, based on a conical failure surface of concrete (see Fig. 3.8).

$$T_r = \lambda \sqrt{f'_c} A_c \quad (\lambda = 0.33 \quad f'_c \text{ in MPa}) \quad (3-19)$$

where A_c is the pull-out cone surface area corresponding to one shear connector²³.

Note that when studs are placed closely together, the full tension cones of the studs cannot be developed due to the intersection of the pull-out cone surfaces, thus A_c given above has to be estimated from the partial tension cone action.

Equilibrium for the top composite and bottom steel section above and below the opening

$$\begin{aligned} 2a[V_c + V_{st}] &= Q_1 \bar{y}_1 - Q_2 \bar{y}_2 \\ &= n_t q [(N_v - 1)H_s + l_{s1} \tan \theta] + n_t q s_t + P_{wt} s_t \end{aligned} \quad (3-20)$$

$$\begin{aligned} 2aV_{sb} &= Q_3 \bar{y}_3 - Q_4 \bar{y}_4 \\ &= P_{wb} s_t \end{aligned} \quad (3-21)$$

and for the composite section at the opening centerline,

$$M = 0.5H[Q_1 + Q_2 + Q_3 + Q_4] + 0.5[Q_1 \bar{y}_1 + Q_2 \bar{y}_2 + Q_3 \bar{y}_3 + Q_4 \bar{y}_4] \quad (3-22)$$

Substitution Eq (3-17) into (3-20) leads to

$$\frac{V_{st}}{V_{pt}} = \frac{\mu\gamma + \sqrt{3\gamma^2 - 3\mu^2 + 9}}{(3 + \gamma^2)} \quad (3-23)$$

in which $\gamma = 2a/s_t$ and $\mu = n_tq/V_{pt}$.

It is of interest to note that Eq. (3-23) has identical form to that given in the previous analysis except for the new definition of μ .

Also, Eq. (3-21) gives

$$V_{sb} = V_{pb} \sqrt{\frac{\alpha_b}{1 + \alpha_b}} \quad (3-24)$$

where $\alpha_b = 3s_b^2/4a^2$.

The total shearing force carried by concrete and steel tees corresponding to point 1 on the interaction diagram can be written

$$V_1 = V_{t1} + V_{b1} = V_c + V_{st} + V_{sb} \quad (3-25)$$

and the maximum moment consistent with this shearing force corresponds to $k_3 = 1$ and is given by Eq. (3-22) as

$$M_1 = dP_{yf}(1 - \beta_b) + 0.5n_tq[(N_v - 1)H_s + l_{s1}\tan\theta - s_t] \quad (3-26)$$

Further, from Eq. (3-23), it is known that V_{st} has a maximum value when μ is equal to γ . With this, the upper bound for the horizontal stud forces corresponding to a vertical member can be formulated as follows.

$$n_tq \leq \frac{2a}{s_t} V_{pt} \quad (3-27)$$

$$V_c \leq \frac{2a}{s_t} V_{pt}\tan\theta \quad (3-28)$$

Also, note that when the studs transferring vertical tension to the steel section are located exactly at the high moment end of the hole, they are not included in estimating N_v and l_{s1} should be considered to be equal to l_{s0} .

3.2.3.2 Bearing Studs Beyond L.M.-Solution II

The stud configuration considered applies when bearing studs are placed away from the low moment end of the hole as shown in Fig. 3.9. The top compressive strut near the high moment end of the hole is assumed to be anchored diagonally at the stud location beyond the low moment end of the hole. Thus, the vertical force transfer from slab to steel occurs beyond the hole length

In treating anchorage of the inclined strut for this type of stud configurations, another possible anchorage may be considered, i.e. at the stud location within the hole length near the low moment end of the hole. If the anchorage of the inclined strut at the position of the studs within the hole length is assumed, the steel tee in a limited region between the low moment end of the hole and the location of the anchorage must resist all of the vertical shear forces alone. As a result, the shear capacity of the top steel tee web (V_{pt}) will limit the maximum shear capacity that can be carried by the composite section above the hole (V_{t1}). However, it is noted that the case with anchorage beyond the low moment end of the hole always provides the higher shear strength in the top tee section compared with that given by the case with anchorage within the hole length. Therefore, further consideration of the latter case is not given.

Following the same procedure used in Solution I, the shear carrying capacity of the top composite section, V_{t1} ($= V_c + V_{st}$), and the maximum moment consistent with this shearing force, M_1 can be written as follows, while all others are identical to the previous Solution I.

$$V_c = n_1 T = n_1 q \tan \theta = n_1 q [N_v H_s + (l_{s1} + l_{s2} - l_{s0}) \tan \theta] / 2a \quad (3-29)$$

in which l_{s0} is the longitudinal spacing of the studs, and l_{s1} and l_{s2} are the distances from the nearest studs to the high and low moment ends of the hole respectively.

Also,

$$V_{st} = V_{pt} \sqrt{\frac{\alpha_t}{1 + \alpha_t}} \quad (3-30)$$

where $\alpha_t = 3s_t^2/4a^2$.

Also,

$$M_1 = dP_{yf}(1 - \beta_b) + 0.5n_tq[(N_v + 1)H_s + (l_{s1} - l_{s2})\tan\theta] \quad (3-31)$$

3.2.3.3 No Studs Within Hole Length -Solution III

The stud configuration considered has no studs within the hole length but some studs placed some distance beyond the ends of the hole, thus vertical force transfer occurs at these two stud locations (see Fig. 3.10).

In applying the truss concept to this type of stud configuration, a fundamental question may arise whether or not the inclined strut action described can be developed with that flat inclination, by crossing the length of the hole. Obviously, this will be dependent on the positions of the studs relative to the ends of the hole. As a simple rule, it is herein assumed that the truss action described above does not exist when studs spaced more than two ribs apart in ribbed slabs and more than 1.5 times the opening length in solid slabs. Actually, the restriction given to the solid slabs is less meaningful because there is no limitation in the stud placement. With respect to this, the possibility of truss action involving no studs within the hole length and with placement one rib distance away will be investigated experimentally.

In the following, using the same procedure used in Solutions I or II, the shear carrying capacity of the top composite section, V_{t1} ($= V_c + V_{st}$), and the maximum moment consistent with this shearing force, M_1 are given. This solution can be considered

as a particular case of Solution II (N_v, l_{s1} and $l_{s2} = 0$).

$$V_c = n_t T = n_t q \tan \theta \quad (3-32)$$

$$V_{st} = V_{pt} \sqrt{\frac{\alpha_t}{1 + \alpha_t}} \quad (3-33)$$

where $\alpha_t = 3s_t^2/4a^2$.

$$M_1 = dP_{yf}(1 - \beta_b) + 0.5n_t q H_s \quad (3-34)$$

To find the load combination on the studs that satisfies the failure criterion Eq. (3-18) as well as provides the maximum shear and moment capacities (V_1 and M_1), the solutions given above require iterative calculations with a chosen value of q . As a trial value for q , 70% ~ 80% of q_r is suggested. Example calculations demonstrating this as well as the overall calculation procedure for solid and ribbed slabs are given in Appendix A.

Further, investigating the three solutions described above and comparing with the previous analysis, the following observations can be made

- i) Of the three configurations of the studs in the hole region, the stud configuration corresponding to Solution I provides the highest shear strength when the identical number of shear connectors are assumed within the length of the hole. Therefore, it can be considered that by placing studs exactly at the low moment end of the hole where the anchorage of diagonal stress fields is expected, the most efficient shear carrying mechanism in composite beams at web holes is achieved.
- ii) From Eqs. (3-27) and (3-28), it is of interest to note that the shearing force that can be carried by the concrete slab is dependent upon the geometry of the top steel tee ($2a/s_t$) as well as the inclination of diagonal struts ($\tan \theta$), if no failure of the studs is assumed (see Fig. 3.11).
- iii) Concerning the top and bottom compression forces in the slab, the proposed truss analogies indicate that these forces are calculated based on a limited number of

shear connectors in the hole region, while in the previous analysis (Chapter 2) these are determined from the number of connectors between the corresponding opening edges and the nearest point of zero moment as given in Eqs (2-1) and (2-2). Following from this, some important aspects related to the slab forces for composite beams at web holes can be pointed out. The established approach adopted in Eqs. (2-1) and (2-2) is originally derived from the bending theory for the treatment of the sagging moment region. However, in hole regions where the secondary hogging moment is normally created due to a high shearing force, transverse cracks in the top of the slab occur at the early stage of load. As shear is increased, these cracks will gradually widen and will spread into the bottom part of the slab, finally leading to full separation of the slab (as might be the case in ribbed slabs). Therefore, this situation can not be treated in the same way to that used in the sagging moment region. The degree of transverse cracks appeared in the top of the slab will have significant influence on the transference of the horizontal connector forces from low to high moment regions through those cracks. In this regard, the truss models proposed involve only studs placed near the opening.

The full comparison of results with those of previous tests are also given in Chapter 4

3.3 Serviceability

While considerable attention has been given to prediction of the ultimate strength of composite beams with web openings, much less has been given to the prediction of serviceability limits. Test results described in Fig. 3.12 demonstrate that at loads of 60% of the ultimate test load, local deflections at the opening significantly exceed usual values of deflection limits ($2a/300$) in most ribbed and some solid slab beams. Again, the limited evidence shows that cracking near the opening and the support can

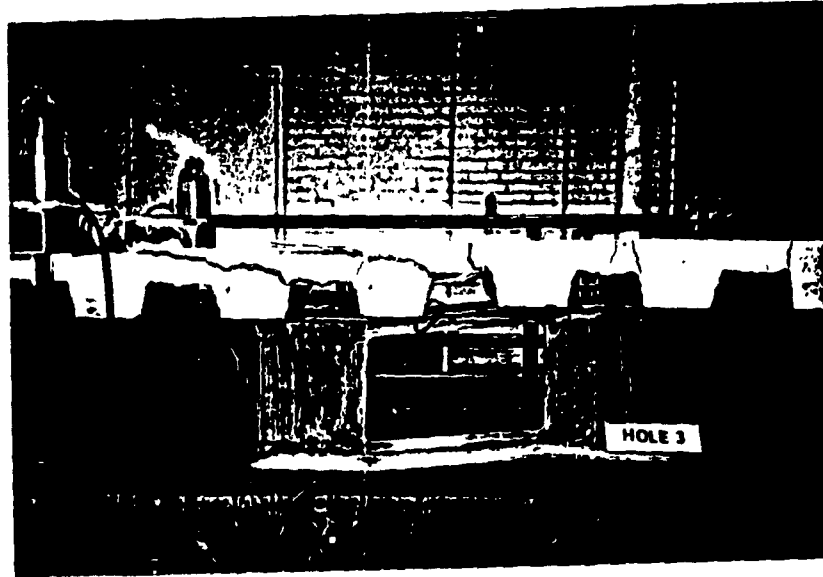
be expected in early stages of loading in some cases. Hence the need to study the beam behaviour at service load levels is evident.

To this end, although several approaches¹⁵ ignoring the flexibility of shear connection and slab cracking can be used to estimate overall beam deflections with acceptable accuracy, it should be noted that for an accurate evaluation of the relative deflections between hole ends and stress distributions in the opening region, incomplete interaction and concrete slab cracking through the whole beam span are of critical importance.

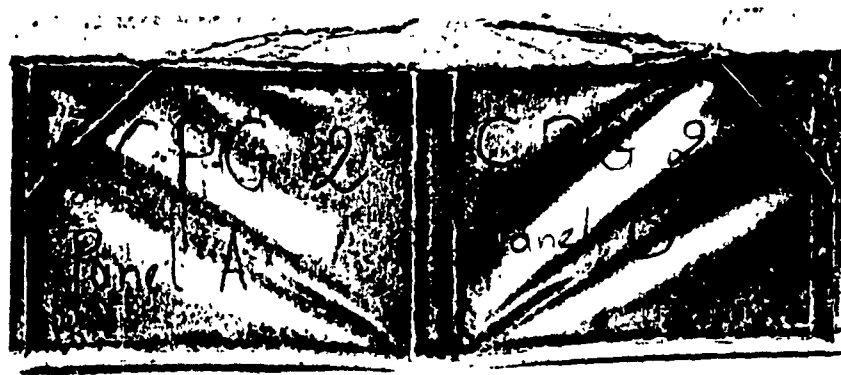
As in the ultimate strength analysis, the slab behaviour observed around the holes and possibly near the supports in ribbed slabs can be simulated in the analytical models based on the truss concept. Figure 3 13 shows frame models to evaluate the service performance of composite beams with web holes. In these, the slab and the steel beam are represented by beam elements at their own centerlines and the shear connectors by spring elements with horizontal (k_h) and vertical (k_v) stiffnesses at their bases. Eccentric zones between the slab mid-depth axis and the studs, and the studs and the steel elements are also modelled by using rigid offset connections. Model I is proposed for the analysis at 30 % of the ultimate load, while Model II, which is consistent with the truss concept explained previously, is implemented to simulate transverse cracks in the region of the web opening at 60 % of the ultimate load level. Elastic plane frame stiffness analysis²⁴ provides the solution for these models.

In arranging compression struts, a single inclined strut which has half the slab width and thickness, and spans between the top and bottom portion of the slab along the opening length is suggested without identifying the details of the truss connectivity.

More details about horizontal and vertical stiffness of the studs and the full comparison of these models with previous tests based on deflections at the beam midspan and relative deflections at the ends of the hole are given in Appendix B.

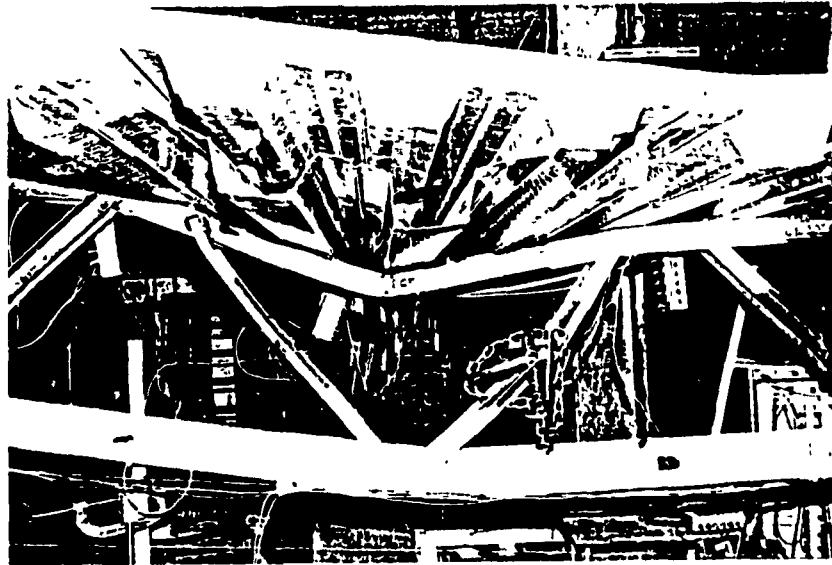


(a) Beam with Hole

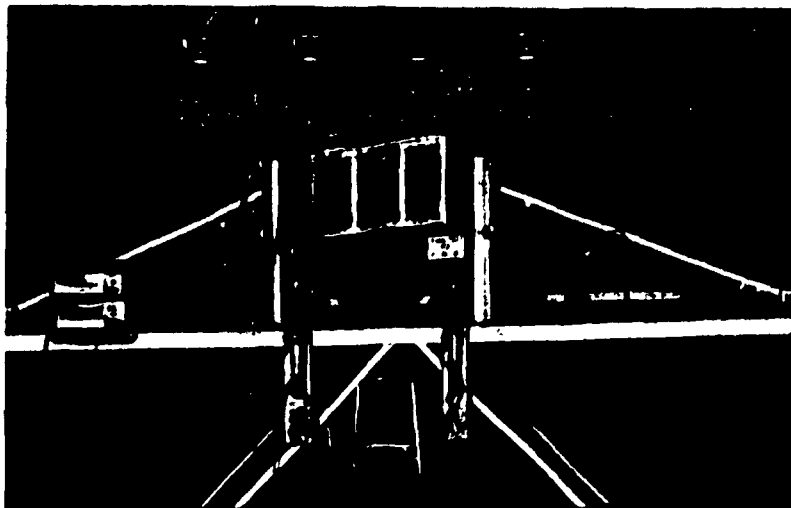


(b) Thin Webbed Girder²

Figure 3.1 Possible Truss Action in the Slabs of Composite Floor Members.

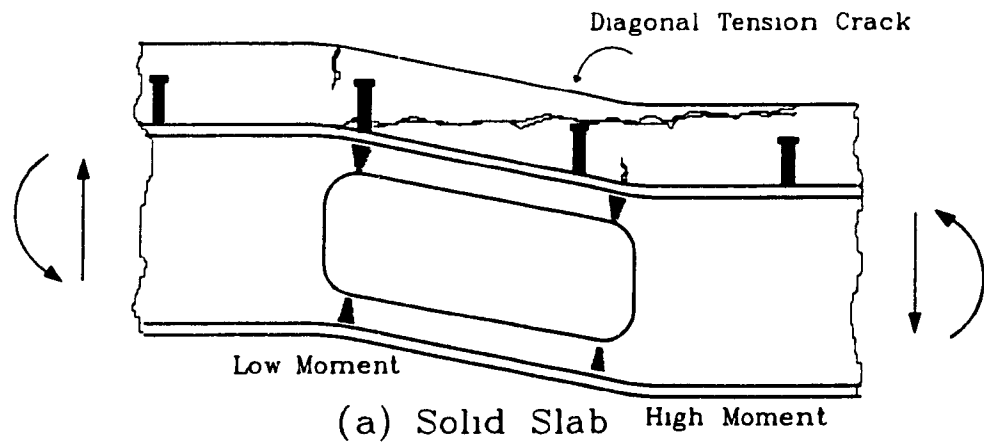


(a) Composite Truss²⁰

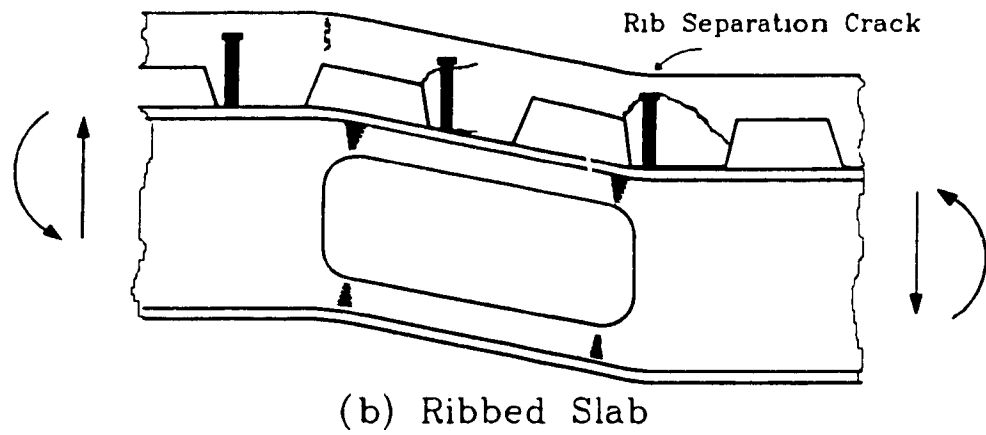


(b) Link Beam of Eccentrically Braced Frames²¹

Figure 3.1 (Cont'd) Possible Truss Action in the Slabs of Composite Floor Members.

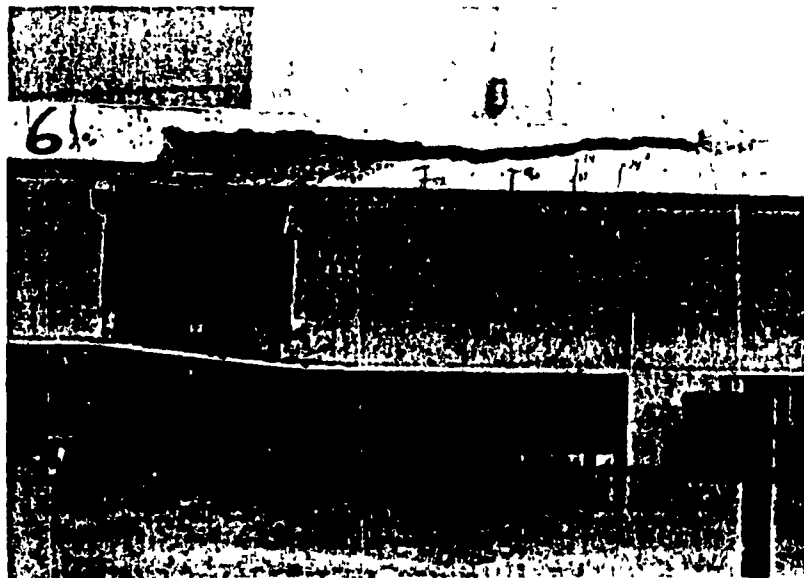


(a) Solid Slab

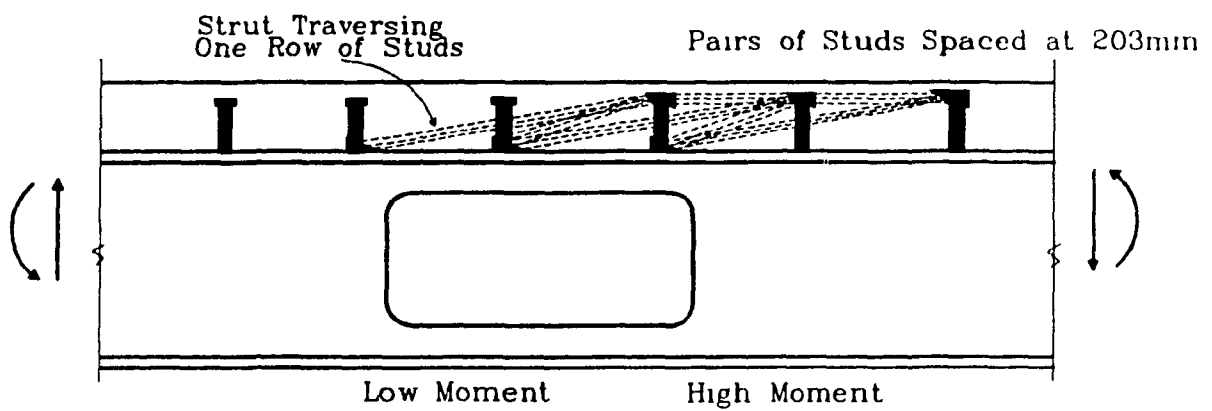


(b) Ribbed Slab

Figure 3.2 Typical Slab Failures at Web Holes.

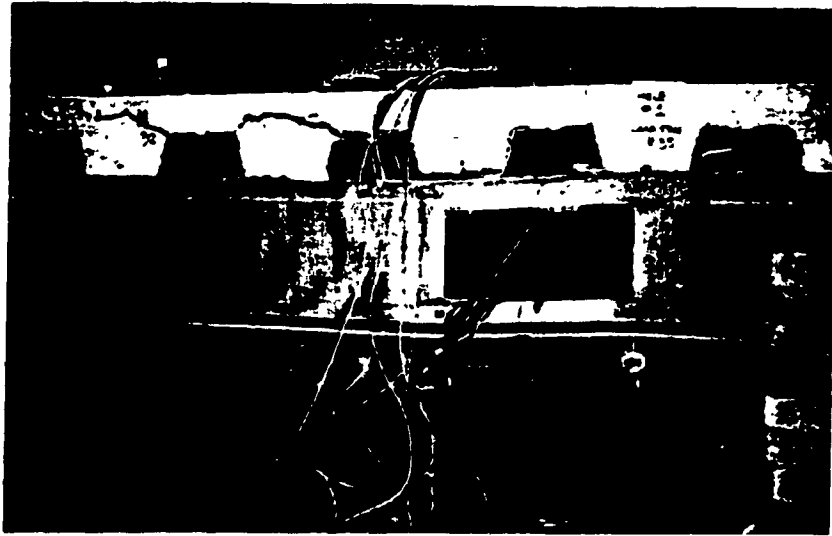


(a) Diagonal Tension Type of Slab Failure

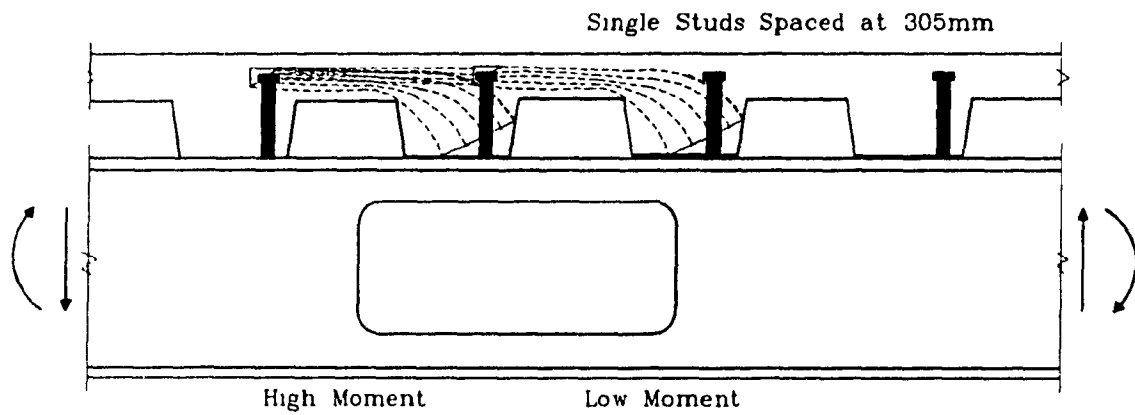


(b) One Possible Compression Field Action

Figure 3.3 A Solid Slab Test at the University of Kansas⁷.

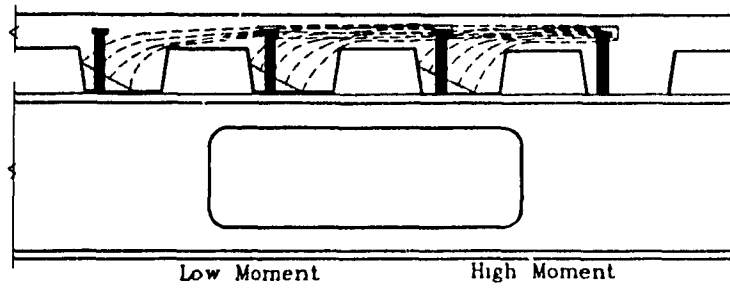


(a) Rib Separation Type of Slab Failure

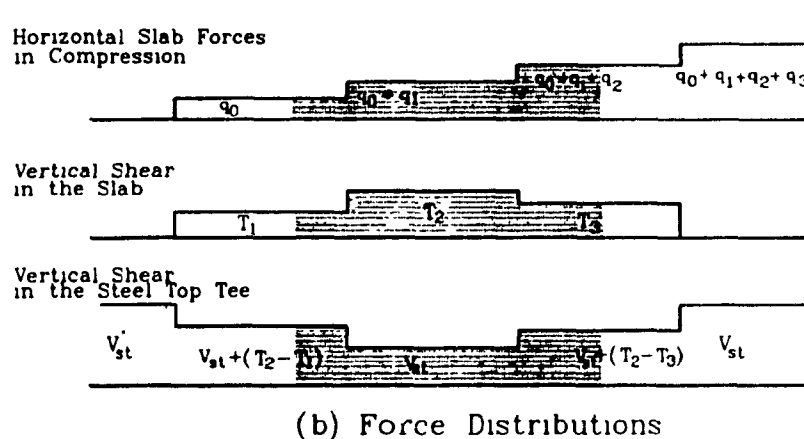


(b) One Possible Compression Field Action

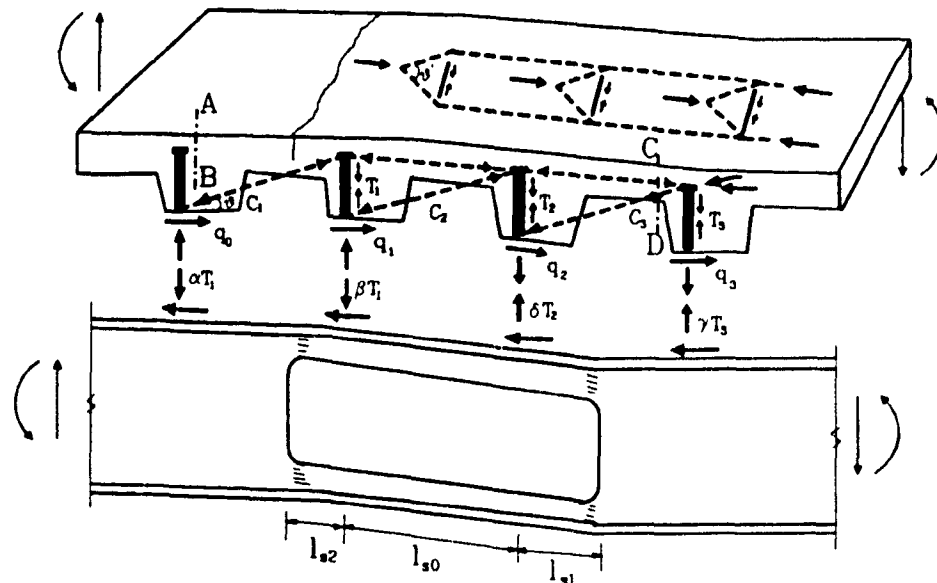
Figure 3.4 A Ribbed Slab Test at McGill University¹⁰.



(a) Stress Fields

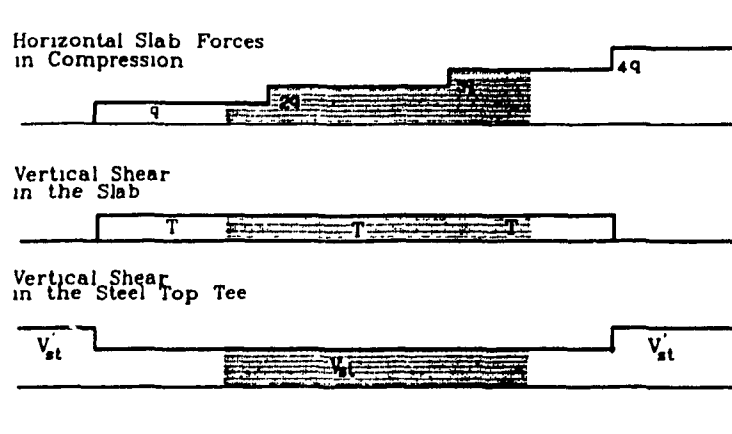


(b) Force Distributions

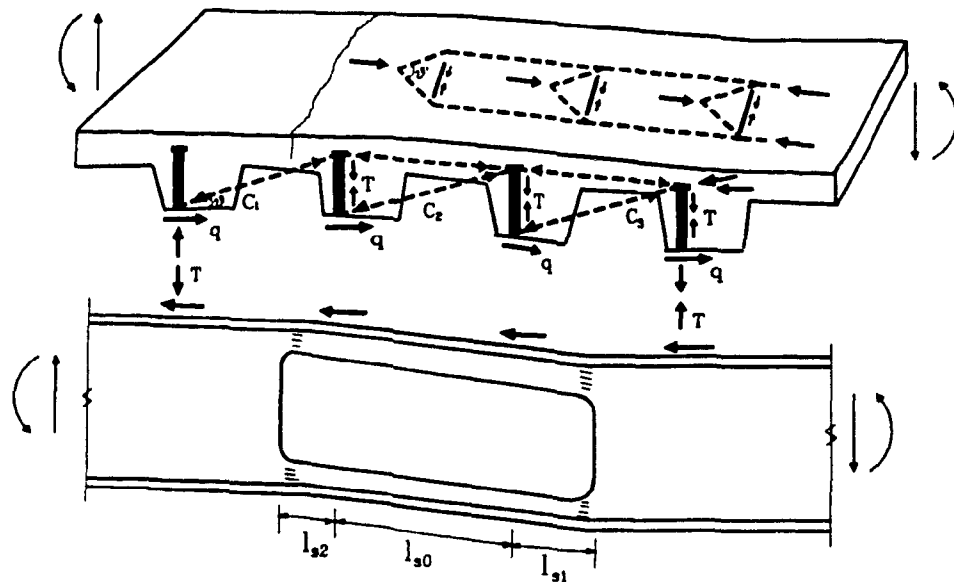


(c) Truss Model

Figure 3.5 Truss Idealization for the Slab in a Composite Beam at a Web Hole.



(a) Force Distributions



(b) Truss Model

Figure 3.6 Truss Model Providing the Maximum Shear Capacity in the Top Composite Section ($\beta \& \delta = 0$, and $q_1 = q$).

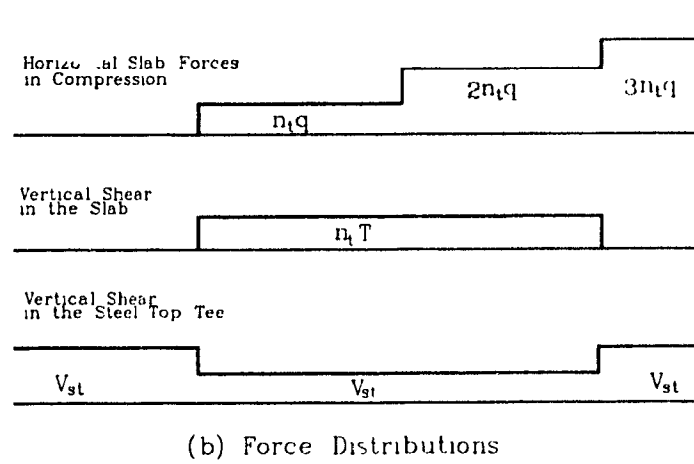
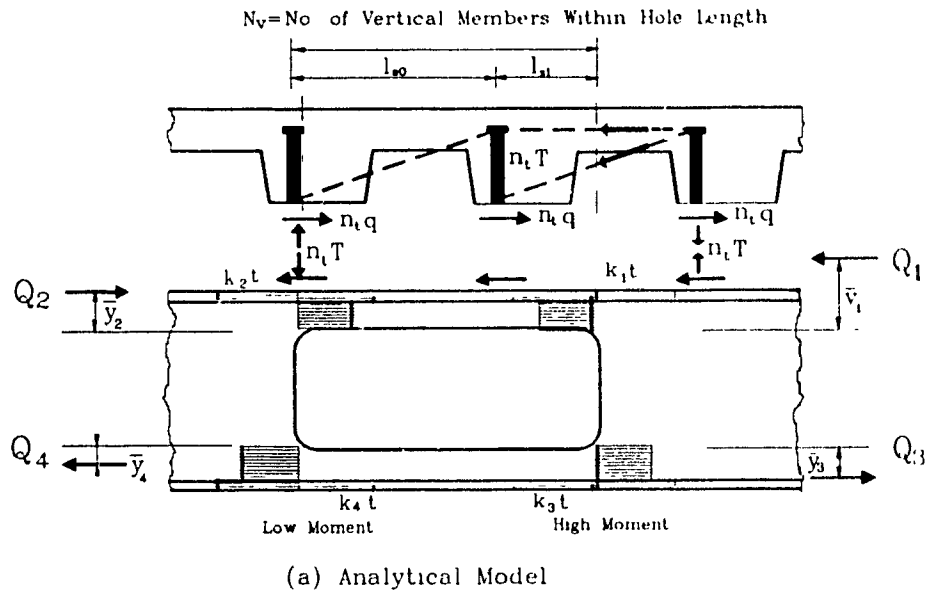
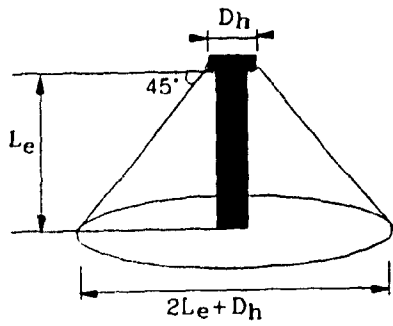
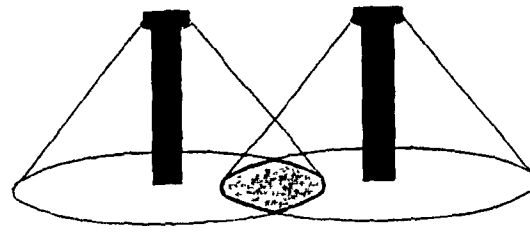


Figure 3.7 Bearing Studs at the Low Moment end of the Hole.



(a) Full Tension Cone



(b) Reduction of Tension Cone

Figure 3.8 Pull-out Cones of Stud Shear Connection

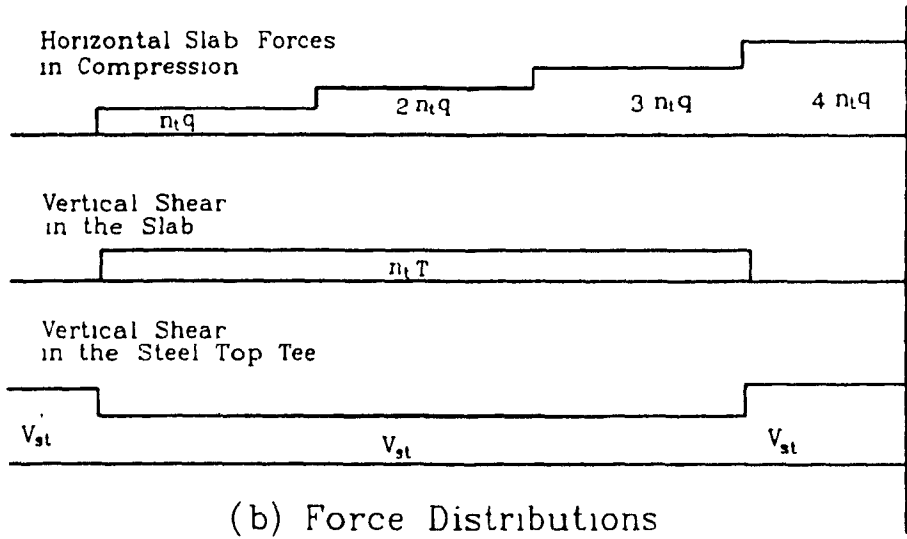
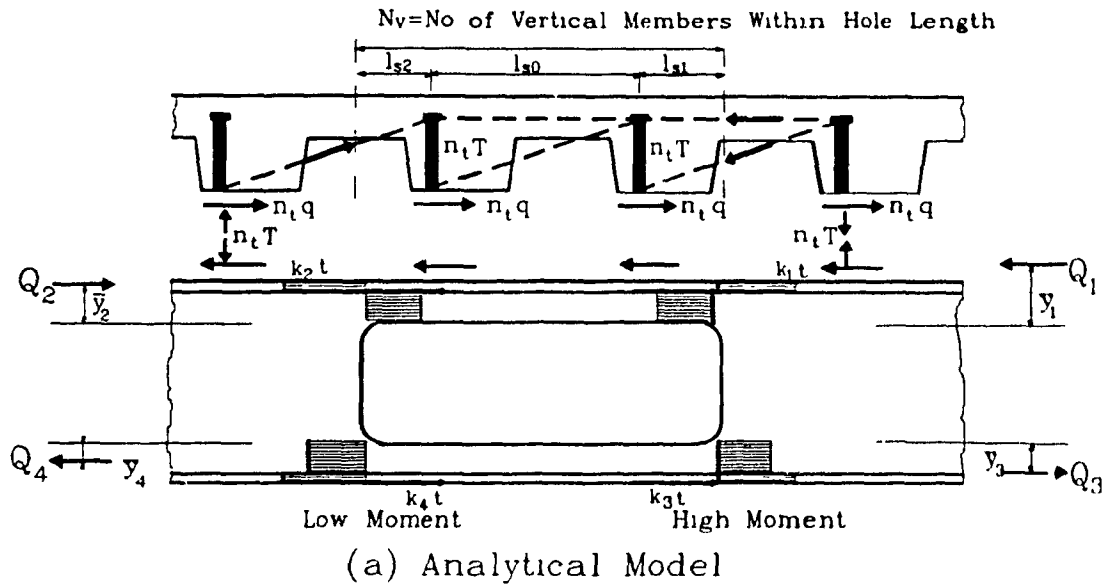


Figure 3.9 Bearing Studs Beyond the Low Moment end of the Hole

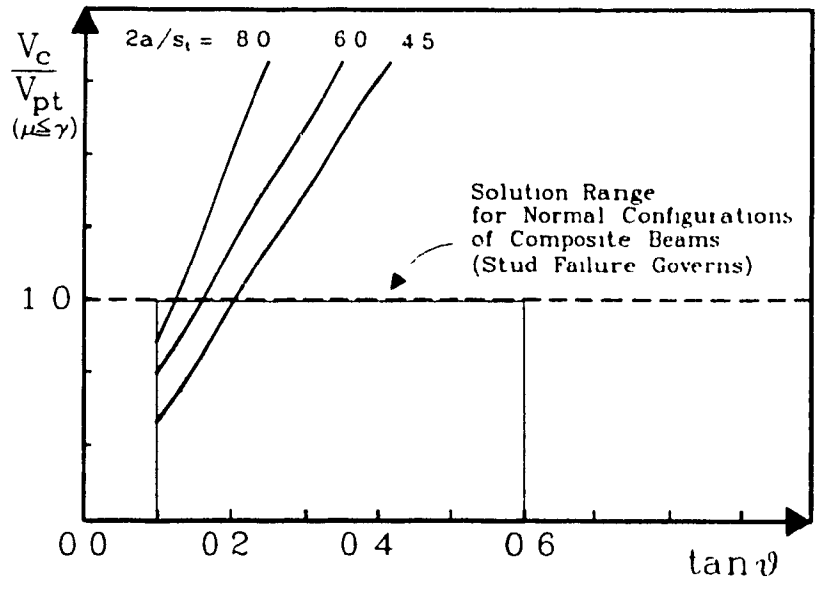


Figure 3.11 Graphical Representation for the Slab Shear Capacity

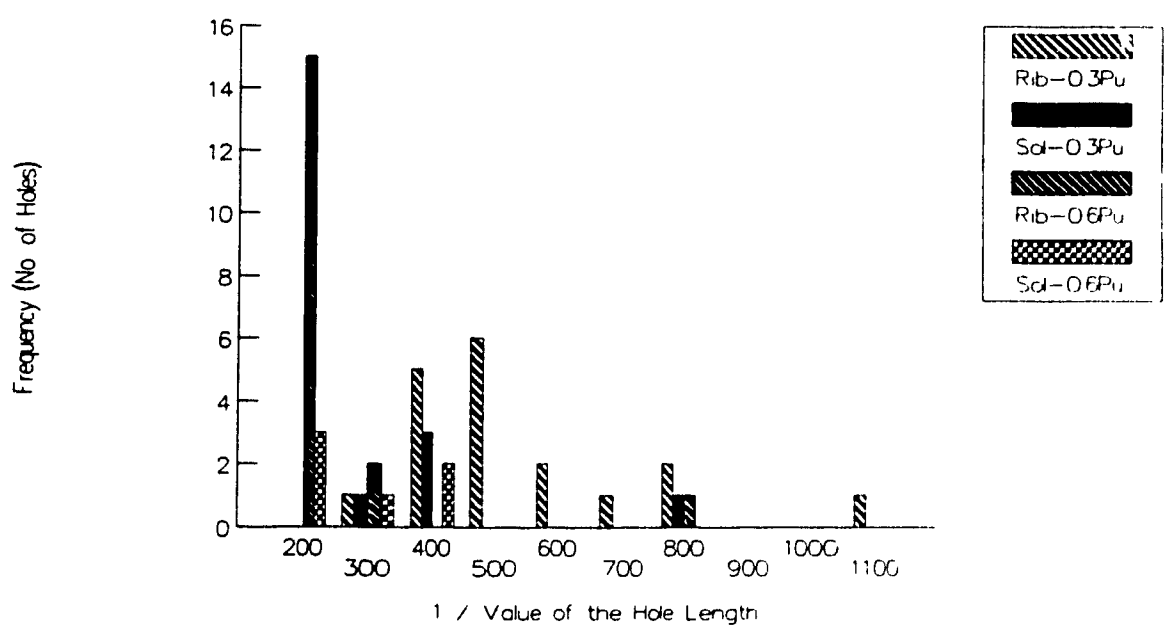


Figure 3.12 Measured Deflections Between Hole Ends

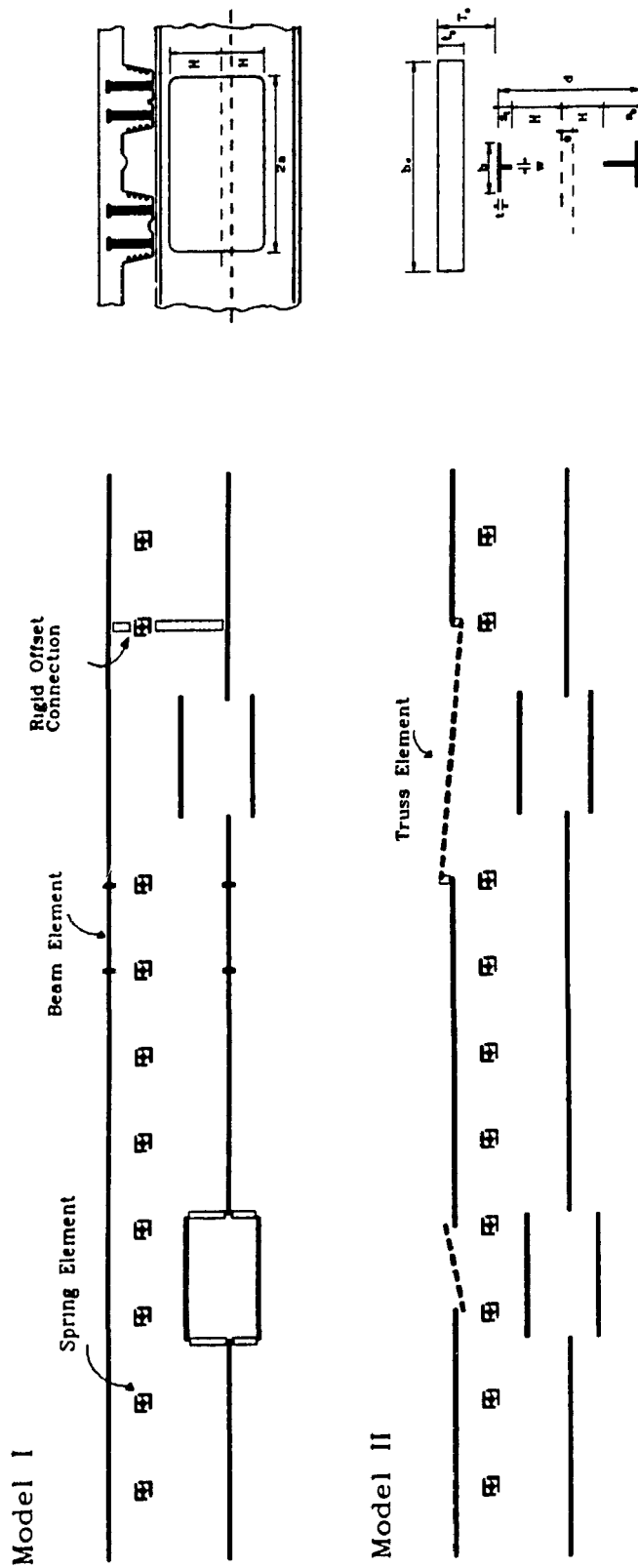


Figure 3.13 Analytical Models for Serviceability Analysis.

CHAPTER 4

COMPARISON WITH PREVIOUS TESTS

4.1 Introduction

The two theories described in the preceding chapters for the estimation of the ultimate strength of composite beams at web holes will now be evaluated by comparison with test results collated from many sources.

A total of thirty five tests form a database which includes eleven beams with solid slabs reported by Granade (1968), Clawson and Darwin (1982), and Cho (1982), and twenty four beams with ribbed slabs reported by Redwood and Wong (1982), Redwood and Poubouras (1983), and Donahey and Darwin (1988)

Material and cross sectional properties of all these beams, and the corresponding horizontal resistance of shear connectors are summarized in Appendix C. Note that the values of connector resistance given for all such beams except those tested at McGill University were estimated from the analytical procedure given in the AISC specifications²⁵. This procedure also incorporates reduction factors for ribbed slabs. In view of the large dependence of the beam strength prediction on shear connector resistance particularly in ribbed slab beams, accurate information about shear connector resistance is desirable if a complete evaluation of the proposed theories is to be achieved.

4.2 Simplified Slab Shear Model

The theory described in Chapter 2 is herein termed a "simplified slab shear model" since the way of considering the slab shear contribution is not general for all beam geometries, resulting from the fact that all vertical shear is firstly assigned to the steel beam, and then the remainder to the concrete slab. It is also noted that in defining shear resistance of the concrete slab, this theory employs a simple formula such as Eq (2-29) which is based on a lower bound theory, rather than on a physical model.

Relevant theoretical values that define the interaction diagrams, such as that shown in Fig 4 1, are summarized in Table 4.1. Note that in the diagram shown, all values are non-dimensionalized by dividing moment by M_0 the pure bending strength of the composite beam assuming full shear connection and an unperforated web, and the shearing force by V_0 , the pure shear capacity of the unperforated steel beam web.

A comparison of actual and predicted failure loads is also given in Table 4.2 and in Table 4 3 a number of parameters are given which identify some features of solutions for the various beams. Since the solution is significantly dependent upon shear connector resistance, Table 4 4 includes all limiting values of connector resistance for the various conditions listed in Table 2 1. Of all the values listed, the smallest will determine the solution category and the corresponding ultimate strength.

Agreement between test and predicted loads for solid and ribbed slab beams is generally satisfactory, as can be seen in Table 4.2. The parameters listed in Table 4.3 also indicate that in some cases a significant portion of the shearing force is carried by the concrete slab, particularly in solid slab beams. This is as much as 1.6 times the pure shear capacity of the steel tee web (CH-1). The ratio T_0/C_0 varies from 0.23 to 1.0 in solid slab beams and from 0.35 to 1.54 in ribbed slab beams, thus representing a wide range of practical configurations.

From Table 4.4, it is of interest to note that in nineteen beams out of thirty five, the solution was governed by the connector resistance q_c that ensures stress reversals

within the steel flange thicknesses, in the sense of satisfying equilibrium of the assumed stress distributions. Note that the connector force determined in this way is only a small portion of its ultimate capacity, particularly when a high number of shear connectors are provided between the low moment end of the opening and the support, such as the case for most solid slabs, and in the ribbed slab tests¹⁵ recently carried out at the University of Kansas. These unrealistic situations also occur in solid slab beams when the slab forces are limited by the yield capacity of one steel flange due to yielding of the steel tee in pure shear, as is the case in recent analysis given by Darwin and Donahey¹⁶. In view of this, it is difficult to see how the ultimate strength of the slab and the associated failure of the beam will take place with such small connector forces. In ribbed slab beams, in particular, most observed slab failure was related to stud failure since tension cone failure occurred.

4.3 Truss Model

Unlike the simplified slab shear model, the truss model described in Chapter 3 is capable of estimating the shearing force carried by the concrete slab independently for all various beam geometries. However, in applying this to some stud configurations of the previous tests which did not conform exactly to the stud configurations defined in the truss analogy, some difficulties arise in distinguishing the corresponding solution category which will be determined from the relative position of bearing studs to the low moment end of the opening.

For these, all possible solutions are applied in the first place, and then the solution that provides the highest strength is selected for the comparison with the strength given in tests. In a practical sense, however, the difficulties mentioned above can be resolved by means of placing studs exactly at the low moment end of the hole where diagonal stress fields have to be anchored, such that a most favourable way of performing truss action as well as carrying vertical shearing forces can be obtained.

Detailed information about the configuration of the studs in the opening region was not usually given in most previous tests, and thus estimation from drawings was necessary. For some ribbed slab tests carried out by Donahey and Darwin¹⁵, this information was obtained from a private communication²⁶.

In Table 4.5, all predicted shearing forces carried by the concrete slab and the top and bottom steel tees are summarized and compared with those predicted by the simplified slab shear model. Inclinations of diagonal struts and solution categories used are also given. Comparisons between measured and predicted failure loads are also shown in Table 4.6. Table 4.7 includes horizontal and vertical resistances, and loads of an individual shear connector that provide the ultimate beam resistances, and the relative ratios indicating the magnitudes of the horizontal compression forces in the slab at the high moment end of the hole according to the two theories.

From Table 4.5, it is noted that the truss model predicts that the shearing forces in the top tees are almost equally shared by the concrete slab and the steel section in solid and ribbed slab beams. All solid slabs, and most of the ribbed slabs tested at McGill University^{10,12} fall into the solution category I, while most of the ribbed slabs tested at the University of Kansas¹⁵ fall into the solution category II. In relation to this, an important aspect can be pointed out for the ribbed slabs having the solution category II, which were tested at the University of Kansas. In those tests, the predicted shear strength of the top composite section above the hole ($V_c + V_{st}$) is much less than the pure shear capacity of the steel tee section alone (V_{pt}), even though high degrees of shear connections were provided along the whole beam span as well as within the length of the hole (usually 4 studs). This may result from the inefficient arrangements of the studs along the hole length in which bearing studs were placed beyond the low moment end of the hole (see Fig. 3.9). In this regard, it is considered that for these tests it was not possible to obtain the full increased strength corresponding to the degree of shear connection provided.

While predictions given by the truss model are generally satisfactory as indicated in Table 4.6, some conservatism is inherent particularly in solid slab beams. Note that the conservative results associated with the ribbed slabs, D-4A and 4B are expected from the ignorance of the puddle welds used over the openings in place of shear connectors.

Concerning high conservatism associated with solid slabs, the following can be considered as the major reasons.

- i) In defining the top compression force in the slab at the high moment end of the hole, the proposed truss model does not take into account the horizontal forces that can be provided by shear connection placed some distance apart from the low moment end of the hole (see Fig. 4.2). In reality, these connector forces will also be transferred to the high moment region depending on the degree of transverse cracks appeared in the top of the slab near the low moment end of the hole. In ribbed slabs, very severe cracks were normally observed in tests due to the thin cover slab thickness, so the connector forces described can be ignored. However, in solid slabs which involve much less severe cracks than ribbed slabs, some transference of the horizontal connector forces is expected. This might be one reason for the conservatism related to solid slabs. No rational method has been found to consider the influence of those horizontal connector forces on the slab forces. If additional connector forces are to be considered, the same number of connectors in tension action need to be assumed to satisfy vertical force equilibrium as shown in Fig. 4.2, however this way of consideration is not very convincing for various cases of stud configurations in solid slabs.
- ii) Another possible reason is related to the pull-out capacity of shear connectors in solid slabs. In most solid slab tests, the pull-out capacity of the stud calculated from the surface area of a tension cone is much less than its horizontal shear capacity (see Table 4.7). In tests, however, no failure associated with the pull-out capacity of the stud was observed for solid slabs. Further, the shear-friction

concept²³ about shear connection indicates that in order to develop a horizontal connector force, the identical magnitude of a vertical tensile connector force is required when the frictional coefficient is equal to 1.0. As a result, the pull-out capacity of the studs used in the analysis might need some modification. One possible modification in which the pull-out capacity of the stud is increased up to its horizontal resistance is incorporated in the analysis, and the results are also shown (as bracketed terms) in Table 4.6.

Table 4.7 shows how shear connectors placed in the opening region perform under the combined horizontal and vertical forces. With the combination predicted, the studs in the opening region were fully exhausted.

4.4 Discussion

Ultimate strengths obtained from two theories have been compared with previous test results, and it has been shown that both theories provide satisfactory predictions for solid and ribbed slab beams. The mean ratios of test to theory by the simplified slab shear and truss models for thirty five tests are 1.064 and 1.196 respectively (see Table 4.6). In view of the accuracy of prediction, the simplified slab shear model (COV=10.9%) provides better agreement with previous tests than the truss model (COV=12.5%), particularly for solid slabs, but the difference is not significant enough to distinguish the two theories.

In an overall sense, the two theories fundamentally adopt the same solution procedure by employing the lower bound approach, however they are significantly different in treating the vertical shear forces carried by the concrete slab. According to this, the slab forces and the role of connectors are defined in different ways.

In the truss analogy a limited number of connectors around the opening are involved in resisting horizontal and vertical forces in the slab, rather than incorporation of all shear connectors provided between the opening edges and the support. As a re-

sult, stress reversals within the steel flange thicknesses can be maintained as assumed without unduly reducing the horizontal connector forces, i e fully exhausting connector resistance. However, above all, the major difference of these two theories is that the truss model provides a detailed appreciation of the slab and connector behaviour in carrying the vertical shear forces because it is based on realistic physical models

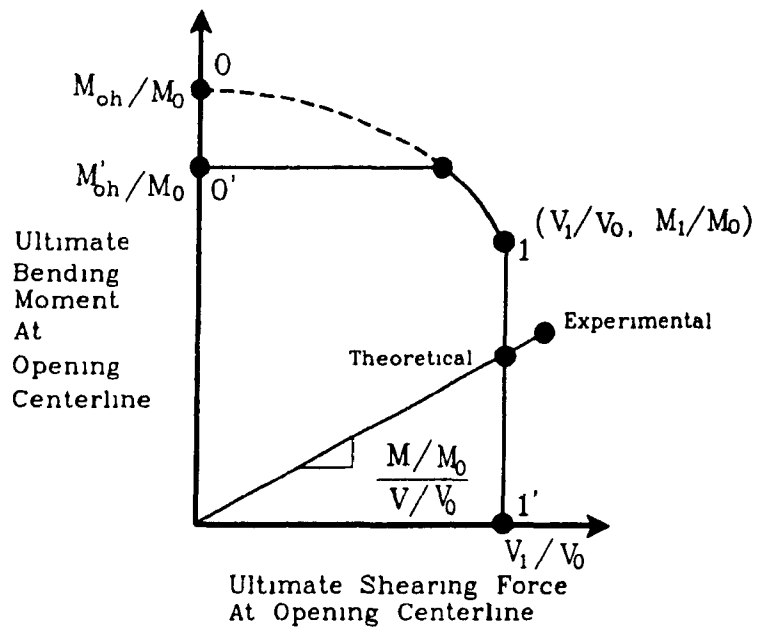


Figure 4.1 Non-dimensionalized Interaction Diagram.

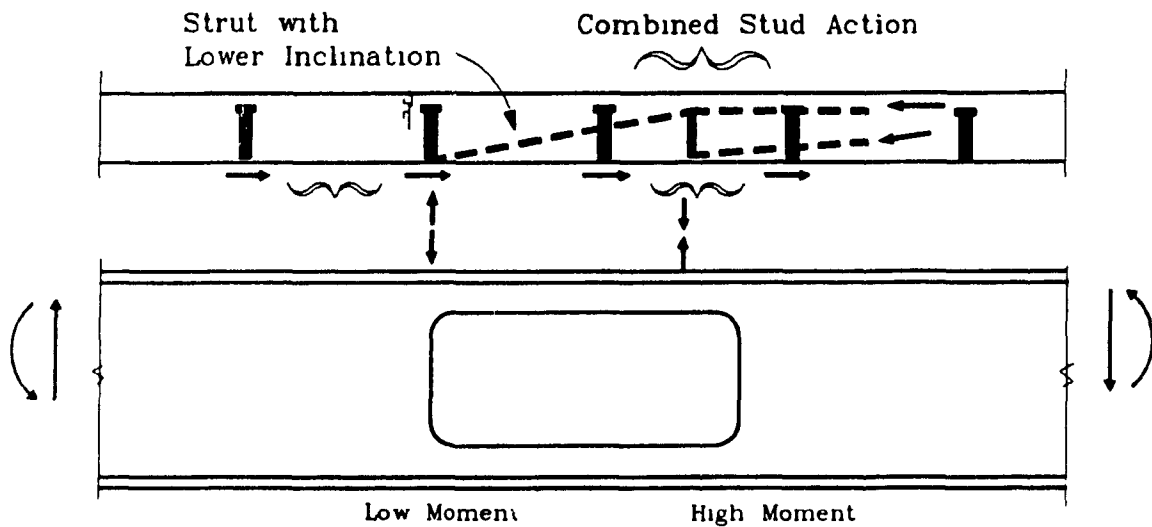


Figure 4.2 Transference of Horizontal Connector Forces in Solid Slabs.

Table 4.1 Theoretical Values Defining Interaction Diagrams

Slab Type	Exp. Inves.	Hole No.	Mo (kN-m)	Moh	Moh'	M1	Vo (kN)	V1	
Solid Slab	Granade	G-1	216.5	184.4	160.3	104.2	273.9	134.0	
		G-2	216.5	184.4	183.8	104.5	273.9	131.9	
	Clawson and Darwin	C-1	410.8	319.3	319.3	165.7	343.3	206.7	
		C-2	673.1	490.3	490.3	230.6	627.9	168.2	
		C-3	686.4	496.8	496.8	230.9	627.9	176.4	
		C-4	758.6	550.9	495.5	251.1	725.4	200.9	
		C-5	736.7	543.5	536.8	263.0	650.2	195.4	
		C-6	461.4	358.9	329.5	183.5	434.1	216.1	
	Cho	CH-1	199.4	168.7	139.5	76.3	213.4	133.9	
		CH-2	360.9	282.2	261.3	122.7	471.2	187.9	
		CH-3	360.9	282.2	267.1	122.8	471.2	187.1	
	Ribbed Slab	Redwood, Wong and Poubouras	R-0	245.8	168.2	121.0	64.4	311.7	103.0
			R-1	462.1	376.4	274.9	174.1	445.2	102.4
			R-2	497.0	402.1	378.3	226.8	494.4	117.7
			R-3	567.2	424.6	424.6	230.9	498.2	147.0
R-4			560.3	433.7	330.3	200.6	508.4	109.9	
R-5			462.1	393.9	292.5	149.8	445.2	115.8	
R-6			458.7	366.6	286.8	170.7	487.5	84.7	
R-7			458.7	366.6	304.0	185.7	487.5	133.2	
R-8		440.3	358.7	299.7	196.8	431.4	120.9		
Donahey and Darwin		D-1	919.1	658.4	558.8	226.3	941.1	177.8	
		D-2	916.1	660.0	635.5	231.6	918.2	157.0	
		D-3	940.7	675.1	639.5	239.1	916.2	162.3	
		D-4A	920.3	664.8	549.7	224.7	918.2	134.0	
		D-4B	942.0	681.2	633.0	234.3	918.2	137.8	
		D-5A	911.3	658.4	532.0	213.9	908.4	152.5	
		D-5B	925.4	646.2	581.0	284.3	908.4	171.6	
		D-6A	887.5	637.6	565.4	242.5	909.4	169.9	
		D-6B	900.0	648.3	616.3	265.7	909.4	193.3	
		D-7A	763.2	509.7	496.9	170.6	710.6	173.3	
		D-7B	765.2	510.5	510.5	170.1	710.6	160.9	
		D-8A	224.3	156.6	130.2	64.3	271.2	96.8	
		D-8B	228.5	152.2	112.2	68.3	271.2	67.3	
		D-9A	892.1	538.0	493.2	243.8	719.3	164.6	
		D-9B	900.7	537.5	496.6	256.8	727.1	247.1	

Table 4.2 Experimental and Predicted Failure Loads

Slab Type	Exp. Inves.	Hole No.	Experimental		Predicted		Test/Theory	
			M (kN-m)	V (kN)	M	V		
Solid Slab	Granade	G-1	88.7	145.5	81.7	134.0	1.085	
		G-2	143.7	117.9	142.0	116.5	1.012	
	Clawson and Darwin	C-1	326.0	148.6	285.2	129.9	1.143	
		C-2	464.0	163.7	384.4	135.6	1.207	
		C-3	616.9	62.3	486.3	49.1	1.268	
		C-4	193.6	211.7	183.7	200.9	1.054	
		C-5	397.8	214.0	346.7	186.5	1.147	
		C-6	164.3	179.7	197.0	215.5	0.834	
	Cho	CH-1	70.7	157.2	60.2	133.9	1.174	
		CH-2	220.3	206.4	148.3	185.4	1.113	
		CH-3	260.9	79.1	266.6	80.8	0.979	
	Ribbed Slab	Redwood, Wong and Pombouras	R-0	81.0	81.0	97.6	97.6	0.830
			R-1	109.1	115.5	96.7	96.7	1.128
R-2			319.5	127.8	280.2	112.1	1.140	
R-3			438.0	73.0	403.2	67.2	1.086	
R-4			350.4	58.4	330.3	55.0	1.061	
R-5			116.0	122.7	109.5	109.5	1.059	
R-6			89.3	94.5	80.1	80.1	1.116	
R-7			128.0	135.5	125.9	125.9	1.017	
R-8		121.4	128.5	114.2	114.2	1.063		
Donahey and Darwin		D-1	181.5	168.1	191.9	177.8	0.946	
		D-2	349.7	173.5	310.8	154.3	1.125	
		D-3	686.4	50.3	639.5	46.8	1.073	
		D-4A	293.9	145.5	269.5	133.3	1.091	
		D-4B	350.0	173.5	276.8	173.2	1.265	
		D-5A	312.9	153.9	303.7	149.4	1.030	
		D-5B	290.3	143.2	343.2	169.3	0.846	
		D-6A	0.0	182.4	0.0	169.9	1.074	
		D-6B	234.0	217.5	208.0	193.3	1.125	
		D-7A	208.2	193.5	186.3	173.2	1.117	
		D-7B	381.8	189.5	299.8	148.8	1.274	
	D-8A	87.3	86.3	93.1	92.0	0.938		
D-8B	48.2	63.6	51.1	67.3	0.945			
D-9A	166.5	153.9	303.7	149.4	1.030			
D-9B	200.7	210.4	235.8	247.1	0.851			

Table 4.3 Non-Dimensional Parameters of Test Beams

Slab Type	Exp. Inves.	Hole No.	Vt/Vpt	Vc/Vcu	To/Co	Moh'/Moh	M/Vd	
Solid Slab	Granade	G-1	1.83	1.00	1.00	0.87	3.000	
		G-2	1.79	1.00	1.00	1.00	6.000	
	Clawson and Darwin	C-1	2.32	0.58	0.23	1.00	6.171	
		C-2	1.01	0.02	0.53	1.00	6.243	
		C-3	1.08	0.10	0.45	1.00	21.818	
		C-4	1.06	0.10	0.57	0.90	2.014	
		C-5	1.11	0.18	0.52	0.99	4.039	
		C-6	1.86	0.94	0.48	0.92	2.571	
	Cho	CH-1	2.65	1.00	0.71	0.83	2.320	
		CH-2	1.51	1.00	0.89	0.93	2.667	
		CH-3	1.51	1.00	0.89	0.95	11.000	
	Ribbed Slab	Redwood, Wong and Pombouras	R-0	1.25	0.30	0.46	0.72	3.943
			R-1	0.79	0.00	1.13	0.73	2.656
			R-2	0.83	0.00	1.14	0.94	7.007
			R-3	1.09	0.67	0.73	1.00	16.835
R-4			0.73	0.00	0.82	0.76	16.830	
R-5			1.23	0.26	1.13	0.74	2.656	
R-6			0.53	0.30	1.46	0.78	2.647	
R-7			0.99	0.00	1.46	0.83	2.647	
R-8		1.03	0.19	1.54	0.84	2.662		
Donahey and Darwin		D-1	0.63	0.00	1.16	0.85	2.059	
		D-2	0.54	0.00	1.04	0.96	3.845	
		D-3	0.57	0.00	0.94	0.95	26.059	
		D-4A	0.42	0.00	1.09	0.83	3.857	
		D-4B	0.44	0.00	0.98	0.93	3.851	
		D-5A	0.53	0.00	1.07	0.81	3.880	
		D-5B	0.60	0.00	1.00	0.90	3.868	
		D-6A	0.62	0.00	1.28	0.89	0.000	
		D-6B	0.74	0.00	1.20	0.95	2.053	
		D-7A	0.89	0.00	0.52	0.98	2.053	
		D-7B	0.81	0.00	0.51	1.00	3.845	
		D-8A	1.34	0.42	0.46	0.83	3.933	
		D-8B	1.04	0.04	0.35	0.74	2.950	
		D-9A	0.44	0.32	0.42	0.92	2.071	
		D-9B	1.90	0.93	0.41	0.92	1.821	

Table 4.4 Various Connector Resistance Related to Each Solution Procedure

Slab Type (1)	Exp. Inves. (2)	Hole No. (3)	qr (kN) (4)	qmax (5)	qo (6)	qc (q ^u) (7)	qe (8)	q/qr (9)	
Solid Slab	Granade	G-1	81.6	157.8	101.1	90.3 (34.7)	-	0.42	
		G-2	81.6	90.2	52.1	48.6 (20.0)	-	0.24	
	Clawson and Darwin	C-1	117.9	85.3	240.4	211.7	59.5	0.50	
		C-2	117.9	101.6	107.9	101.6	63.5	0.54	
		C-3	117.9	101.6	126.7	119.3	63.5	0.54	
		C-4	117.9	183.8	238.1	202.4	113.3	0.96	
		C-5	117.9	111.3	135.9	121.3	71.4	0.61	
		C-6	117.9	140.8	214.6	182.4	95.3	0.81	
	Cho	CH-1	47.1	77.8	75.7	65.6 (15.3)	-	0.32	
		CH-2	47.1	70.5	49.5	44.7 (22.8)	-	0.48	
		CH-3	47.1	63.5	43.6	39.7 (20.5)	-	0.44	
	Ribbed Slab	Redwood, Wong and Pombouras	R-0	93.4	166.2	301.6	208.4	87.6	0.94
			R-1	91.2	303.9	251.3	173.6	-	1.00
			R-2	59.8	71.8	45.3	38.0	-	0.76
			R-3	81.8	65.3	64.8	49.1	43.1	0.53
R-4			107.1	296.4	181.0	181.0	-	1.00	
R-5			91.2	303.9	251.3	173.6	-	1.00	
R-6			64.6	248.6	124.3	124.3	-	1.00	
R-7			64.6	124.3	157.6	82.9	-	1.00	
R-8		62.2	118.1	149.7	78.7	-	1.00		
Donahey and Darwin		D-1	76.6	162.3	190.9	101.4	-	1.00	
		D-2	73.2	80.0	61.0	44.0	35.8	0.49	
		D-3	79.8	92.5	77.7	54.5	41.7	0.52	
		D-4A	113.1	344.1	172.1	172.1	-	1.00	
		D-4B	73.2	103.9	53.2	53.2	36.7	0.50	
		D-5A	79.8	245.8	232.5	143.4	-	1.00	
		D-5B	79.8	115.4	101.6	66.0	57.4	0.72	
		D-6A	70.8	121.6	126.3	73.0	-	1.00	
		D-6B	74.4	78.0	91.8	48.8	59.4	0.80	
		D-7A	73.0	63.4	111.4	78.3	36.4	0.50	
		D-7B	74.4	63.	90.7	71.9	33.5	0.45	
		D-8A	65.5	77.2	139.4	95.8	42.7	0.65	
		D-8B	69.8	99.4	274.3	169.8	59.3	0.85	
		D-9A	121.3	128.7	289.4	189.2	78.8	0.65	
		D-9B	125.4	161.2	300.7	226.1	100.0	0.80	

* q is minimum value in columns 4 through 8

Table 4.5 Calculated Shearing Forces for Test Beams

Slab Type	Exp. Inves.	Hole No.	Vsb (kN)	Truss Model							Simplified Slab Shear Model					
				θ (degs.)	Vc (kN)	Vst	Vst'	V1	M1 (kN-m)	Sol.	Vc (kN)	Vst	V1	M1 (kN-m)		
Solid Slab	Granade	G-1	21.9	20	42.7	42.3	84.5	106.8	94.0	94.0	I	50.8	61.2	134.0	104.2	
		G-2	21.8	20	42.7	42.3	84.5	106.4	94.0	94.0	I	48.7	61.2	131.9	104.5	
	Clawson and Darwin	C-1	24.3	11	41.8	57.0	99.2	123.7	125.1	125.1	I	103.8	78.6	206.7	165.7	
		C-2	35.6	11	40.1	64.5	104.6	140.2	187.5	187.5	I	1.8	130.9	168.2	230.6	
		C-3	35.6	11	40.9	65.4	106.4	142.0	187.7	187.7	I	10.0	130.8	176.4	230.9	
		C-4	41.2	18	57.9	66.8	124.2	165.5	210.3	210.3	I	8.4	151.3	200.9	251.1	
		C-5	39.5	17	52.5	66.3	118.8	158.4	214.6	214.6	I	15.2	140.7	195.4	263.0	
		C-6	30.8	21	58.7	56.1	114.8	146.0	148.7	148.7	I	85.5	99.8	216.1	183.5	
	Cho	CH-1	15.4	32	35.3	34.3	102.9	118.6	68.4	68.4	I	74.0	44.8	133.9	76.3	
		CH-2	36.0	27	35.3	60.8	130.3	165.6	100.2	100.2	I	109.9	100.3	187.9	122.7	
		CH-3	36.0	27	35.3	60.8	130.3	165.6	100.2	100.2	I	50.8	100.3	187.1	122.8	
	Ribbed Slab	Redwood, Wong and Pombouras	R-0	19.2	20	29.9	31.5	61.4	80.6	32.9	32.9	I	16.7	67.1	103.0	64.4
			R-1	26.6	20	29.1	38.4	67.6	143.0	94.2	94.2	I	0.0	75.7	102.4	174.1
			R-2	29.8	20	38.0	45.3	83.3	113.1	148.9	148.9	I	0.0	87.8	117.7	226.8
R-3			29.9	20	51.2	50.5	101.7	131.7	140.1	140.1	I	10.0	107.0	147.0	230.9	
R-4			30.6	9	16.6	30.6	47.1	77.7	148.4	148.4	III	0.0	79.4	109.9	200.6	
R-5			57.0	20	29.1	13.3	42.4	99.4	120.3	120.3	I	10.9	48.0	115.8	149.8	
R-6			29.5	7	15.4	29.5	44.9	74.4	149.9	149.9	III	0.0	55.3	84.7	170.7	
R-7			29.5	20	40.4	45.8	86.2	115.7	145.0	145.0	I	0.0	103.7	133.2	185.7	
R-8		25.6	20	39.0	41.2	80.2	105.7	157.7	157.7	I	3.1	92.2	120.9	196.8		
Donahey and Darwin		D-1	54.5	21	48.1	54.3	102.8	157.5	185.3	185.3	II	0.0	123.3	177.8	226.3	
		D-2	53.2	21	49.8	53.4	102.8	155.8	181.4	181.4	II	0.0	103.8	157.0	231.6	
		D-3	53.0	21	49.8	53.0	103.2	156.2	185.5	185.5	II	0.0	109.3	162.3	239.1	
		D-4A	53.2	7	13.4	53.4	66.8	119.7	173.7	173.7	III	0.0	80.9	134.0	224.7	
		D-4B	53.2	7	19.6	53.4	72.6	125.5	176.4	176.4	III	0.0	84.6	137.8	234.3	
		D-5A	52.6	21	47.2	52.5	76.1	128.6	175.2	175.2	II	0.0	99.9	152.5	213.9	
		D-5B	30.7	21	49.8	79.7	129.5	160.2	225.3	225.3	II	0.0	140.0	171.6	284.3	
		D-6A	52.7	21	44.5	52.5	97.0	149.5	190.8	190.8	II	0.0	117.2	169.9	242.5	
		D-6B	52.7	21	87.2	187.2	174.4	227.0	185.0	185.0	I	0.0	140.7	193.3	265.7	
		D-7A	41.1	24	67.6	63.6	131.7	172.7	124.7	124.7	I	0.0	132.3	173.3	170.6	
		D-7B	4.1	29	55.2	56.1	111.3	152.2	132.7	132.7	I	0.0	119.9	160.9	170.1	
		D-8A	17.3	23	46.3	34.3	80.5	97.9	42.5	42.5	I	20.3	59.2	96.8	64.3	
		D-8B	7.7	23	49.8	22.7	73.0	80.5	47.3	47.3	I	2.3	57.3	67.3	68.3	
		D-9A	21.5	25	77.4	21.4	99.2	120.6	194.6	194.6	II	36.2	106.9	164.6	243.8	
		D-9B	32.4	25	80.1	38.3	117.9	150.4	189.5	189.5	II	101.9	112.9	247.1	256.8	

Table 4.5 Calculated Shearing Forces for Test Beams

Slab Type	Exp. Inves.	Hole No.	Vsb (kN)	Truss Model							Simplified Slab Shear Model				
				θ (degs.)	Vc (kN)	Vst	Vst'	V1	M1 (kN-m)	Sol.	Vc (kN)	Vst	V1	M1 (kN-m)	
Solid Slab	Granade	G-1	21.9	20	42.7	42.3	84.5	106.8	94.0	I	50.8	61.2	134.0	104.2	
		G-2	21.8	20	42.7	42.3	84.5	106.4	94.0	I	48.7	61.2	131.9	104.5	
	Clawson and Darwin	C-1	24.3	11	41.8	57.0	99.2	123.7	125.1	I	103.8	78.6	206.7	165.7	
		C-2	35.6	11	40.1	64.5	104.6	140.2	187.5	I	1.8	130.9	168.2	230.6	
		C-3	35.6	11	40.9	65.4	106.4	142.0	187.7	I	10.0	130.8	176.4	230.9	
		C-4	41.2	18	57.9	66.8	124.2	165.5	210.3	I	8.4	151.3	200.9	251.1	
		C-5	39.5	17	52.5	66.3	118.8	158.4	214.6	I	15.2	140.7	195.4	263.0	
		C-6	30.8	21	58.7	56.1	114.8	146.0	148.7	I	85.5	99.8	216.1	183.5	
	Cho	CH-1	15.4	32	35.3	34.3	102.9	118.6	68.4	I	74.0	44.8	133.9	76.3	
		CH-2	36.0	27	35.3	60.8	130.3	165.6	100.2	I	109.9	100.3	187.9	122.7	
		CH-3	36.0	27	35.3	60.8	130.3	165.6	100.2	I	50.8	100.3	187.1	122.8	
	Ribbed Slab	Redwood, Wong and Pombouras	R-0	19.2	20	29.9	31.5	61.4	80.6	32.9	I	16.7	67.1	103.0	64.4
			R-1	26.6	20	29.1	38.4	67.6	143.0	94.2	I	0.0	75.7	102.4	174.1
			R-2	29.8	20	38.0	45.3	83.3	113.1	148.9	I	0.0	87.8	117.7	226.8
R-3			29.9	20	51.2	50.5	101.7	131.7	140.1	I	10.0	107.0	147.0	230.9	
R-4			30.6	9	16.6	30.6	47.1	77.7	148.4	III	0.0	79.4	109.9	200.6	
R-5			57.0	20	29.1	13.3	42.4	99.4	120.3	I	10.9	48.0	115.8	149.8	
R-6			29.5	7	15.4	29.5	44.9	74.4	149.9	III	0.0	55.3	84.7	170.7	
R-7			29.5	20	40.4	45.8	86.2	115.7	145.0	I	0.0	103.7	133.2	185.7	
R-8		25.6	20	39.0	41.2	80.2	105.7	157.7	I	3.1	92.2	120.9	196.8		
Donahey and Darwin		D-1	54.5	21	48.1	54.3	102.8	157.5	185.3	II	0.0	123.3	177.8	226.3	
		D-2	53.2	21	49.8	53.4	102.8	155.8	181.4	II	0.0	103.8	157.0	231.6	
		D-3	53.0	21	49.8	53.0	103.2	156.2	185.5	II	0.0	109.3	162.3	239.1	
		D-4A	53.2	7	13.4	53.4	66.8	119.7	173.7	III	0.0	80.9	134.0	224.7	
		D-4B	53.2	7	19.6	53.4	72.6	125.5	176.4	III	0.0	84.6	137.8	234.3	
		D-5A	52.6	21	47.2	52.5	76.1	128.6	175.2	II	0.0	99.9	152.5	213.9	
		D-5B	30.7	21	49.8	79.7	129.5	160.2	225.3	II	0.0	140.0	171.6	284.3	
		D-6A	52.7	21	44.5	52.5	97.0	149.5	190.8	II	0.0	117.2	169.9	242.5	
		D-6B	52.7	21	87.2	187.2	174.4	227.0	185.0	I	0.0	140.7	193.3	265.7	
		D-7A	41.1	24	67.6	63.6	131.7	172.7	124.7	I	0.0	132.3	173.3	170.6	
		D-7B	41.1	29	55.2	56.1	111.3	152.2	132.7	I	0.0	119.9	160.9	170.1	
		D-8A	17.3	23	46.3	34.3	80.5	97.9	42.5	I	20.3	59.2	96.8	64.3	
		D-8B	7.7	23	49.8	22.7	73.0	80.5	47.3	I	2.3	57.3	67.3	68.3	
	D-9A	21.5	25	77.4	21.4	99.2	120.6	194.6	II	36.2	106.9	164.6	243.8		
D-9B	32.4	25	80.1	38.3	117.9	150.4	189.5	II	101.9	112.9	247.1	256.8			

Table 4.6 Experimental and Predicted Failure Loads

Slab Type	Exp. Inves.	Hole No.	Experimental		Truss Model		Simplified Model		
			M (kN-m)	V (kN)	Predicted V	Test/Theory	Predicted V	Test/Theory	
Solid Slab	Granade	G-1	88.7	145.5	106.8	1.365 (1.176)	134.0	1.085	
		G-2	143.7	117.9	101.0	1.170 (1.067)	116.5	1.012	
	Clawson and Darwin	C-1	326.0	148.6	104.1	1.424 (1.395)	129.9	1.143	
		C-2	464.0	163.7	120.6	1.358 (1.312)	135.6	1.207	
		C-3	616.9	62.3	48.5	1.289 (1.285)	49.1	1.268	
		C-4	193.6	211.7	165.5	1.281 (1.137)	200.9	1.054	
		C-5	397.8	214.0	154.4	1.385 (1.267)	186.5	1.147	
		C-6	164.3	179.7	146.0	1.233 (1.030)	215.5	0.834	
	Cho	CH-1	70.7	157.2	118.6	1.330 (1.060)	133.9	1.174	
		CH-2	220.3	206.4	163.7	1.261 (1.174)	185.4	1.113	
		CH-3	260.9	79.1	78.4	1.002 (0.990)	80.8	0.979	
	Solid Slab Summary:					Mean	Co. of Var.	Mean	Co. of Var.
						1.282	(1.172)	9.2%	(11.1)
					1.092		11.0%		
Ribbed Slab	Redwood, Wong and Pombouras	R-0	81.0	81.0	76.3	1.061	97.6	0.830	
		R-1	109.1	115.5	94.2	1.227	96.7	1.128	
		R-2	319.5	127.8	102.5	1.247	112.1	1.140	
		R-3	438.0	73.0	64.7	1.129	67.2	1.086	
		R-4	350.4	58.4	55.0	1.061	55.0	1.061	
		R-5	116.0	122.7	99.4	1.235	109.5	1.059	
		R-6	89.3	94.5	74.4	1.270	80.1	1.116	
		R-7	128.0	135.5	115.7	1.172	125.9	1.017	
	R-8	121.4	128.5	105.7	1.215	114.2	1.063		
	Donahey and Darwin	D-1	181.5	168.1	157.5	1.068	177.8	0.946	
		D-2	349.7	173.5	150.9	1.151	154.3	1.125	
		D-3	686.4	50.3	46.7	1.073	46.8	1.073	
		*D-4A	293.9	145.5	118.8	1.226	133.3	1.091	
		*D-4B	350.0	173.5	124.2	1.397	173.2	1.265	
		D-5A	312.9	153.9	126.8	1.214	149.4	1.030	
		D-5B	290.3	143.2	156.2	0.917	169.3	0.846	
		D-6A	0.0	182.4	150.9	1.210	169.9	1.074	
		+D-6B	234.0	217.5	225.2	0.966	193.3	1.125	
		**D-7A	208.2	193.5	170.9	1.134	173.2	1.117	
		**D-7B	381.8	189.5	139.3	1.355	148.8	1.274	
D-8A		87.3	86.3	89.0	0.970	92.0	0.938		
D-8B	48.2	63.6	79.7	0.797	67.3	0.945			
D-9A	166.5	153.9	120.6	1.272	149.4	1.030			
D-9B	200.7	210.4	150.4	1.399	247.1	0.851			
Ribbed Slab Summary:					Mean	Co. of Var.	Mean	Co. of Var.	
					1.157	12.8%	1.051	10.9%	
Overall Summary:					Mean	Co. of Var.	Mean	Co. of Var.	
					1.196	(1.162)	12.5%	(12.2)	
					1.064		10.9%		

* Puddle weld used over the opening

** Longitudinally ribbed slab

+ Deck pan used

Table 4.7 Horizontal and Vertical Resistance of Shear Connection

Slab Type	Exp. Inves.	Hole No.	qr (kN)	Tr (kN)	Truss Model		Simplified Model	*Slab Force at H.M. of Hole
					q/qr	T/Tr	q/qr	Truss / Simplified
Solid Slab	Granade	G-1	81.7	34.0	0.70	0.63	0.42	0.56
		G-2	81.7	34.0	0.70	0.63	0.24	0.49
	Clawson and Darwin	C-1	118.0	58.7	0.89	0.36	0.50	0.39
		C-2	118.0	47.2	0.84	0.42	0.54	0.44
		C-3	118.0	51.2	0.87	0.40	0.54	0.46
		C-4	118.0	48.8	0.73	0.59	0.96	0.76
		C-5	118.0	46.3	0.75	0.57	0.61	0.41
		C-6	118.0	44.4	0.66	0.66	0.81	0.82
	Cho	CH-1	47.0	23.4	0.58	0.75	0.32	0.91
		CH-2	47.0	29.3	0.73	0.60	0.48	0.43
		CH-3	47.0	29.3	0.73	0.60	0.44	0.42
	Ribbed Slab	Redwood, Wong and Pombouras	R-0	93.4	73.5	0.86	0.41	0.94
R-1			91.2	71.5	0.85	0.41	1.00	0.28
R-2			59.8	46.0	0.85	0.41	0.76	0.28
R-3			81.8	56.7	0.84	0.45	0.53	0.18
R-4			107.1	79.7	0.95	0.21	1.00	0.19
R-5			91.2	71.5	0.85	0.41	1.00	0.7
R-6			64.6	44.5	0.96	0.17	1.00	0.48
R-7			64.6	44.5	0.84	0.45	1.00	0.42
R-8		62.2	43.3	0.84	0.45	1.00	0.42	
Donahey and Darwin		D-1	76.7	54.7	0.84	0.44	1.00	0.84
		D-2	**73.2	53.0	+0.82	0.47	0.49	0.61
		D-3	79.8	56.1	0.84	0.44	0.52	0.61
		D-4A	113.1	104.8	0.98	0.13	1.00	0.20
		D-4B	**73.2	55.2	+0.96	0.18	0.50	0.23
		D-5A	79.8	46.3	0.79	0.51	1.00	0.47
		D-5B	79.8	54.3	0.83	0.46	0.72	0.58
		D-6A	70.8	48.1	0.83	0.46	1.00	0.62
		D-6B	74.4	42.1	0.78	0.52	0.80	0.65
		D-7A	73.0	21.5	0.52	0.79	0.50	0.69
		D-7B	74.4	41.4	0.66	0.67	0.45	0.55
	D-8A	65.5	55.2	0.85	0.42	0.65	0.44	
D-8B	69.8	61.9	0.85	0.40	0.85	1.00		
D-9A	121.3	61.9	0.70	0.63	0.65	1.08		
D-9B	125.4	63.2	0.70	0.63	0.80	0.37		

* Horizontal compression force

** Average value considering four and two studs in a rib

+ Based on two studs in a rib

CHAPTER 5

EXPERIMENTAL PROGRAMME

5.1 Introduction

A series of six composite beam tests incorporating a total of nine rectangular web holes was carried out to investigate the slab behaviour under high shear, particularly in relation to the verification of truss action identified in Chapter 3.

All test beams involved the same size of steel sections W360×51 (W14×34), and each contained one or two isolated web cut-outs centered at the mid-depth of the steel member. Five beams had metal deck supported slabs with ribs oriented transversely to the steel beam-axis, while one beam had a solid slab.

In order to obtain a clearer indication of the slab behaviour in carrying vertical shear, the height of the opening for all tests was fixed to the maximum possible value that corresponds to 70 % of the steel beam depth, and the location of the opening was also restricted to the high shear region. Three holes were placed at the point of zero moment.

Further, in view of the truss analogy, shear connectors in hole regions for all test specimens were carefully arranged to play their role in resisting vertical tensile forces as well as providing bearing at the corresponding edges of the opening in an efficient manner. More details are given below. Layouts for all test beams are shown in Fig. 5.1

5.2 Details of Test Specimens

All test specimens were designed primarily with emphasis on the performance of shear connection in the hole region, since it is the major factor to determine the slab behaviour in a composite beam at a web hole, particularly when using truss analogy. The specific test parameters included were stud configurations, and the width of the slab as well as detailing of the studs, associated with the performance of shear connection that provides bearing as well as tensile resistance.

The ribbed slab was constructed using a standard 20 gauge (0.914 mm) wipe coat galvanized deck 76 mm deep, with average width 156 mm. A single layer of wire mesh consisting of 4 12 mm diameter (8 gauge) wires spaced at 152 mm was placed at the mid-depth of the cover slab, resulting in a reinforcement ratio of 0.0012 based on the slab thickness above the rib. In solid slab specimens double layers of this mesh was necessary to obtain a shrinkage and temperature reinforcement ratio of 0.002.

Shear connection was provided by 19 mm diameter headed studs, with initial length of 124 mm for ribbed slabs, and with initial length of 81 mm for solid slabs. In ribbed slab specimens, the studs placed in pairs in a rib were staggered at 91 mm longitudinally and 85 mm transversely, while single studs were placed at the beam centerline in the low moment side of the flute, this being the more favorable position to provide bearing.

In the preparation of test specimens, 32 mm diameter holes were firstly drilled at the opening corners to minimize the effect of stress concentrations, and then the opening was cut using an oxy-acetylene torch. No stiffeners and plates were placed on the steel beam. After steel decking was positioned on the steel flange, shear studs were installed through the deck using a welding gun. At this time, supports were provided at the beam ends and at one third points of the span. During pouring of concrete, shoring was also installed to support the steel decks.

Geometric properties of all test specimens are summarized in Table 5.1, and specific

reasons for individual tests are given below.

5.2.1 Hole 1

Shear stud distribution and hole configuration on Beam 1 are shown in Fig. 5.2, which provided a pure shear loading condition at the hole centerline.

This specimen had an effective slab width equal to 750 mm based on the span between supports. It did not contain any studs within the hole length, but a pair of studs were placed close to each end of the hole so that inclined strut action along these studs might be developed. For this stud configuration, the truss model indicates that the studs placed even beyond the opening length are important in carrying vertical shear unless they are far beyond the edges of the opening. On the other hand, the simplified slab shear model presented in Chapter 2 ignores the participation of studs beyond the ends of the hole in carrying vertical shear, thus predicting lower resistance of the beam. This difference is examined by this test.

5.2.2 Holes 2 and 3

Beams 2 and 3, comprising Holes 2 and 3 respectively, were identical in every aspect except for the effective width of the concrete slab used. Beam 2 was constructed with the effective width of the slab equal to 750 mm which is normally required to treat the slab as part of the beam for this composite beam configuration, while in Beam 3 one-half of this required width (375 mm) was considered. Each beam contained a single opening at a point of zero moment and incorporated uniform distribution of the studs along the whole beam span, so that two single studs were located within the hole length. The details of these beams are shown in Fig 5.3.

A major concern of this pair of tests was to investigate the effect of the width of the concrete slab on the ultimate resistance of the beam. Note that the effective width of the concrete slab used in Hole 2, calculated in the usual manner, relates to

the treatment of the slab participation in resisting horizontal forces caused by bending, not for vertical shear forces. Therefore, this way of considering the effective width of the concrete slab can not be justified in the hole region where the slab behaviour is determined by shear, rather than bending. With respect to this, the truss concept indicates that the width of the concrete slab that can be effective in resisting vertical shear in the hole region will correspond to the width of the corresponding stud tension cone to be developed, in the sense that vertical shear is mainly carried by stud action in tension. As a result, no significant reduction in the ultimate load carrying capacity is expected in Hole 3 compared with Hole 2. Minor reduction might be possible resulting from the difference of horizontal resistance of the studs. It is on the other hand noted that a smaller width of the concrete slab specimen(Hole 3) will provide a clearer observation for the diagonal compressive struts near the stud locations.

The test Hole 2 also included a comparison with Hole 1 on ultimate and serviceability load level performance. In both holes four studs were provided between the high moment end of the opening and the support, while within the hole length only Hole 2 had two studs. For these stud configurations, the simplified slab shear model predicts the ultimate strength of Hole 2 to be significantly greater than that of Hole 1 because of the larger eccentricity involved in the slab force system, resulting from the higher degree of shear connection within the hole length. In contrast with this, however, the truss model predicts both holes to be similar in strength. These aspects will be investigated

5.2.3 Holes 4 and 7

Holes 4 and 7 were in the same beam, each having the same loading condition, as shown in Fig. 5.4. The actual width was equal to the effective width of the concrete slab (1000mm), based on one-quarter of the span. Each specimen contained six studs between the high moment end of the opening and the support, and two studs within

the hole length. However, different stud arrangement were used within the hole length, i.e. single and a pair of studs per rib for Holes 4 and 7 respectively. With these stud configurations, the simplified slab shear model predicts the same strength at both holes because the numbers of studs between the opening ends and the supports are identical. However, the truss model predicts that Hole 7 has higher strength than Hole 4, for the reason that the larger tensile resistance of the studs was provided near the high moment end of the hole. This aspect will be investigated.

5.2.4 Holes 5 and 8

Holes 5 and 8 examine one possible detailing method to enhance vertical resistance of the studs near the high moment end of the opening, such that the inclined strut action similar to that found in solid slabs could be fully developed without premature failure associated with rib separation. The steel bars (No. 10) were welded longitudinally and transversely to the top of the studs placed near the high moment region of the opening. The details of these specimens are shown in Figs. 5.5 and 5.6.

In Hole 5, no studs were placed within the hole length, but instead, a longitudinal bar was welded at the heads of the studs placed beyond the high moment end of the opening and was extended through the low moment end. Additional transverse reinforcement was also provided following the truss model representing the slab forces across the width of the slab. Similarly, in Hole 8 transverse bars estimated from the truss model across the width of the slab were welded to the heads of the studs where vertical tensile forces should be resisted by tensile stud action. Both tests provide direct comparisons with Holes 4 and 7 respectively. Note that Hole 4 contained two studs within the opening length while Hole 5 no studs, and Holes 7 and 8 had the same conditions in all other aspects except for reinforcement associated with the enhancement of vertical resistance of the studs.

An indication of the stud performance in resisting vertical tensile forces near the

high moment end of the hole will be obtained from these tests.

5.2.5 Holes 6 and 9

Holes 6 and 9 were constructed with a solid slab 500 mm wide, which was half the required width, according to several codes^{18,25}, to consider the slab as part of the beam for this composite beam configuration. The details of these specimens are shown in Fig 5 7.

The number of studs provided between the high moment end of the opening and the support were identical for both holes. However, within the length of the hole different numbers of studs were placed, two and three studs for Holes 6 and 9 respectively. Also, note that in Hole 9, the stud spacing used was taken as the minimum value to develop the full stud tension cone, and the relatively low degree of shear connection was provided between the low moment end of the opening and the support. With this distribution of shear connection, the inclined struts involving single or combined action of the studs and possibly, the effect of shear connection between the low moment end and the support on the development of the inclined struts will be investigated.

Further, using the narrow width of the concrete slab, the slab failure associated with the bearing zone near the low moment end of the opening will also be investigated.

5.3 Material Properties

5.3.1 Concrete

The concrete used in all specimens was obtained from a local concrete ready mix company and had the following specifications: 20 MPa design strength, Type 30 (High early strength) cement, 20 mm maximum aggregate size, 100 mm slump, and 5~7% entrained air. Concrete strengths were measured for each beam from a minimum of three standard cylinder tests (150 mm×300 mm) cured under the same conditions as the test specimens.

The compressive strength of the concrete covering the time period of testing is shown in Fig. 5.8 with the best fit curve, and the corresponding strength of each specimen is summarized in Table 5.2.

5.3.2 Steel

The steel section used in all specimens was W360×51 (W14×34) corresponding to Class 1 in bending defined by CSA Standard S16.1-M84, and the steel conformed to CSA Standard G40.21-M Grade 300W. At least two pairs of tensile coupons for each beam, taken from the web and the flange, were tested on an Instron test machine. The average material properties, yield and ultimate stresses, elongation in a gauge length of 50 mm and reduction in area at fracture are given in Table 5.3.

Welded wire fabric used for slab reinforcement in all specimens conformed to CSA standards G30.5 and G30.15 with a specified yield strength of 400 MPa, and the designation was 152×152 MW 13.3× MW 13.3. The additional No. 10 bars welded to the top of the studs on Beam 5 conformed to CSA Standard G30.12 with a specified yield strength of 400 MPa and also, the welding rod used was type CSA E48014.

The steel deck used in all specimens was type P-2432-12 L2C Hi-bond supplied by Les Acier Canam Inc. with a minimum specified yield strength of 230 MPa. A cross-sectional detail of a sheet of deck material is shown in Fig. 5.9.

5.3.3 Shear Connection

All shear studs, 19 mm×124mm or 19 mm×81 mm, were supplied by the Nelson Stud Welding Division of TRW with a specified tensile strength of 413 MPa.

Six push-out tests having the same slab dimensions as well as stud configurations as the beam specimens were carried out to provide information on the stiffnesses and ultimate shear capacities of the studs. The details of each specimen and the test results are summarized in Table 5.4. The predicted ultimate shear load using the AISC

approach²⁵ is also included. Note that in Test 5 transverse bars (No. 10) were welded to the heads of the studs in a similar manner to that used in Holes 5 or 8.

The test setup used for the push-out test specimens is shown in Fig. 5.10. Load was applied to the top of the steel wide-flange section through a ball and socket platen on a universal testing machine of 2000 kN capacity. The slips were measured from four Linear Voltage Differential Transformers (LVDT's) attached on the top and bottom of the steel beam, which measured the relative movement of the slab to the steel beam.

In all ribbed slab specimens except for Test 5, concrete-related failure such as rib separation or rib shearing was observed, while accompanying transverse cracks were more apparent than longitudinal ones. Failure patterns and load-slip relationships for all push-out tests are shown in Figs. 5.11 and 5.12.

Test 1 had unequal thickness of the slab on each side of the specimen due to inadequate formwork used, therefore the adjustment to the strength and stiffness was necessary by comparing with the test results obtained from Test 2.

Comparison of results between Tests 2 and 3 indicates that the use of half the width of the concrete slab did not reduce horizontal shear resistance of the studs significantly in ribbed slabs (7% reduction). Shearing off at the stud base occurred for the two studs in Test 5 due to additional reinforcement welded to the heads of the studs. Also, severe rib separation cracks occurred at the stud which was not fully sheared off, while the other stud was pulled out from failure of the weld. Using additional reinforcement related to the enhancement of vertical resistance of the studs, a 16% increase in horizontal shear resistance per stud was obtained compared with Test 4.

In Test 6 having the solid slab, failure was triggered by the chopping-out of the concrete across the width of the slab at the stud positions, which is an unusual mode of failure in solid slab specimens. However, this might be possible due to the fact that the steel beam was in a slightly oblique position due to the problem associated with the formwork. Adjustment of this is not considered.

5.4 Instrumentation and Test Procedure-Beam Tests

All test beams were simply supported at their ends or at the ends of interior spans, and loaded at one or two points using hydraulic jacks beneath the reaction floor (see Fig. 5.13). At a loaded section of a beam, two loading rods spaced at 250 mm each side of the steel web passed through cast-in sleeves in the slab, and reacted on a bridge beam bedded with plaster across the entire width of the slab. The top flange of the steel beam above the supports was braced to prevent any lateral movement at these points.

For beams having two holes, when considerable damage had occurred at the first hole, indicated by the measurement of relative deflections between the hole ends and by the observed cracking of the slab, the load was slowly removed, and reinforcement was welded diagonally across the hole. Then loads were applied again until failure took place at the other hole.

The applied loads were monitored using load cells. Vertical deflections were measured using LVDT's at midspan, ends of the hole and the load points. For slip measurements between the concrete slab and steel beam, LVDT's were also installed at both ends of the beam and the nearest stud positions to the hole edges. Slip readings taken at the hole ends were obtained from small steel bars embedded in the concrete and projecting down through the steel deck in the bottom of the rib.

On each specimen, 45° strain rosettes were placed on the steel tee webs above and below the opening to measure shear strains, and uni-axial strain gauges on the top and bottom steel flanges measured longitudinal strains. All gauges were recessed from the edges of the opening to avoid the regions of stress concentration.

In order to have information about the stud action in tension, uni-axial strain gauges were also placed on the shanks of the studs at about two thirds of the stud height under head for a number of stud locations. Prior to placing concrete, these were protected by a waterproof coating. All strain gauges and LVDT's were read from the

OPTILOG Data Acquisition System linked to an IBM PC.

The same test procedure was followed for all test specimens. At the start of each test, several cycles of load at a low level were applied to seat the supports and loading system and to relieve residual stresses. Load was then applied in small increments of about 4 kN up to about 50% of the estimated ultimate load, and cycled several times at this load level to resemble the loading condition on the floor in a realistic way, then continued up to failure.

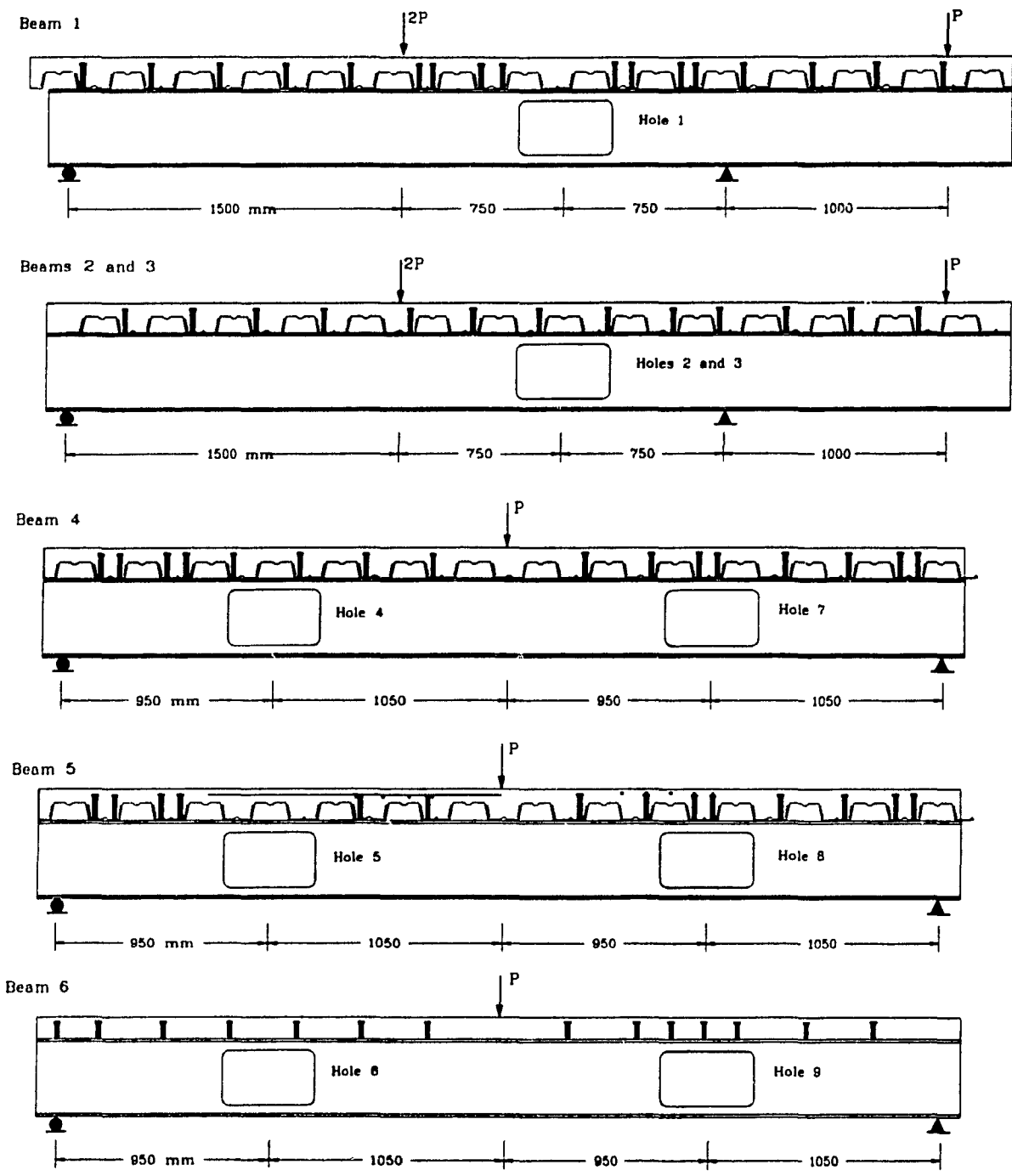


Figure 5.1 Test Beams.

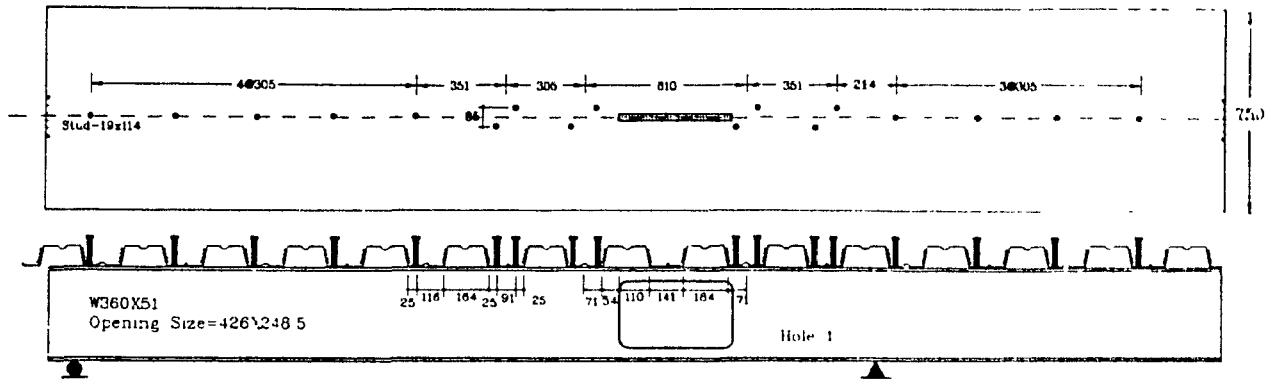


Figure 5.2 Details of Beam 1 (Hole 1).

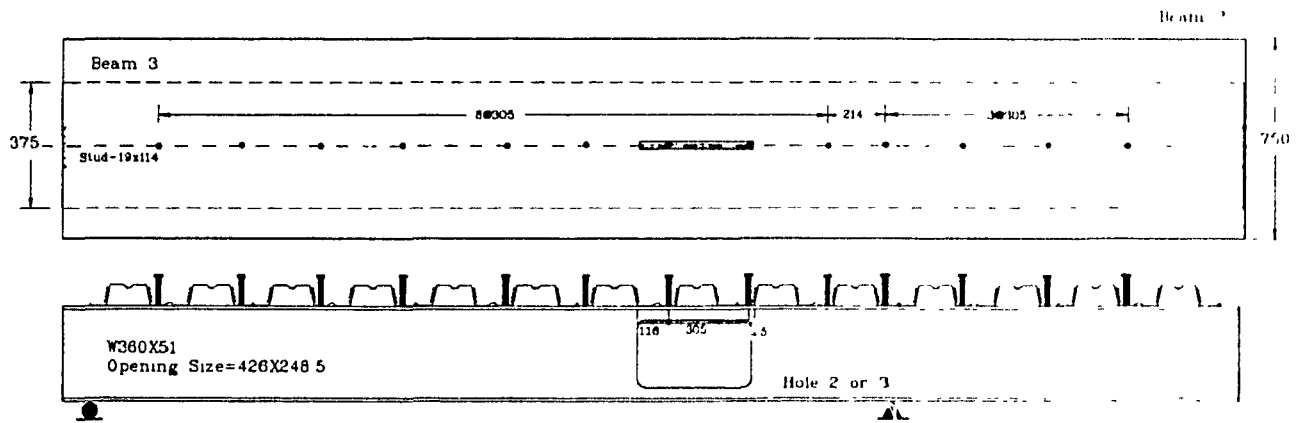


Figure 5.3 Details of Beams 2 (Hole 2) and 3 (Hole 3)

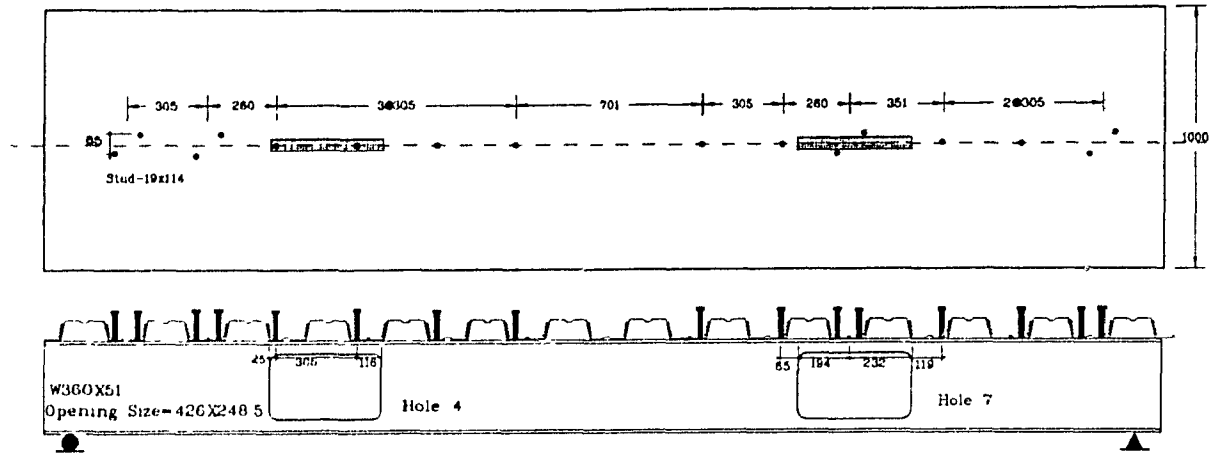


Figure 5.4 Details of Beam 4 (Holes 4 and 7).

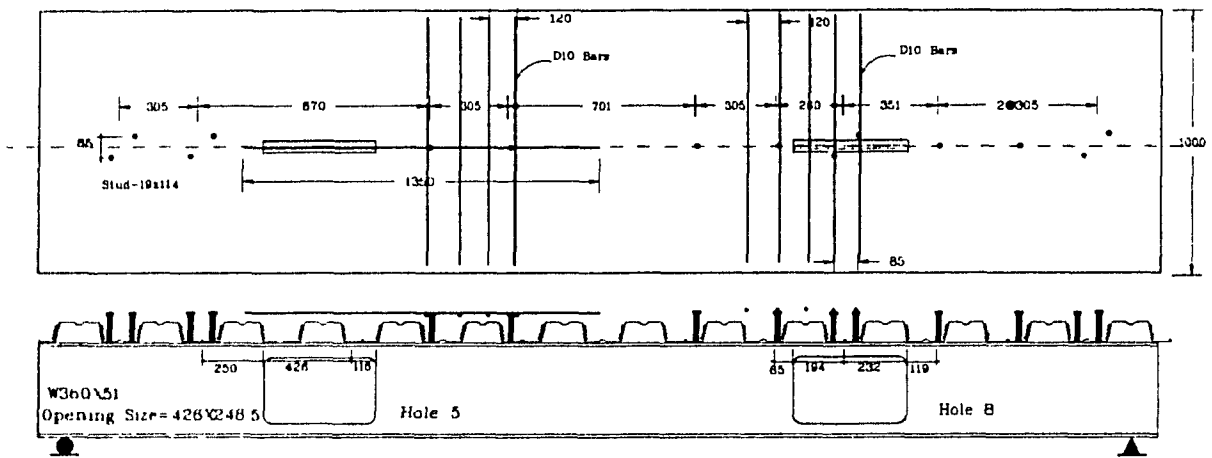


Figure 5.5 Details of Beam 5 (Holes 5 and 8).

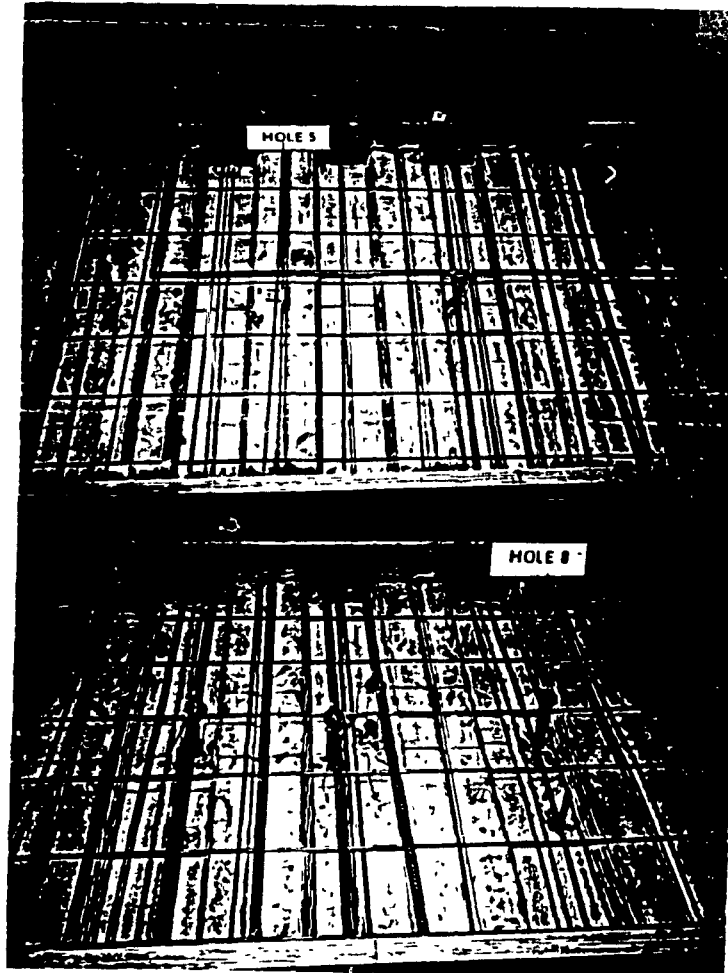


Figure 5.6 Stud Detailing for Holes 5 and 8

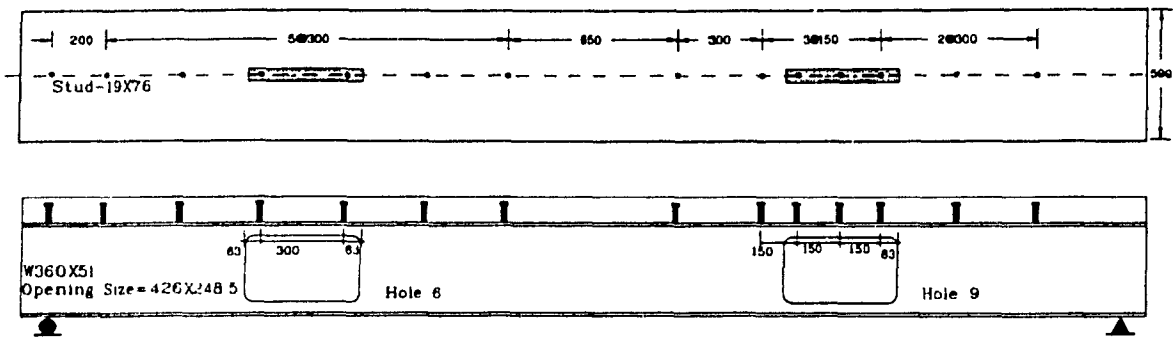


Figure 5.7 Details of Beam 6 (Holes 6 and 9).

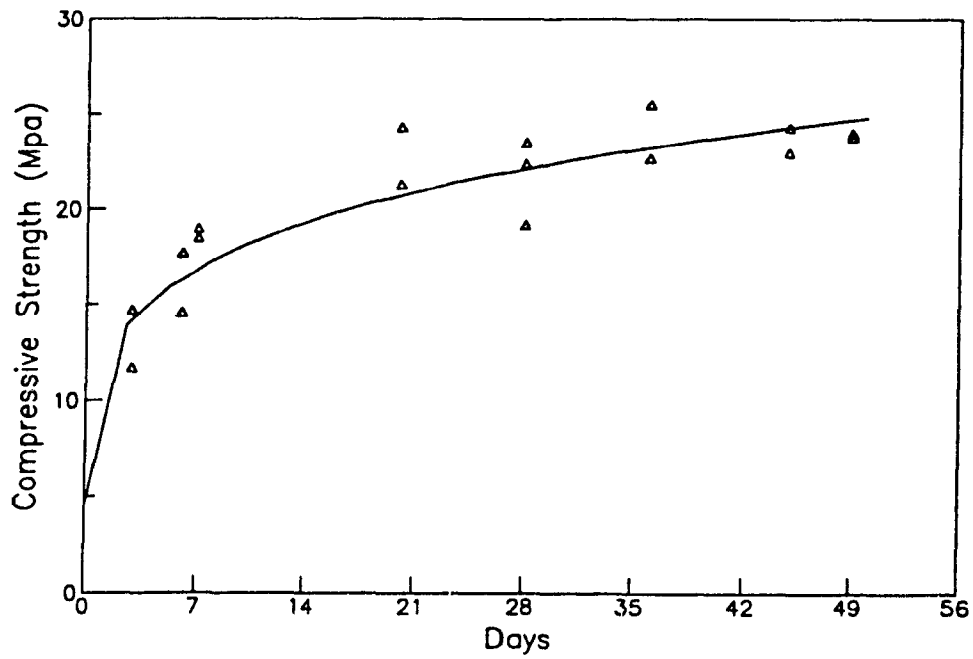
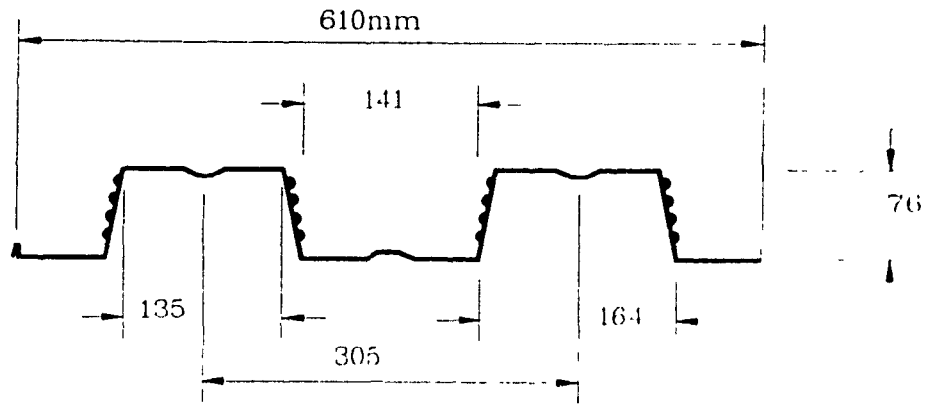


Figure 5.8 Concrete Strength During Testing Period.



Thickness=0.97mm (20gauge)

Figure 5.9 Deck Profile

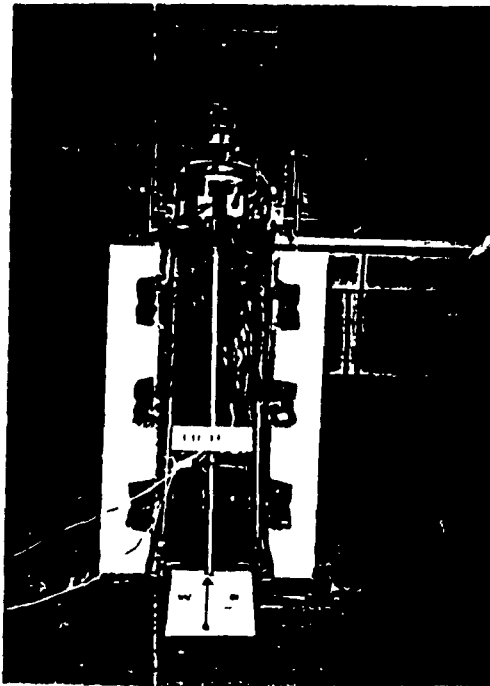


Figure 5.10 Test Setup for Push-out Specimens

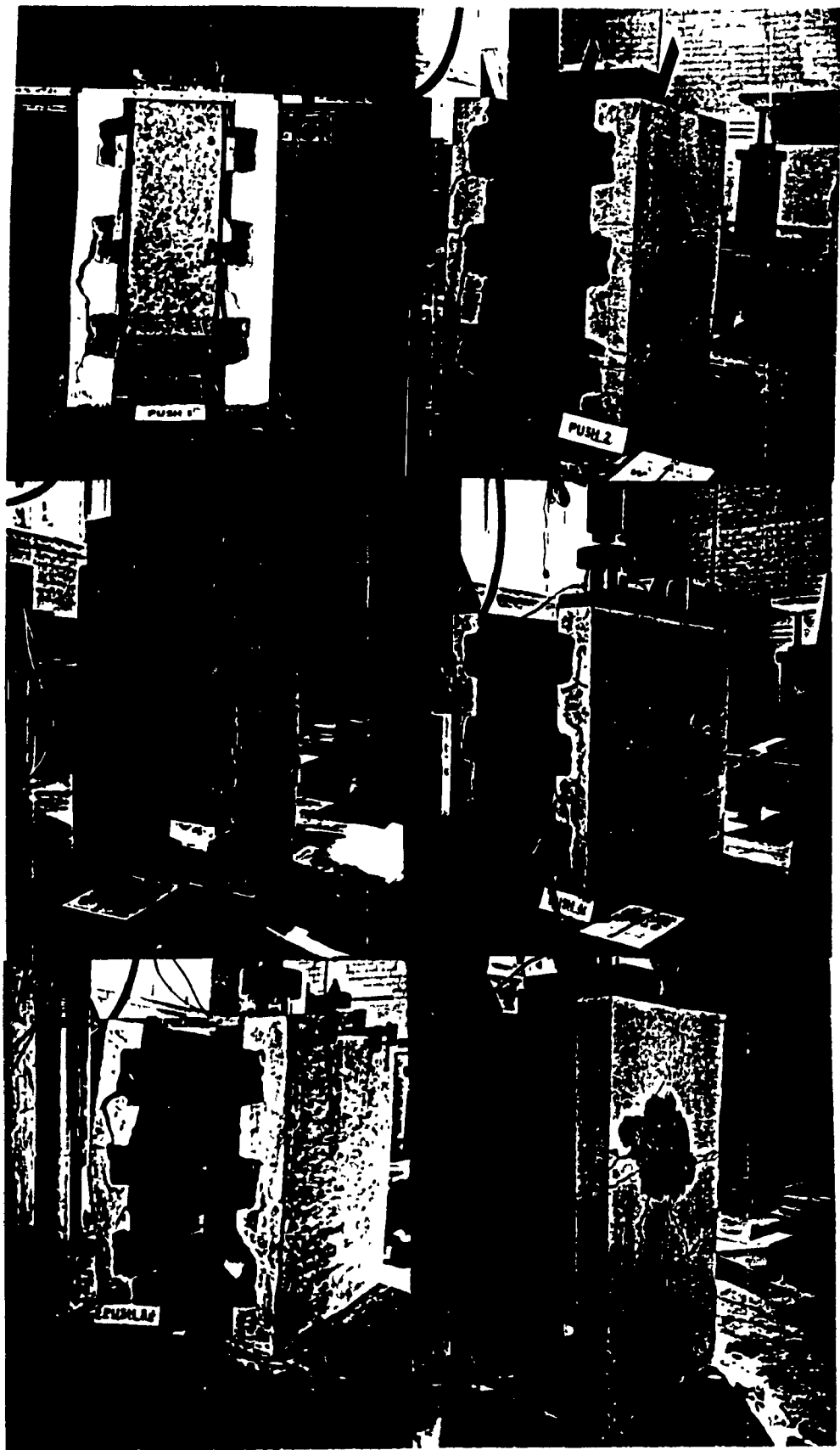


Figure 5.11 Failure Modes for Push-out Tests

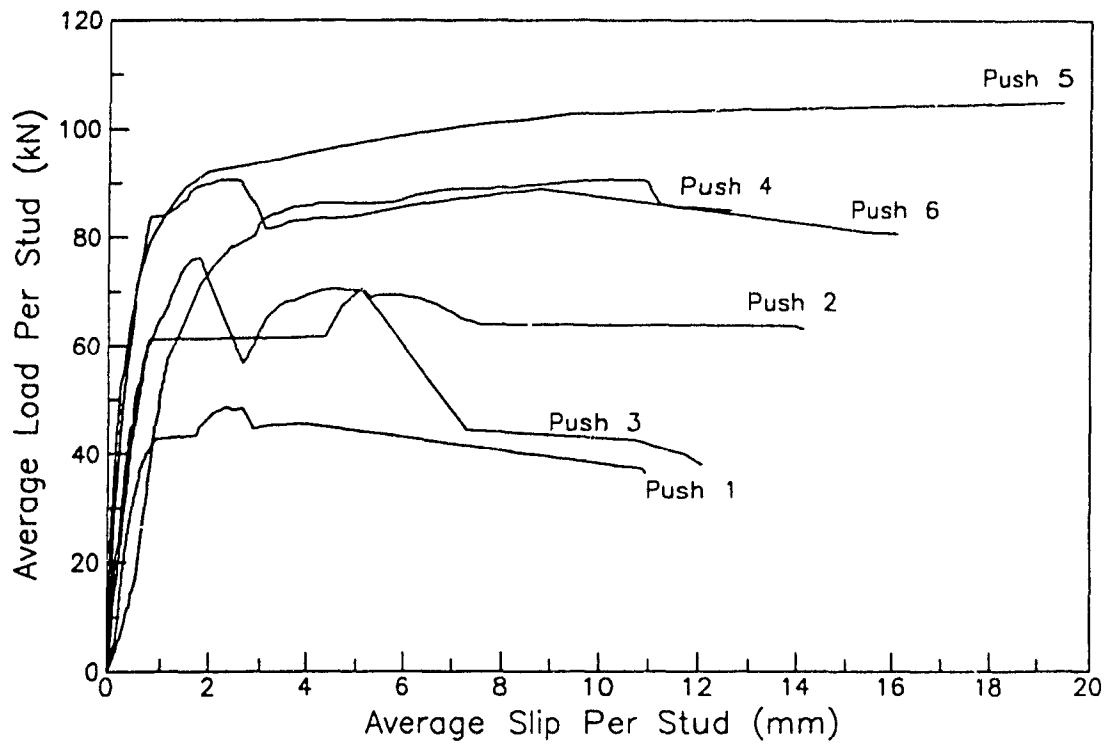


Figure 5.12 Shear Load Versus Slip on Push-out Tests

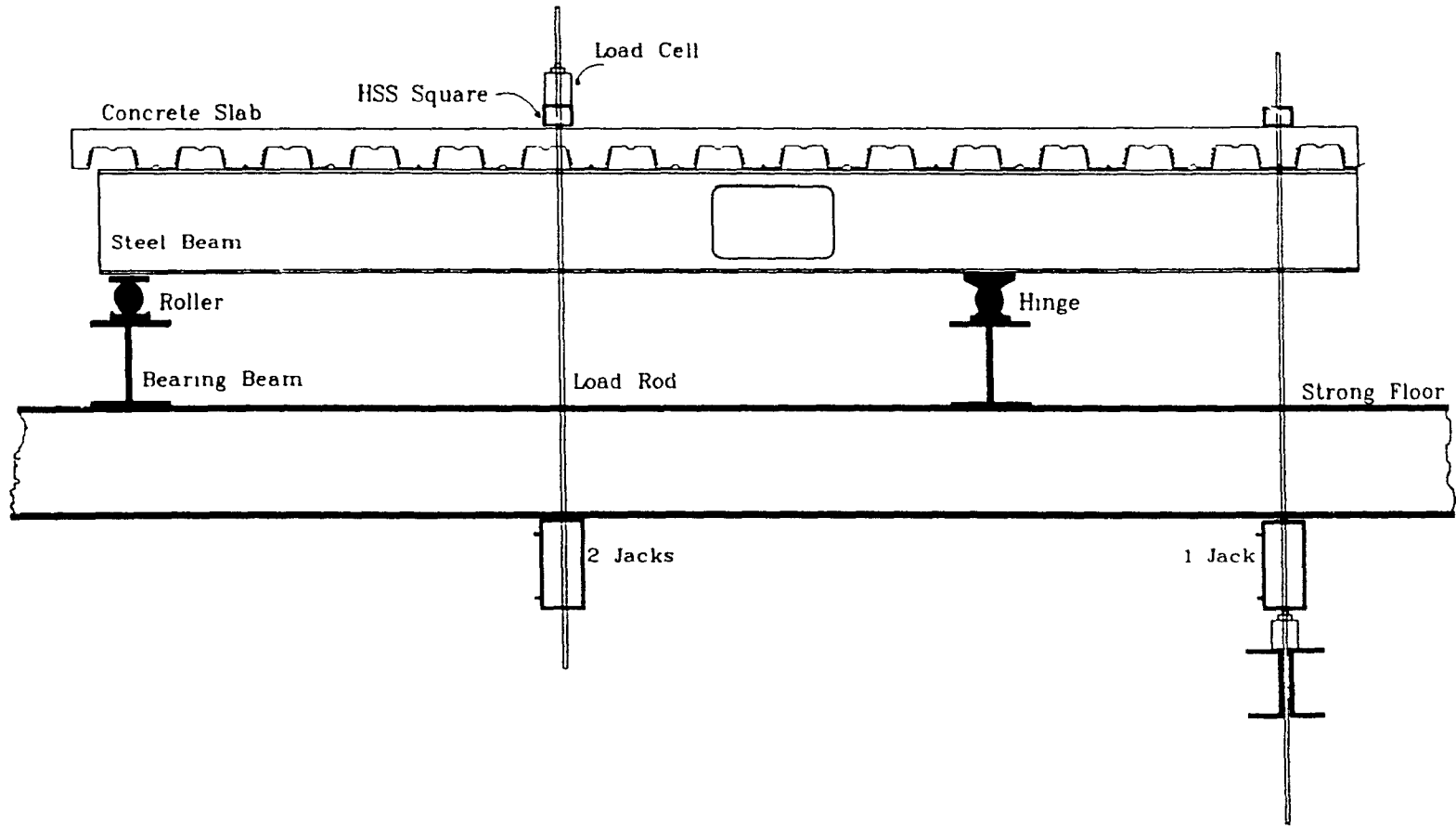


Figure 5.13 Loading System

Table 5.1 Geometric Properties of Test Specimens.

Beam No.	Hole No	M/V of Opening (m)	Steel Beam Dimensions* (mm)				Hole Dimensions** (mm)		Slab Dimensions+ (mm)			No of Studs	
			<i>d</i>	<i>b</i>	<i>t</i>	<i>w</i>	<i>2a</i>	<i>2H</i>	<i>t_s</i>	<i>T_s</i>	<i>b_e</i>	<i>n</i>	<i>n_h</i>
1	1	0 0	357 0	173 5	10 86	7 58	424	246	67	143	758	4	0
2	2	0.0	358 0	171 0	11 55	7.36	424	247	69	145	750	4	2
3	3	0 0	359 5	171 5	10.64	7.90	425	248	67	143	380	4	2
4	4	0 95	357 8	171 0	11 56	7 40	425	248	68	144	1005	6	2
	7	1 05	357 8	171 0	11 56	7 40	423	247	68	144	1005	6	2
5	5	0 95	358 5	171.1	11 52	7.36	424	247	67	143	1005	4	0
	8	1 05	358 5	171 1	11 52	7 36	424	248	67	143	1005	6	2
6	6	0 95	358 3	171 5	11 51	7 32	425	246	104	104	510	5	2
	9	1 05	358 3	171 5	11 51	7 32	425	247	104	104	510	5	2

* Designation of steel beam is W360x51

** Nominal size of hole is 426x248 5mm (1 2dx0 7d)

+ Nominal thickness of ribbed Slab is 65mm (*t_s*) and 141mm (*T_s*), and of solid slab is 100mm

Nominal width of slab for Beams 1 and 2 is 750mm,

for Beam 3 375mm, for Beams 4 and 5 1000mm, and for Beam 6 500mm

Table 5.2 Summary of Concrete Strengths.

Test Beam	f'_c (MPa)	Age (Days)
1	24.4	44
2	24.6	46
3	24.9	50
4	22.7	31
5	22.2	27
6	23.8	38

Table 5.3 Material Properties of Steel Sections.

Beam No	*Flange				*Web			
	F_{yf} (MPa)	F_u (MPa)	Elong (%)	Red in Area (%)	F_{yw} (MPa)	F_u (MPa)	Elong (%)	Red. in Area (%)
1	335.0	453.2	37	64	345.5	460.9	34	59
2	301.5	476.6	42	71	347.5	481.0	38	65
3	329.0	508.0	37	62	339.5	503.8	35	57
4	312.5	477.5	38	70	331.0	484.7	38	68
5	303.5	479.0	36	71	334.0	488.2	38	68
6	306.5	476.6	35	70	332.0	487.0	36	64

* Average values from a minimum of two coupons are given, and are based on a 50mm gauge length

Table 5.4 Summary of Push-out Test Results.

Test* Specimen	No of Studs per Slab	Stud Size $d_s \times H_s$ (mm × mm)	f'_c (MPa)	Slab Width (mm)	Stud Resistance (kN per Stud)		Initial Stiffness (kN/mm per Stud)
					AISC	Test	
1	4	19x114	24.6	750	66.6	52.0**	69.4**
2	2	19x114	24.9	750	97.4	76.1	101.5
3	2	19x114	24.9	375	97.4	70.5	89.1
4	2	19x114	23.6	1000	94.0	90.6	81.2
5+	2	19x114	21.5	1000	87.0	105.0	203.8
6++	2	19x76	23.8	500	110.0	90.5	171.2

* Each specimen corresponds to the corresponding beam specimen

** Adjusted from the values given in Test 2 corresponding to the AISC strength

+ Transverse bars welded to the heads of the studs

++ Solid slab test

CHAPTER 6

EXPERIMENTAL RESULTS

6.1 Introduction

Test results described in the following consist of two parts. In the first, the overall aspects on the opening behaviour are treated by means of investigating load-deflection relationships, measured strains as well as the first occurrence of slab cracking. Then, the second part deals with the specific slab behaviour in carrying vertical shear forces, in association with stud configurations, the width of the concrete slab and detailing of the studs around the hole.

Predictions of the ultimate strength by the simplified slab shear and truss models are given. Elastic deflections predicted with the truss concept are also provided.

6.2 Overall Behaviour

Relative deflections between hole ends for all test specimens are shown in Figs. 6.1 to 6.3, in which they are grouped based on the moment-to-shear ratios at the hole centerlines.

The first group includes Holes 1, 2 and 3, which were tested with the pure shear loading condition at their centerlines. The actual M/V ratio of Hole 1 corresponded to 118mm due to 80% of the designed load being applied at the tip of the external span.

All three holes had the same number of shear connectors between the high moment end of the opening and the support (4 studs), but within the hole length, two of those studs were placed in Holes 2 and 3, while no studs were in Hole 1. Further, note that Hole 3 had half the slab width compared with that used in the other two holes. As indicated by load deflection curves in Fig. 6.1, Hole 1 (143.1 kN(2P)) shows the highest strength out of three holes even though its initial stiffness is less than Hole 2 and similar to that of Hole 3. It is further indicated that Holes 2 (109.3 kN) and 3 (106.2 kN) failed at almost the same load level, although there is a significant reduction in the stiffness for Hole 3 and much greater ductility associated with the smaller width of the concrete slab used.

In the second and third groups, Holes 4, 5 and 6 which were tested with the moment-to-shear ratio of 950 mm at their centerlines, and Holes 7, 8 and 9 with ratio equal to 1050 mm are shown (see Figs. 6.2 and 6.3).

Holes 4 and 5 comprised four studs between the low moment end of the opening and the support in the same pattern. However, within the hole length two additional studs were provided in Hole 4, and no studs in Hole 5. In Hole 5, instead of shear connection, an additional longitudinal bar was welded to the heads of the studs located beyond the high moment end of the opening, and then it was extended over the other end of the opening. With this detailing of studs, Hole 5 (183.6 kN) exhibited a surprisingly large increase of the ultimate strength up to that given in Hole 4(183.9 kN) having two additional studs within the hole length, even though a large difference in the stiffnesses was found between two holes.

Holes 7 and 8 were the same in every aspect except that Hole 8 had additional transverse bars were welded to the heads of the studs near the high moment end of the opening on the same reason given in Hole 5. With these additional transverse bars to enhance vertical resistance of the studs, a 13% increase in the ultimate load carrying capacity was achieved in Hole 8 compared with Hole 7. In relation to this, it is also of

interest to note that in the push-out tests a 16% increase was achieved under the same situations (Tests 2 and 3).

Holes 6 and 9, which were constructed with the solid slab, comprised five studs between the high moment end of the opening and the support. But within the hole length, two and three of those studs were assigned for Holes 6 and 9 respectively. A 15% increase in the ultimate load carrying capacity was achieved in Hole 9 compared with Hole 6, and a similar stiff behaviour was observed in both holes.

Longitudinal strains measured on the steel flanges as well as steel tee webs above and below the opening are shown in Figs. 6.4(a) to (i). In most tests, these measured strains are quite consistent with the stress distributions assumed for the ultimate strength analysis. High strains are found in the web near the hole edges, and initial yielding is evident at a relatively low load level. For all specimens except for Hole 5, first yielding occurred in the bottom tee web at the low moment end of the opening or in the top tee web at the high moment end.

Shear strains obtained from the rosettes on the webs of the four tees are shown in Figs. 6.5(a) to (i). In most cases, these strains showed the increasing trend up to near the ultimate load level. High strains are found in the top as well as bottom tee webs, which might be indicating that "vertical shear transfer" from the concrete slab to the steel beam does not necessarily occur at the sections coincident with the edges of the holes where strain gauges were attached, since it will depend upon the locations of the studs. Also, note that the magnitude of these strains is in proportion to the degree of contribution given by the concrete slab for various conditions of shear connection.

In all specimens, transverse cracks occurred first in the top of the slab near the low moment end of the opening at a range of 10 % to 49% of the ultimate load. As load was increased, longitudinal cracks near the hole or load points (except for Holes 3, 4 and 7) were also accompanied at an average 59 % of the ultimate load for ribbed slabs, and 83 % of the ultimate load for solid slabs. In solid slab specimens, a quite

severe longitudinal cracks occurred, resulting from the use of the smaller width of the concrete slab as well as the smaller longitudinal spacing of the studs (Hole 9). However, all longitudinal cracks which occurred in Holes 6 and 9 did not seem to have significant effect on the opening and beam behaviour at either ultimate or serviceability load levels. More discussion of this will be given later. All ribbed slab tests except for Hole 8 exhibited a rib separation type of crack at the stud locations near the high moment end of the opening, whereas in Hole 8 a diagonal tension crack similar to that found in solid slabs was developed due to the enhanced vertical resistance of the studs provided.

Larger interfacial slips between the concrete slab and the steel section were recorded in the hole regions than at the ends of the beams for all specimens (see Figs. 6.6(a) to (f)). Test results described above are summarized in Table 6.1

6.3 Slab Behaviour

A typical shear crack pattern observed in all ribbed slab tests can be described stepwise as shown in Fig. 6.7(a). At a first stage, part of a tension cone crack was formed at the nearest stud to the high moment end of the opening in the low moment side of the flute. This occurred at an average of about 59 % of the ultimate load. Then, this crack propagated towards the high moment end of the opening, while at the same time the other part of a tension cone crack was developed in the high moment side of the flute. Finally, near collapse these cracks were fully extended towards each end of the opening and towards the load point, resulting in a diagonal tension type of cracking.

In solid slab specimens, the first significant crack was observed on the soffit of the concrete slab at a load of about 72 % of the ultimate load level. This crack was initially located adjacent to the beam-axis near the low moment end of the hole, and then spread towards the edges of the slab in a chevron shape as load was increased.

Near collapse, the chevron shaped crack on the soffit of the concrete slab was dispersed diagonally through the slab thickness linking top and bottom parts of the slab at high and low moment ends of the opening respectively. Finally, this resulted in a diagonal tension type of crack in solid slabs. Further, this diagonal tension crack propagated towards the load point (see Fig. 6.7(b)).

6.3.1 Stud Configurations

In the truss analogy, the configuration of the studs in the hole region is of critical importance in determining the slab shear carrying capacity, since it will affect the geometrical arrangement of inclined compression struts.

Ribbed Slabs

Holes 1 and 2 represented different arrangements of the studs in the hole region, even though they were identical in all other aspects such as the hole geometry and loading condition. The slab crack patterns after failure for Holes 1 and 2 are shown in Figs. 6.8 and 6.9 respectively.

For Hole 1, due to the absence of shear connection within the length of the hole, an inclined strut involving the nearest studs beyond the hole length was expected in a flat angle of inclination. From the observed crack pattern, however, it is difficult to see whether or not the expected diagonal compression strut was developed by linking the nearest studs beyond the hole length. Only the stud action in tension near the high moment end of the opening is clearly visible. No clear indication was found concerning the stud action providing bearing near the low moment end of the opening.

With respect to this, measured strains on the shanks of the studs near the ends of the hole indicated that the studs at both high and low moment ends of the hole were highly strained with similar magnitude of vertical tensile strains, and were bent towards the high moment side of the flute (see Fig. 6.10). This might be a major reason for the significantly higher ultimate strength obtained for the stud configuration used in

Hole 1 (143.2 kN), compared with that given in Hole 2 (109.3 kN). Therefore, it can be deduced that the studs near the low moment end of the hole must have participated in carrying vertical shear, even though the formation of the bearing zone at this location is not obvious. In addition, at a load of 63% of the ultimate load (90 kN) for Hole 1, transverse cracks appeared in the top of the slab near the high moment end of the opening, and these as well as previous cracks at the low moment end served to make the slab between these cracks act in a rigid body mode.

For Hole 2 involving the uniform distribution of shear connection along the whole beam span, diagonal compressive struts linking the heads of the studs and the bases of the nearest studs were well developed in the hole region as would be expected (see Fig. 6.9). A smaller spacing of transverse cracks was found on the top surface of the slab compared with Hole 1. Further, vertical strains measured on the shank of the studs in their compression or tension sides near or far from the hole region indicated that the studs placed near the hole region were much more severely strained than those placed apart from the hole region (see Fig. 6.11). With this test evidence, it can be considered that only the studs near the hole region reach their ultimate capacities when the beam fails.

Different arrangements of the studs along the hole length were also considered in Holes 4 and 7. Hole 4 had two ribs within the hole length in which each rib contained a single stud, while Hole 7 had one rib with a pair of studs. As a result, the numbers of studs between the high moment end of the opening and the support, and within the hole length were identical in both tests. The slab crack patterns after failure for Holes 4 and 7 are shown in Figs. 6.12 and 6.13 respectively.

Both holes behaved in a similar manner except that a uniform pattern of transverse cracks on the top surface of the slab was developed in Hole 4. At 80% of the ultimate load, both holes exhibited a tension cone type of crack in the low moment side of the flute near the high moment end of the hole. Near collapse, another (Hole 4) or

several (Hole 7) transverse cracks occurred near the low moment end, while previous tension cone cracks were widened and propagated towards the load point. With the double studs placed in a rib along the hole length, a 15% increase of the ultimate load carrying capacity for Hole 7 (210.3 kN) was obtained compared with Hole 4 (183.6 kN). After removing the cracked slab at Hole 7, the slab takes a form as shown in Fig. 6.14, and it is shown that reinforced bars passing through the diagonal crack were in dowel action.

Solid Slabs

Holes 6 and 9 also incorporated different stud arrangements along the hole length, while the same number of studs were provided between the high moment end of the opening and the support. The slab crack patterns after failure for Holes 6 and 9 are shown in Figs. 6.15 and 6.16 respectively.

Unlike ribbed slabs, transverse cracks also developed in the bottom of the slab at the high moment end of the opening at an average 50% of the ultimate load. As would be expected, Hole 9 comprising three studs within the hole length failed at a higher load (191.6 kN) corresponding to a 15% increase of the ultimate load carrying capacity compared with Hole 6 (167.2 kN) having two studs within the hole length. Prior to development of a diagonal tension crack in both tests, a chevron shaped crack with its apex towards the low moment end of the hole was formed on the soffit of the concrete slab near the low moment end of the hole as shown in Fig. 6.17. Then, the diagonal crack through the slab thickness was initiated from the bottom of the slab where a chevron shaped crack was formed. This crack pattern in solid slabs indicated that the bearing zone to anchor the diagonal strut was formed in the bottom part of the slab where the severe negative curvature of the top steel flange occurred. From the crack development described, it can be also judged that failure of the bearing zone resulted in the diagonal tension type of crack.

6.3.2 Slab Width

The truss analogy indicated that the magnitude of vertical shear carried by the concrete slab is largely dependent upon the vertical resistance of the shear connectors provided. Therefore, the reduction of the slab width should not influence the slab shear carrying capacity if there is a sufficient width of the concrete slab to develop the full stud tension cones.

To verify this, Hole 3 had half the slab width compared with Hole 2, while all other parameters were identical in both tests. Figures 6.9 and 6.18 show the slab crack patterns after failure for Hole 2 and 3 respectively. Both holes failed at the almost same load level, although Hole 3 showed a much less stiff behavior. In this regard, the truss concept in which the slab shear carrying capacity is related to vertical resistance of the studs can be justified. Both holes behaved in a similar manner except that Hole 3 caused more severe transverse and rib separation cracks.

With the smaller width of concrete slab, a very clear observation of the diagonal compressive struts as they spread from the heads of the studs and are anchored at the bases of the nearest studs was made as shown in Fig. 6.18. Measured strains on the shanks of the studs around Hole 3 are shown in Fig. 6.19

Holes 6 and 9 with a solid slab also had half the required width of the slab to compare with that recommended for full flexural beam action. Due to the use of a narrower width of concrete slab, some longitudinal cracks resulted from vertical as well as horizontal dispersal of the concentrated loads at the bases of the studs into the smaller width of the concrete slab. It is however noted that the width of the concrete slab provided in the solid slab specimens was greater than the required width to obtain horizontal resistance of shear connection based on dowel action²⁷, i.e. it was sufficient to avoid longitudinal splitting of the concrete slab. Therefore, the longitudinal cracks which appeared in Holes 6 and 9 did not seem to reduce either shear connector or beam resistances. In view of this, it can be also deduced that in solid slabs, the width of the

concrete slab will not significantly affect the slab shear carrying capacity unless the longitudinal splitting of the slab governs shear connector resistance.

6.3.3 Stud Details

From the truss concept, it is obvious that if vertical resistance of the studs near the high moment end of the opening is enhanced, the slab shear carrying capacity will be increased and thereby, produce an increase in the beam ultimate resistance

To verify this, Holes 5 and 8, which were identical to Holes 4 and 7 respectively in all other aspects, included longitudinal or transverse bars welded to the heads of the studs near the high moment end of the opening. Although this way of detailing does not represent normal practice, it provides valuable information about the stud behaviour in the hole region. With the enhanced vertical resistance of the studs, it was expected that diagonal compression strut action similar to that found in solid slabs could be fully developed without premature failure associated with rib separation in Hole 8, and hopefully in Hole 5 as well.

The slab crack patterns after failure for Hole 5 and 8 are shown in Figs. 6.20 and 6.21 respectively.

Due to the absence of shear connection in the two ribs within its length, Hole 5 exhibited severe transverse and rib separation cracks concentrated at the nearest stud locations to the ends of the hole. As load was increased, transverse cracks in front of the studs near the low moment end of the hole were widened, and then finally caused separation the slab in this region. Although additional bars were provided for the prevention of the premature failure related to the pull-out failure of the studs and hopefully, for the development of a diagonal compression strut traversing two ribs, it is difficult to see whether or not the diagonal strut was developed in the way expected by linking the nearest studs to the ends of the hole. However, with the enhanced vertical resistance of the studs, this hole failed at a considerably higher load level-comparable

with that obtained with two more studs within the hole length, as in Hole 4.

Due to the uniform distribution of the studs for Hole 8, the uniform pattern of transverse cracks was observed as shown in Fig. 6.21. Although there was an indication of the rib separation type of cracking beyond its high moment end, this hole eventually failed by a diagonal tension type of crack spanning between top and bottom parts of the cover slab over the opening. This is similar to that found in solid slabs. Unlike the other pair of tests (Holes 4 and 5), a relatively small increase (13%) of the ultimate load carrying capacity was obtained between Holes 7 and 8. This can be explained from the fact that due to the significant penetration of transverse cracks from the top to bottom of the slab at the low moment end of the hole, failure of the slab might have resulted from failure of the bearing zone, and this might prevent the full utilization of vertical resistance of shear connectors provided. Measured strains on the shanks of the studs around Holes 5 and 8 are shown in Fig. 6.22. Unfortunately, information at only one stud location for each hole is available.

6.4 Predictions

6.4.1 Ultimate Strength

Ultimate strengths for the nine tests in the present study have been evaluated using both the simplified slab shear and truss models. All predicted values that define the three co-ordinates on the interaction diagram are given in Table 6.2, and predicted values are compared with experimental results in Table 6.3. Horizontal and vertical connector forces that can be resisted by one shear connector at the stage of the beam failure are also predicted by both theories and summarized in Table 6.4. Moment-to-shear interaction curves are shown in Fig. 6.23.

Concerning shear connector resistance used in the analysis for Holes 4, 5, 7 and 8 which comprise single as well as double studs in a rib, it should be noted that different

values of connector resistance need to be considered in both theories because the truss model involves shear connection in the hole region, while the simplified slab shear model requires the inclusion of all shear connection provided between the high moment end of the hole and the support. Thus, when the simplified slab shear model is applied to those tests, connector resistances corresponding to both one and two studs in a rib should be defined in the first place. To do this, connector resistance for two studs in a rib was determined from the resistance obtained in push-out tests by multiplying by the reduction factor (0.71) following the AISC approach²⁵.

Then, weighted values of connector resistance based on the corresponding numbers of single and double studs in a rib between the high moment end of the hole and the support were calculated and finally incorporated in the analysis (see Table 6.4).

In using the truss model for Holes 1, 7 and 8 in which their low moment ends are located within the ribbed part of the slab, Solution I was adopted from the fact that anchorage of the inclined struts sufficiently close to the low moment end of the hole was evident. Also, for Holes 5 and 8 having additional reinforcement welded to the heads of the studs near the high moment end of the hole, no failure related to vertical resistance of the studs was assumed, thus permitting full development of horizontal connector resistance. In these holes, however, it was not possible to consider the enhanced vertical resistance of the studs directly in the solution procedure, since the horizontal forces determined from bearing studs at the low moment end of the hole limited the magnitude of vertical forces to be developed. On the other hand, in Hole 5 no indication of diagonal compressive strut action was found in test. It is however evident from the observed crack pattern in the slab as well as measured strains on the stud that the stud having additional reinforcement welded to its head beyond the high moment end of the hole participated in carrying vertical shear forces. For this, anchorage of the inclined strut was assumed at the end of the hole rather than the location of the stud, and full development of the horizontal connector force was also

permitted in the analysis.

From the comparison given in Table 6.3, it has been found that the simplified slab shear model generally overestimates the test strength for most ribbed slabs in the present tests, while the truss model provides safe assessments of the strength for both ribbed and solid slabs. One major reason for this is that the simplified slab shear model does not account for slab failure related to stud action in tension. It is therefore considered that the simplified model is more adequate for solid slabs in which stud failure is not involved. By contrast, the truss model seems to be more adequate for ribbed slabs in that stud failure governs the beam behaviour and the geometrical arrangement of the inclined struts is more clearly determined than in solid slabs.

6.4.2 Elastic Deflections

Load-deflection response up to 60% of the ultimate load level for the nine tests has been evaluated using the analytical models proposed in Chapter 3. This analysis includes the flexibility of shear connectors in both horizontal and vertical directions, and simulates transverse cracks observed in top and bottom parts of the concrete slab at the ends of the opening using the concept of diagonal strut action. For horizontal stiffnesses of the studs, the test values obtained from the present push-out tests were used, while their vertical stiffnesses were assumed as 25 kN/mm per stud in ribbed slabs and 50 kN/mm per stud in solid slabs. These latter values were based on a number of previous tests^{28,29}.

The comparison with test results is shown in Fig. 6.24, and indicates that a generally satisfactory agreement between experimental and predicted deflections at mid-span as well as at hole ends was achieved except for Holes 1, 2 and 3 that included the negative moment region in a beam span. Note that the unsafe prediction in Holes 1, 2 and 3 resulted from the neglect of the concrete slab cracking occurred in the negative moment region.

In general, the accuracy of the prediction using the proposed analytical models is subjected to the degree of refinement for the connector behaviour by means of horizontal and vertical stiffnesses, and particularly the horizontal stiffness. Note that this is also consistent with the present test results in which relative deflections between hole ends are significantly affected by the degree as well as configuration of shear connection within and beyond the hole length. Therefore, although there exists a fundamental uncertainty in defining the connector behaviour by means of push-out or pull-out tests and a complicated modelling problem arises for the practical use, these behavioural aspects of shear connectors should be included even in elastic analysis. Otherwise, the basic behavioural aspects of the composite beam structures will be lost.

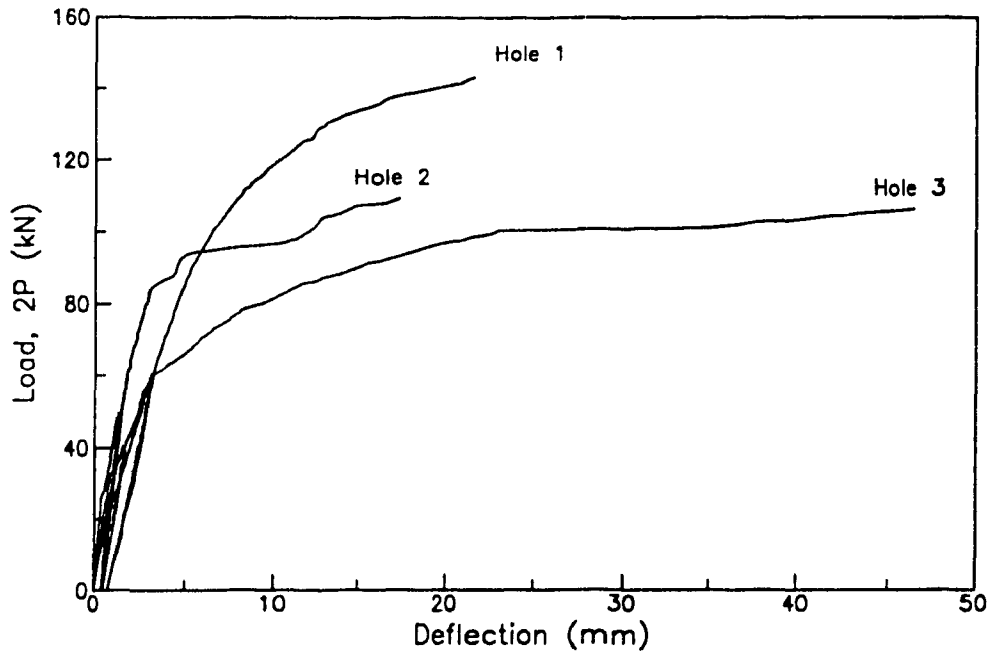


Figure 6.1 Relative Deflections Between Hole Ends ($M/V=0$).

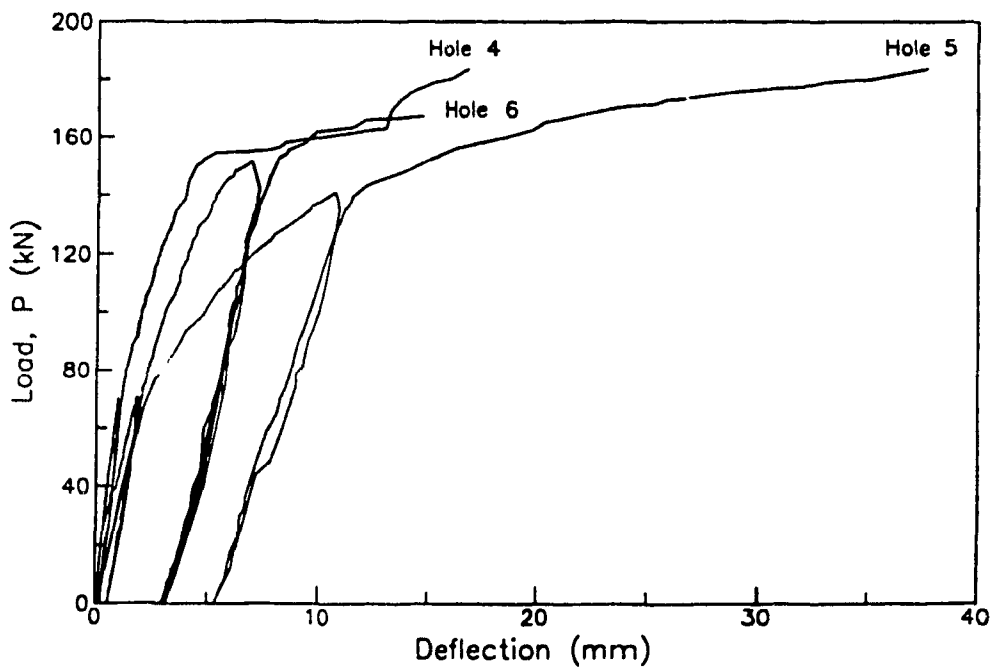


Figure 6.2 Relative Deflections Between Hole Ends ($M/V=0.50$).

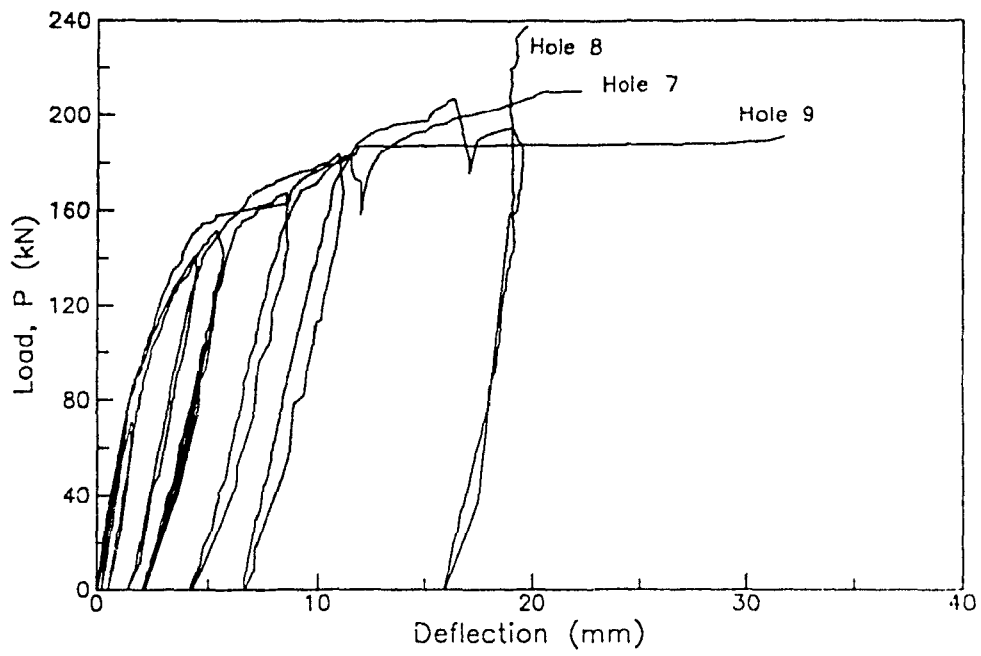


Figure 6.3 Relative Deflections Between Hole Ends ($M/V=1050$).

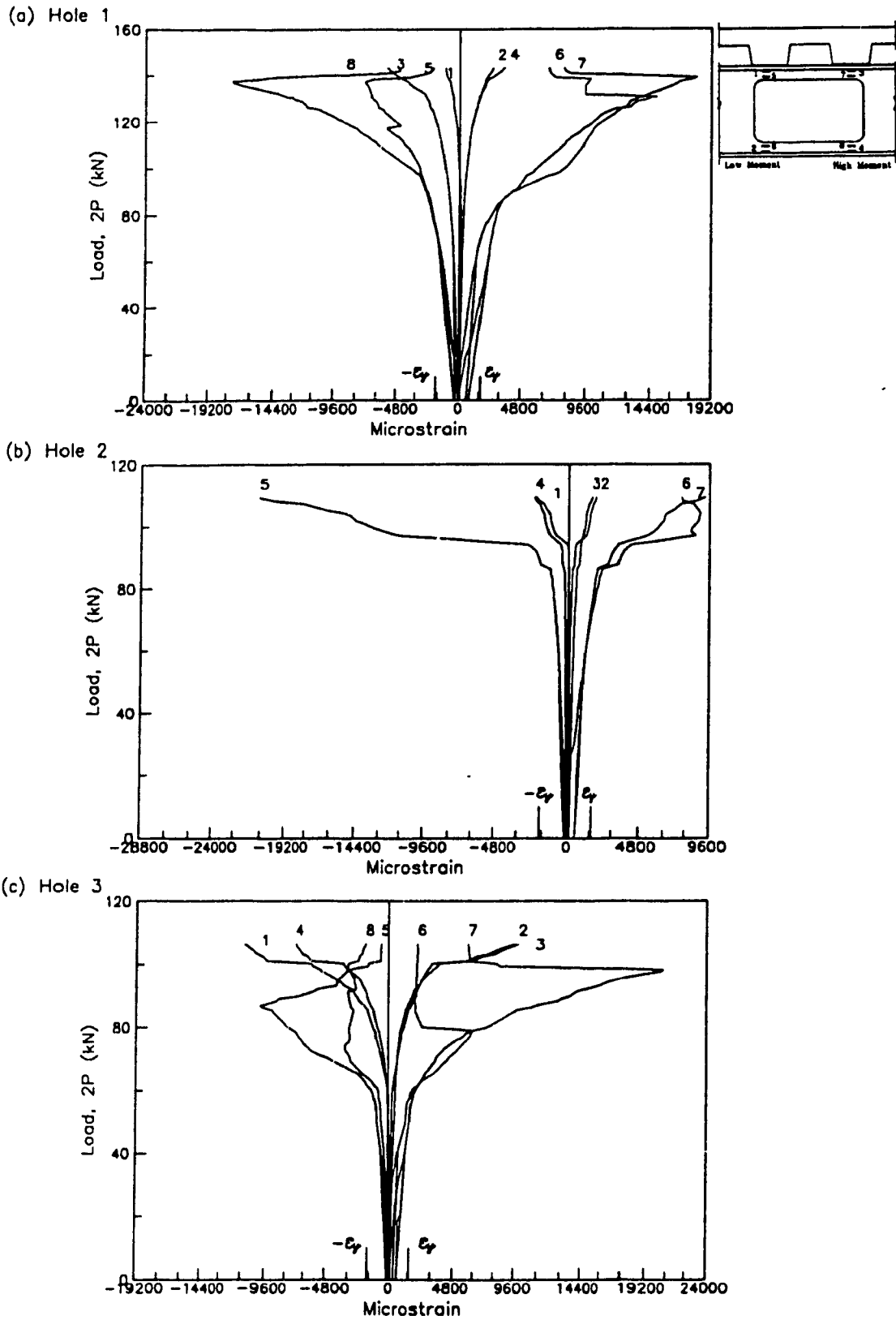


Figure 6.4 Longitudinal Strains Around Web Holes.

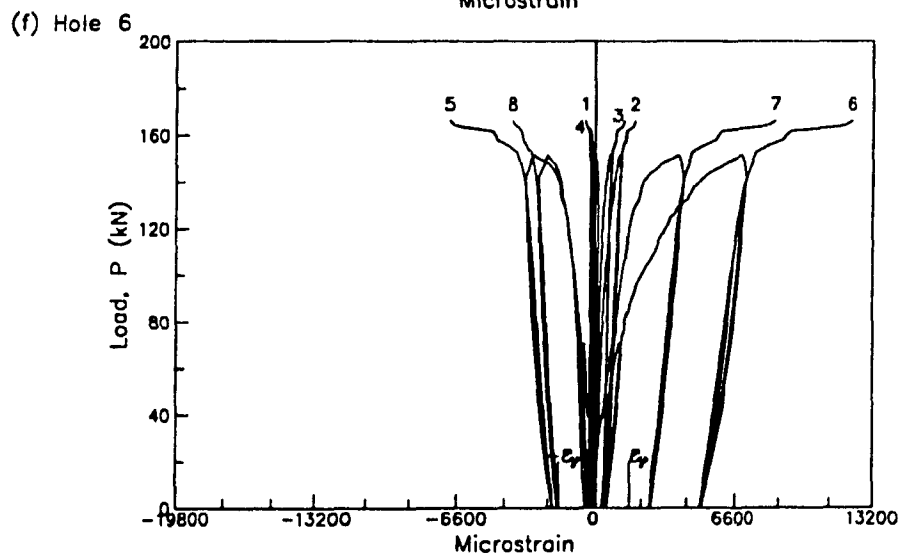
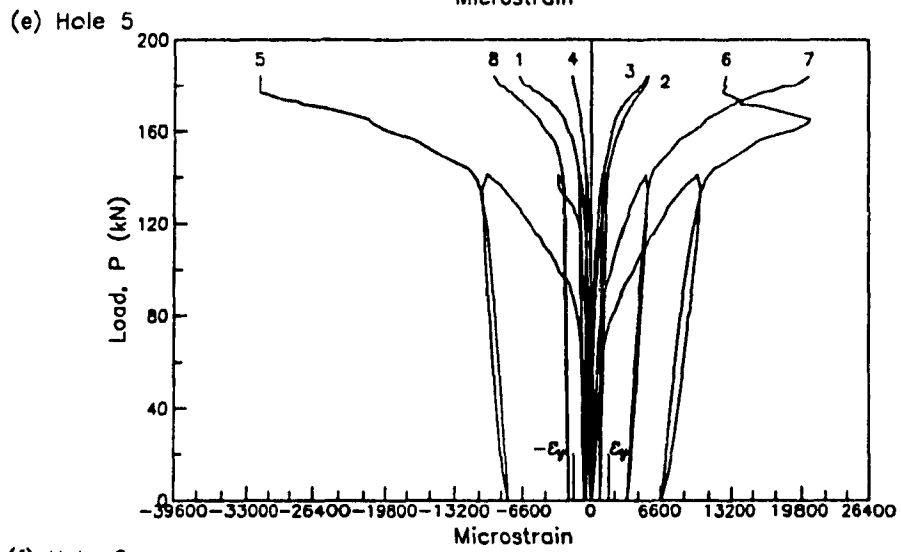
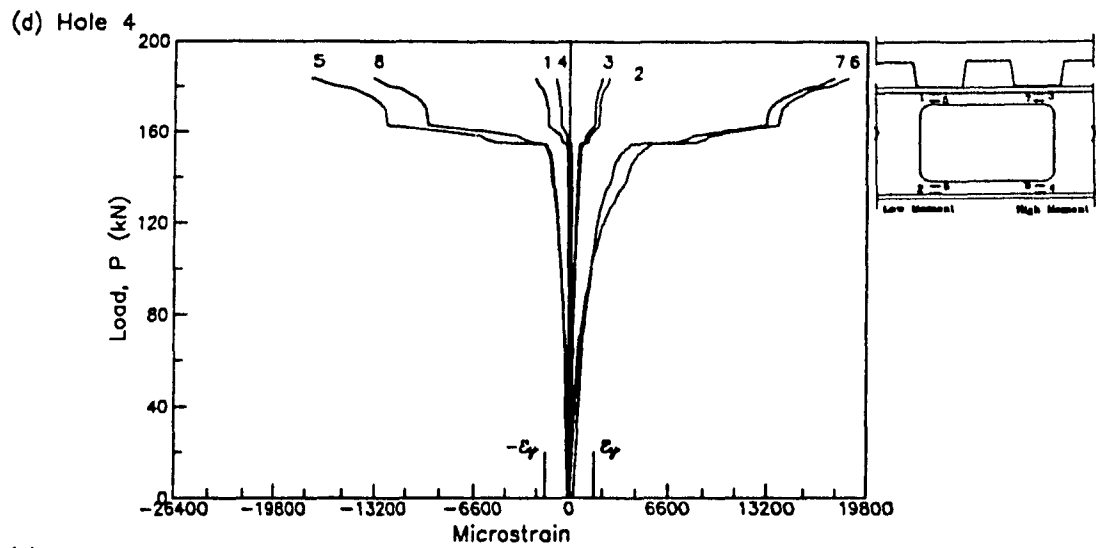
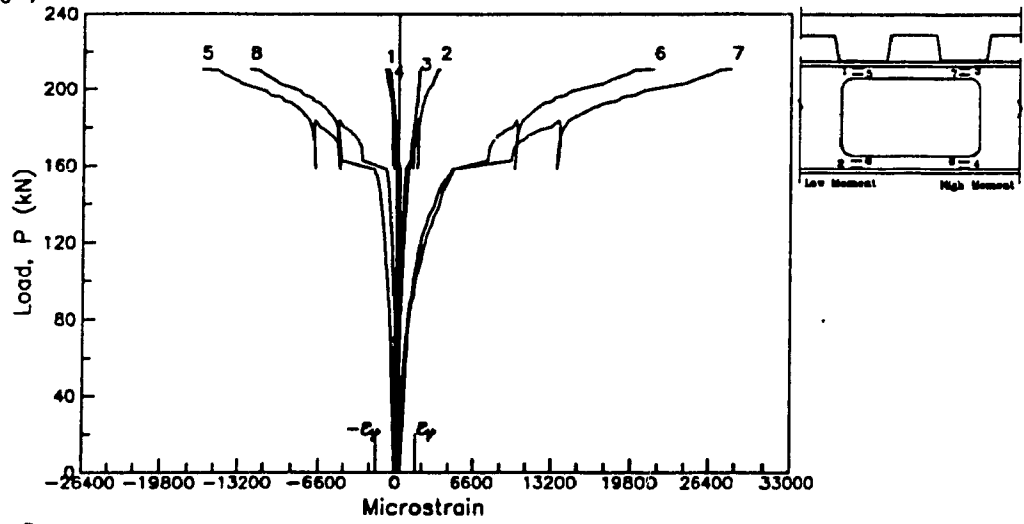
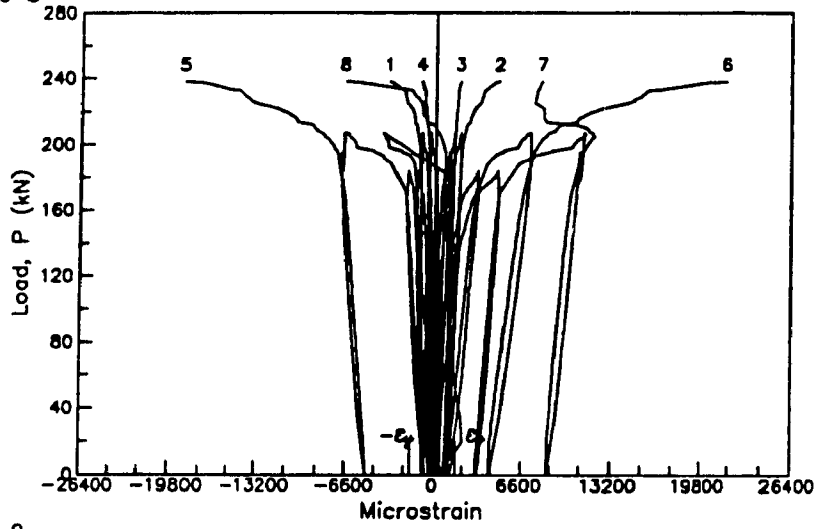


Figure 6.4 (Cont'd) Longitudinal Strains Around Web Holes.

(g) Hole 7



(h) Hole 8



(i) Hole 9

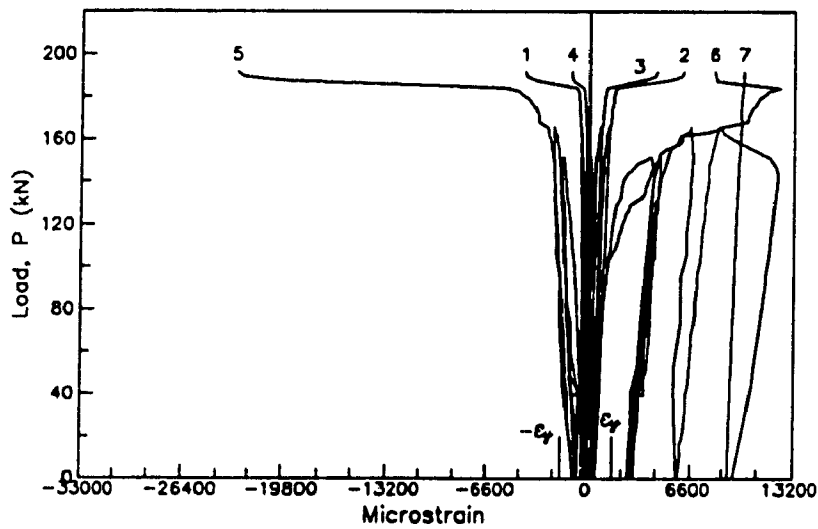


Figure 6.4 (Cont'd) Longitudinal Strains Around Web Holes.

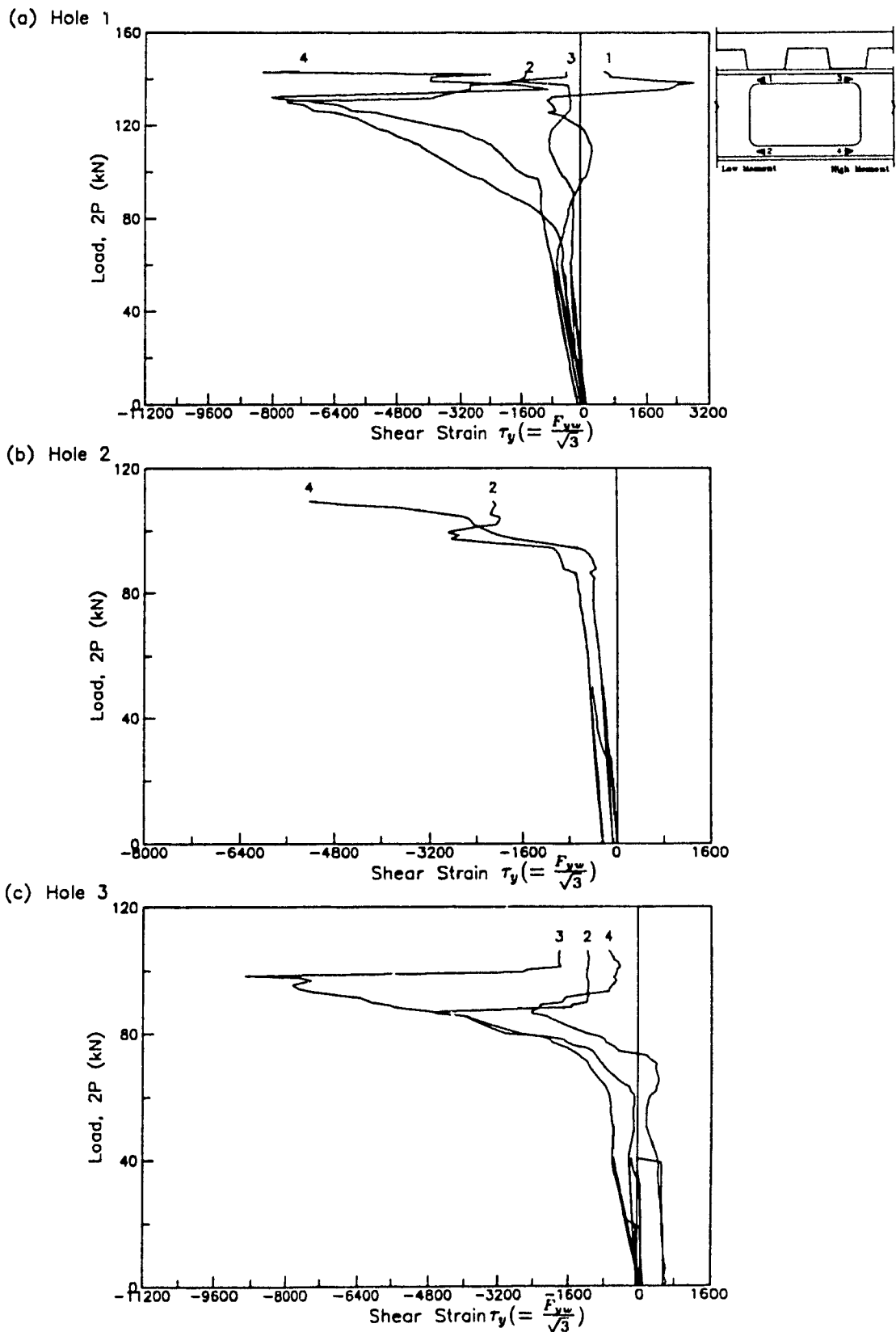


Figure 6.5 Shear Strains Around Web Holes.

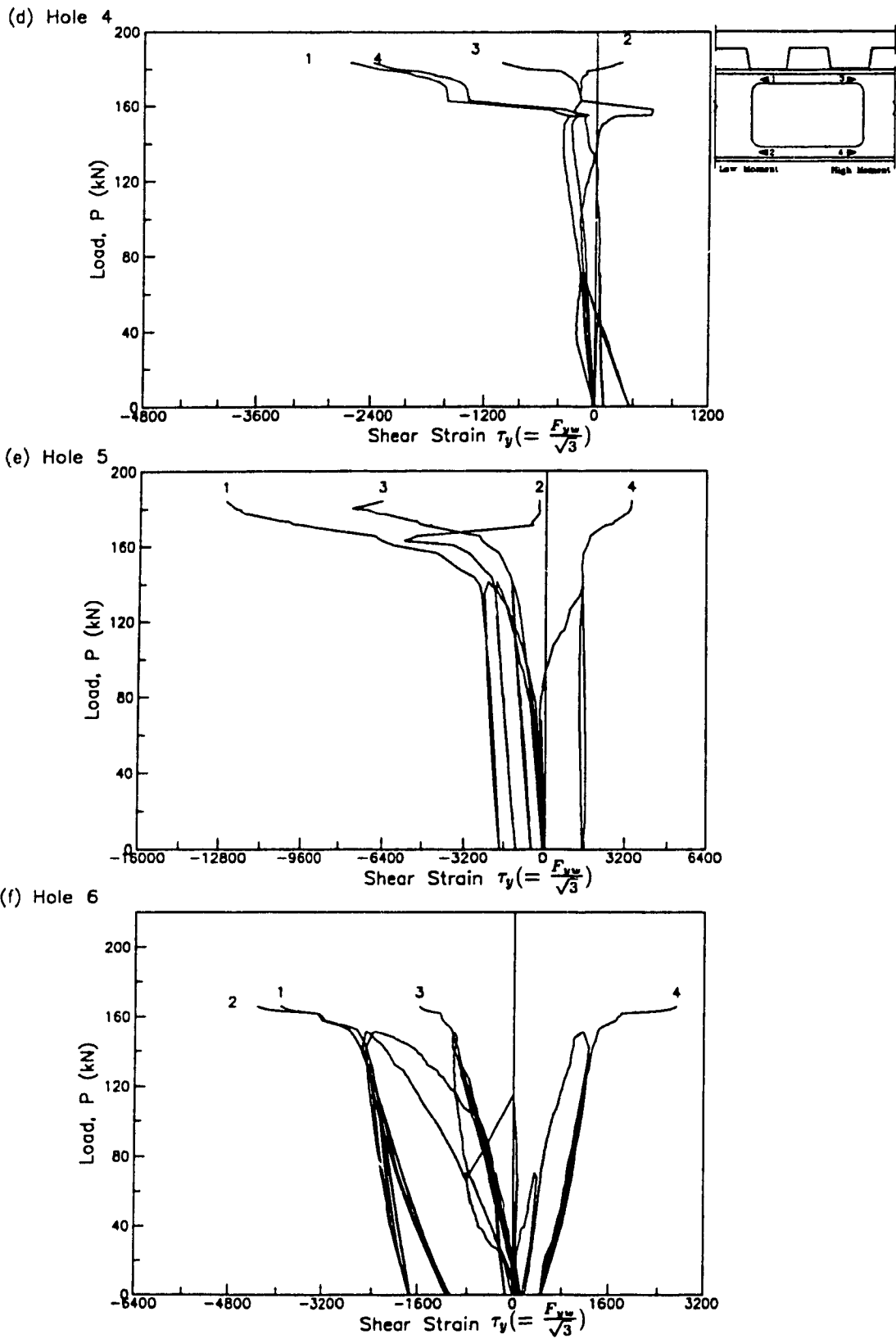


Figure 6.5 (Cont'd) Shear Strains Around Web Holes.

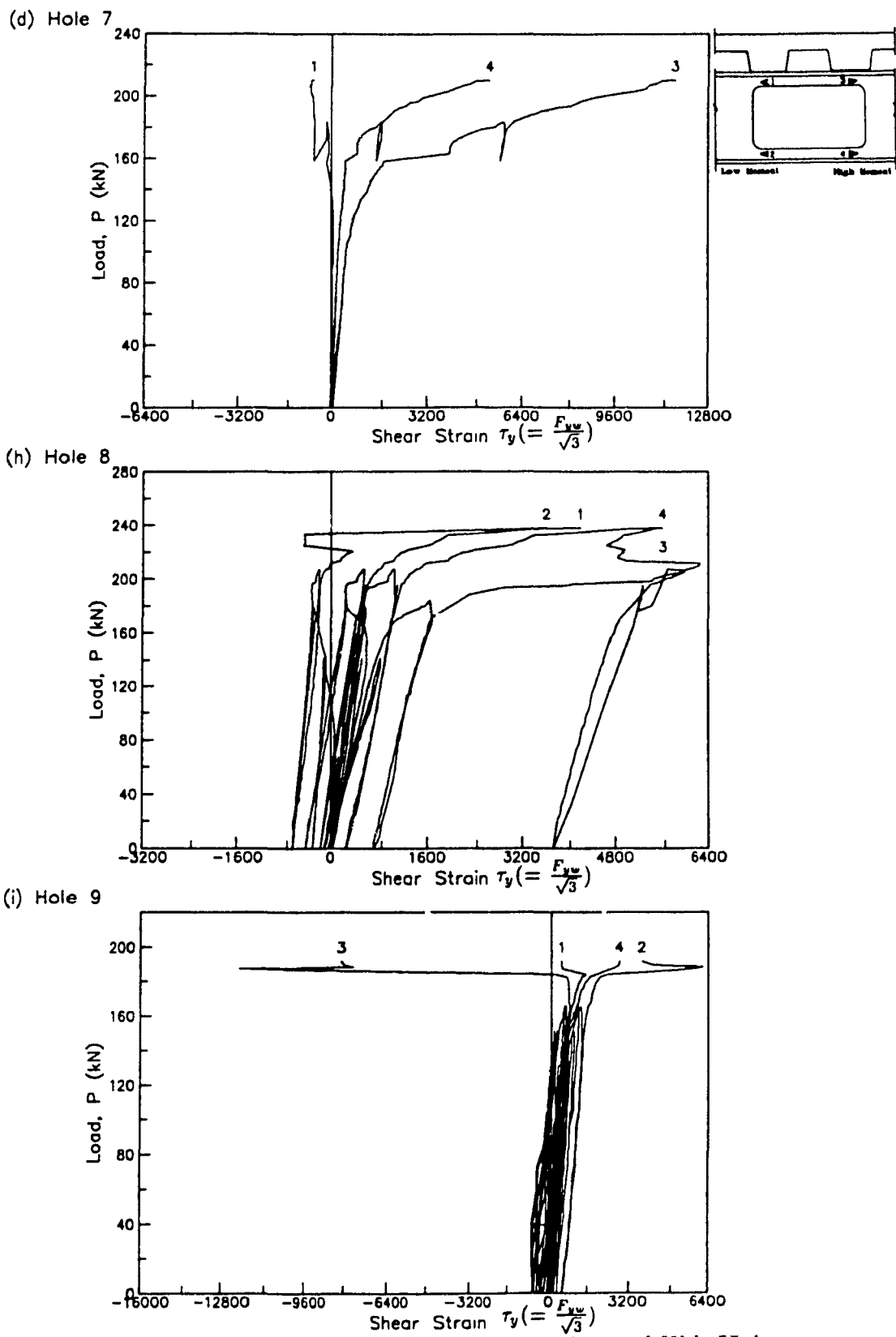


Figure 6.5 (Cont'd) Shear Strains Around Web Holes.

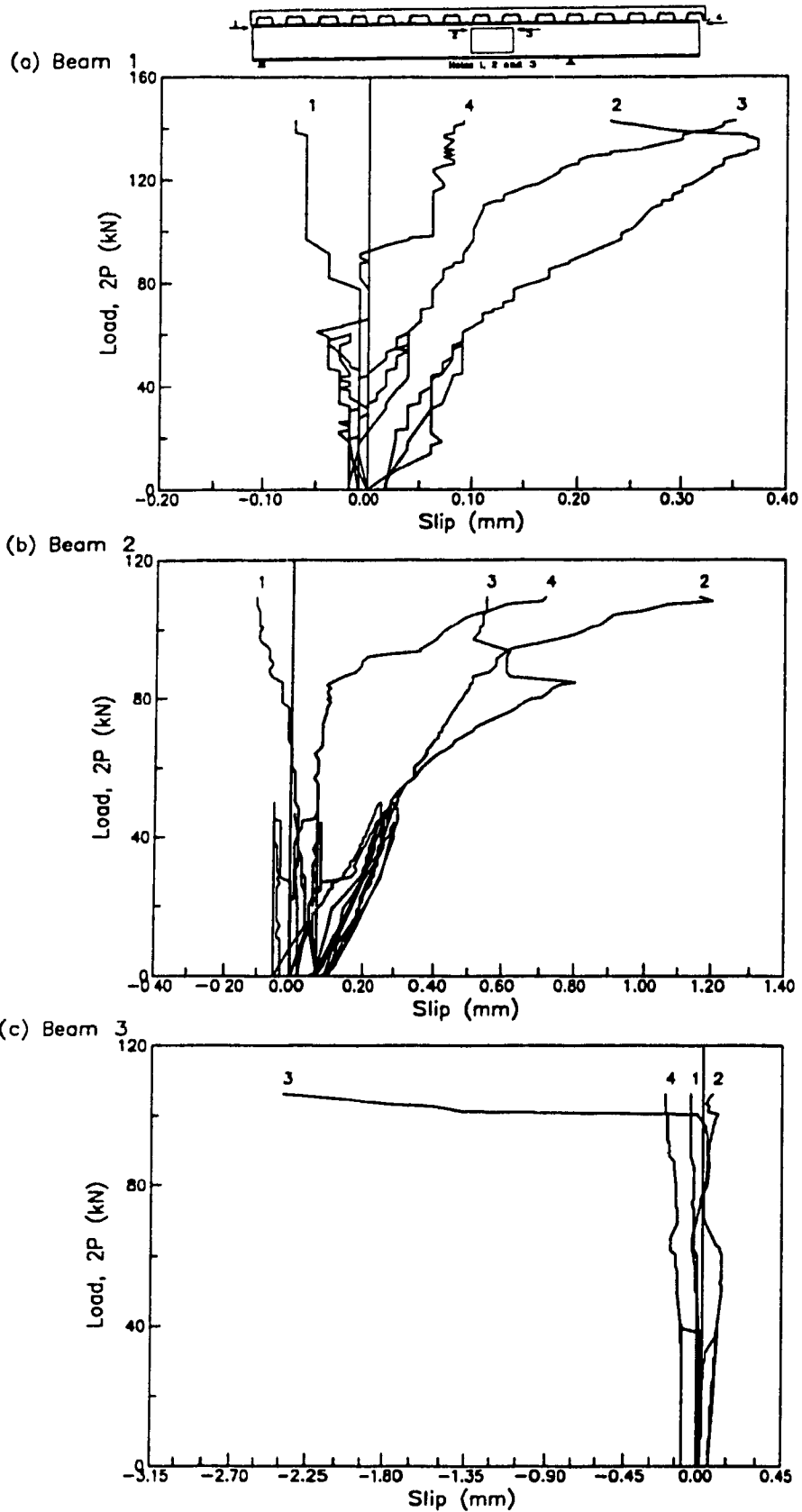


Figure 6.6 Slips Along Length of Beam.

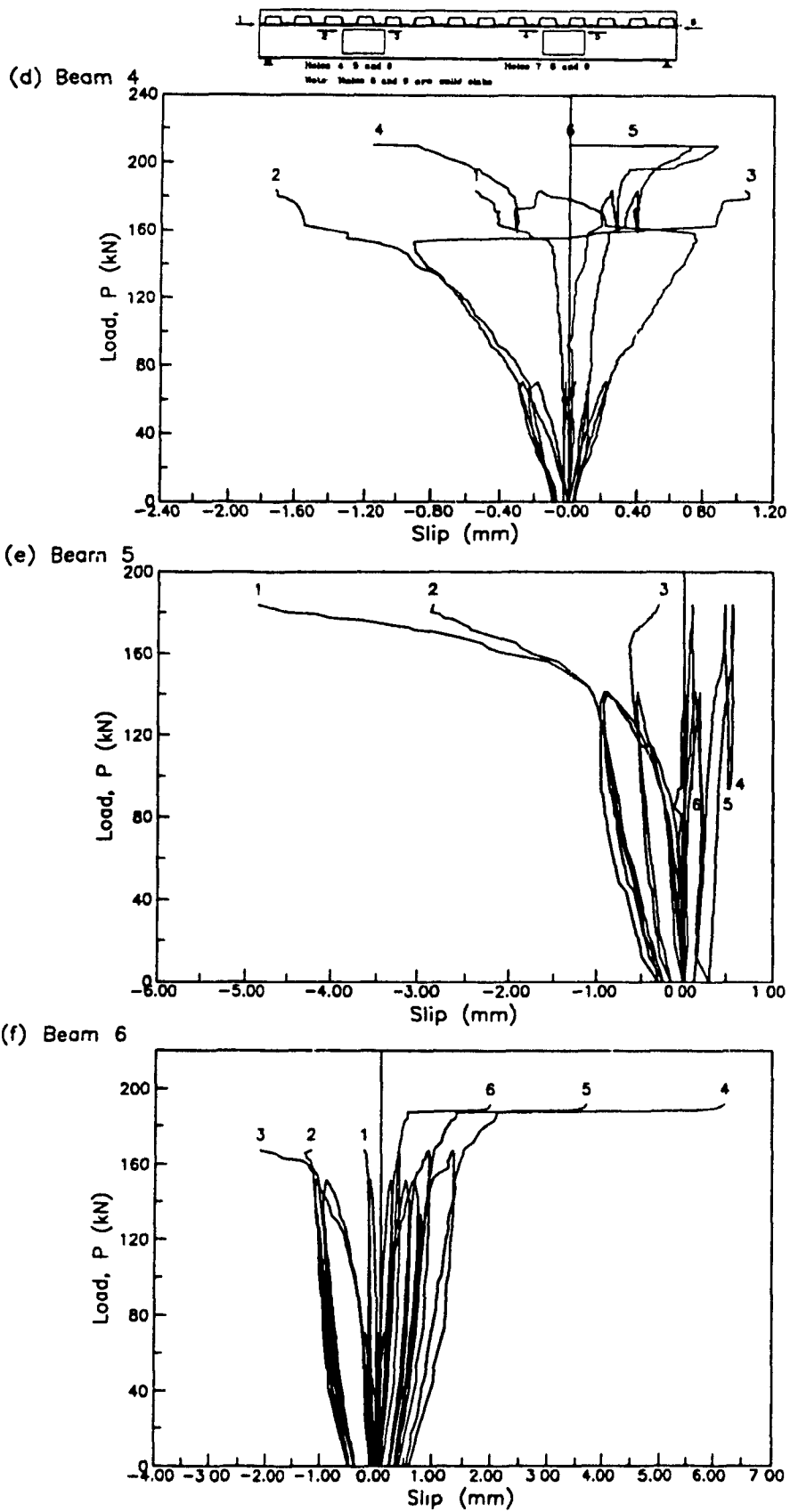


Figure 6.6 (Cont'd) Slips Along Length of Beam.

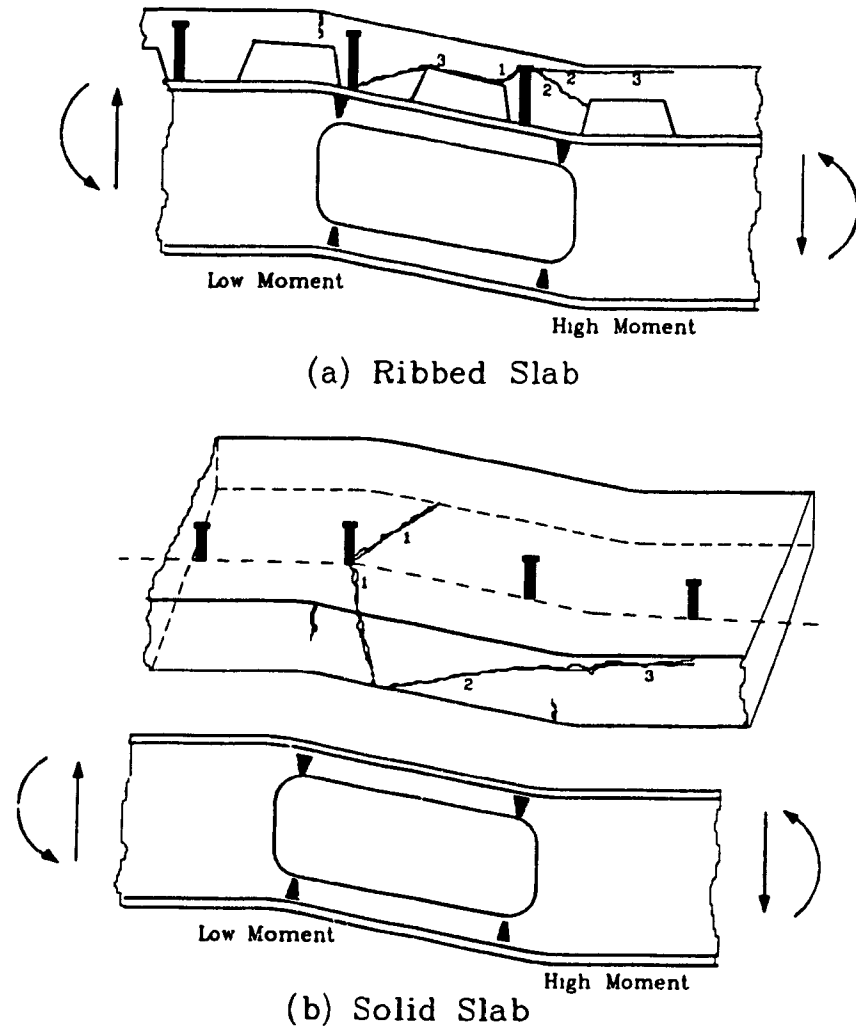
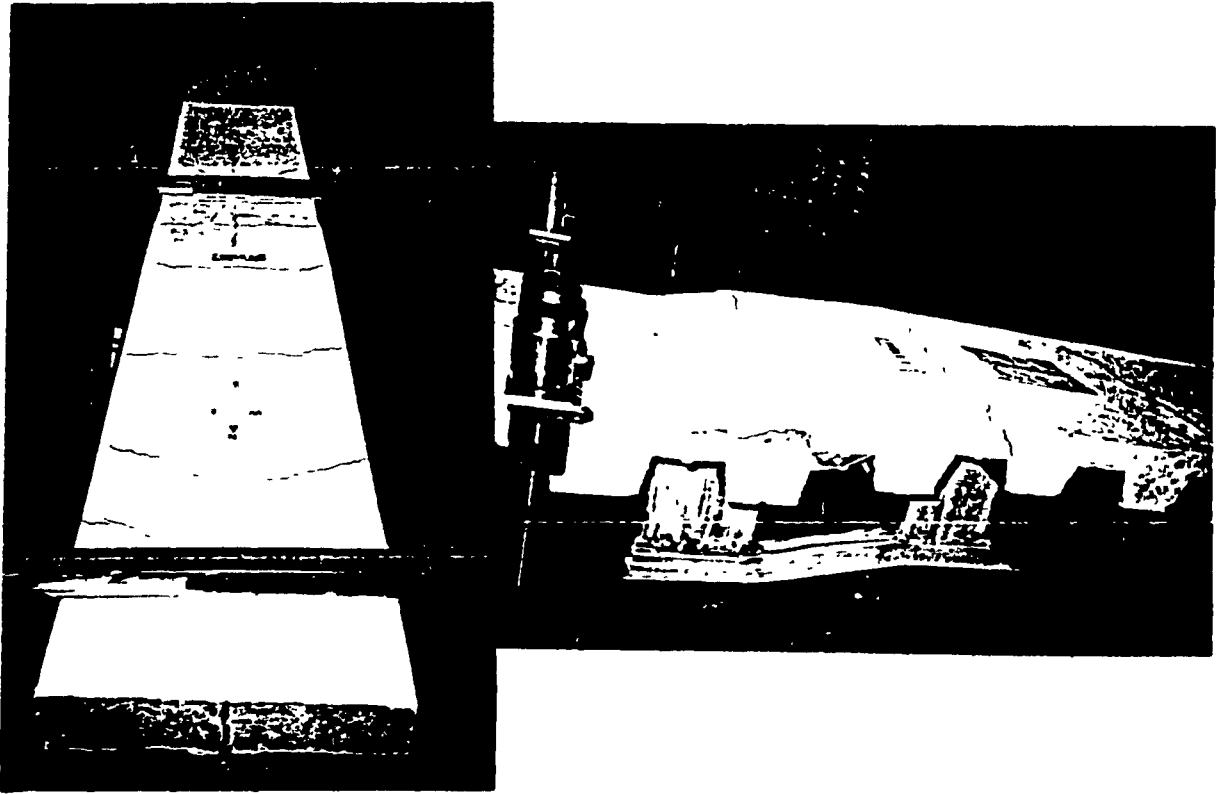


Figure 6.7 Schematic Representation of Crack Development

(a) Hole Deformation



(b) Slab Cracks

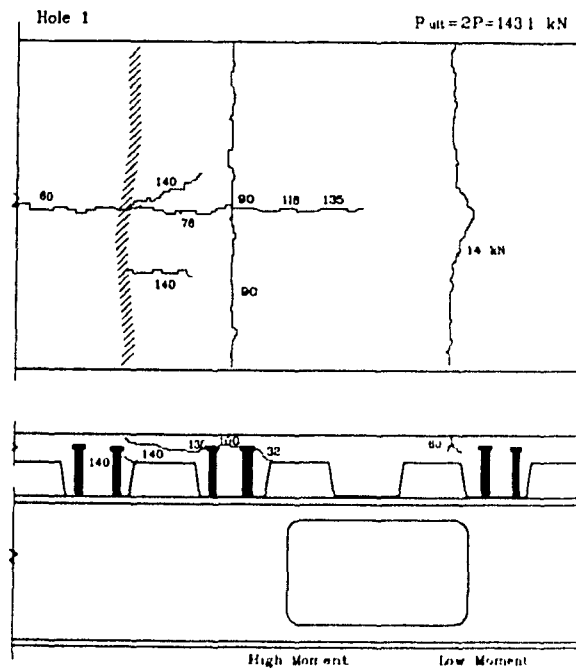
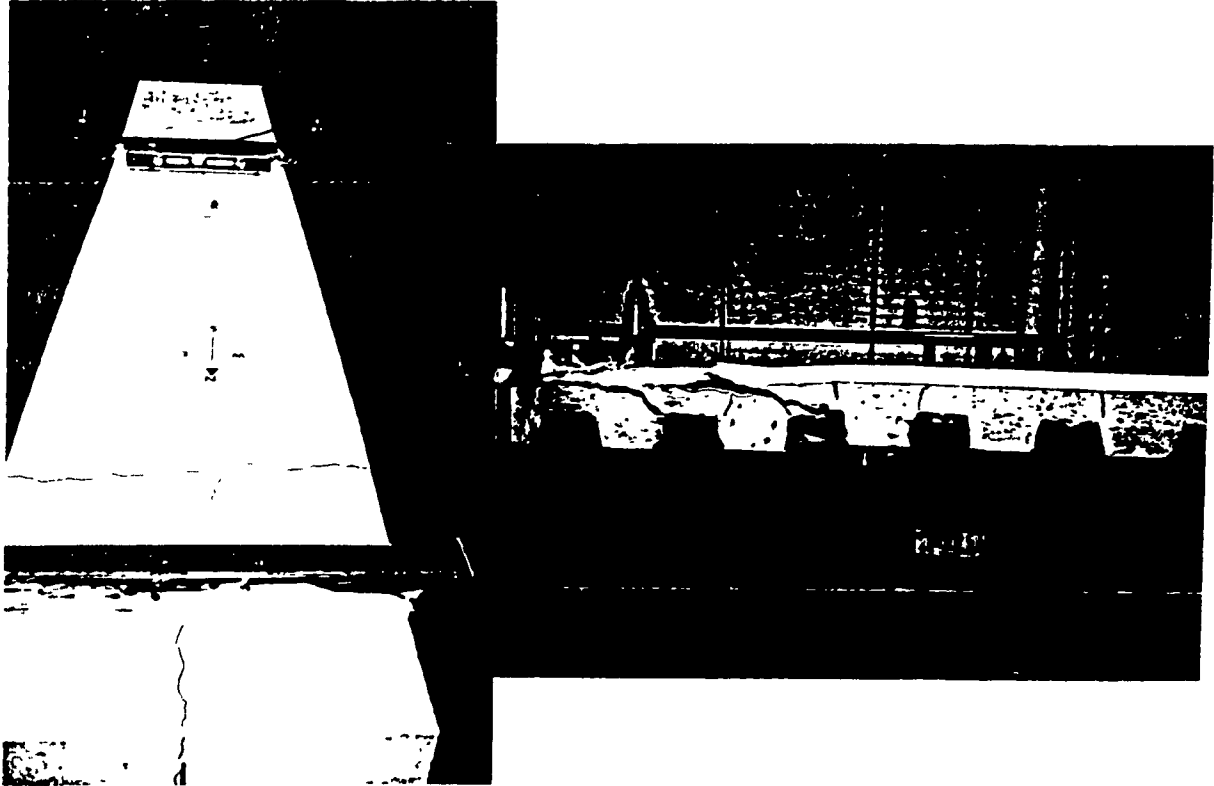


Figure 6.8 Failure of Hole 1

(a) Hole Deformation



(b) Slab Cracks

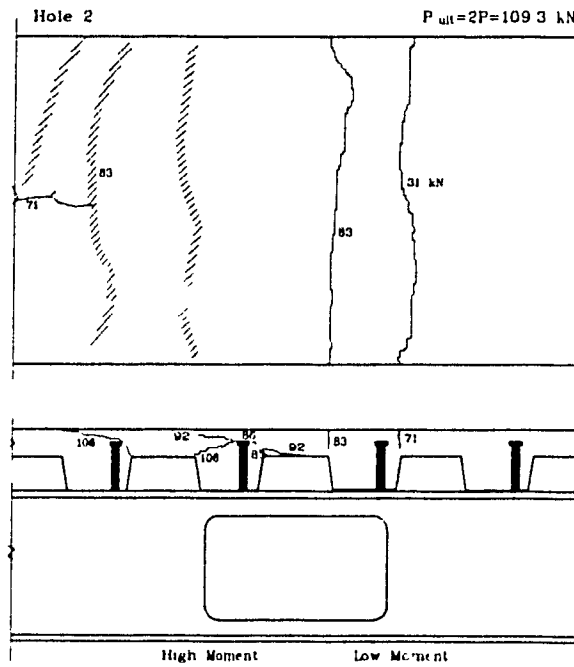


Figure 6.9 Failure of Hole 2

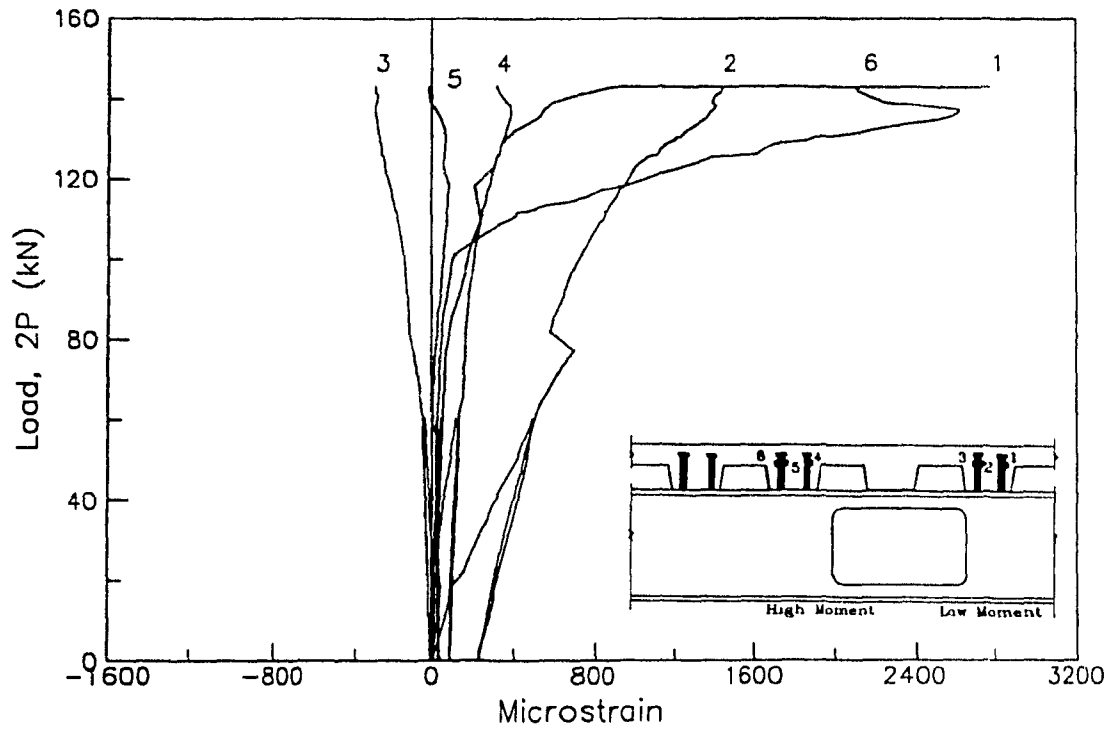


Figure 6.10 Stud Strains Around Hole 1.

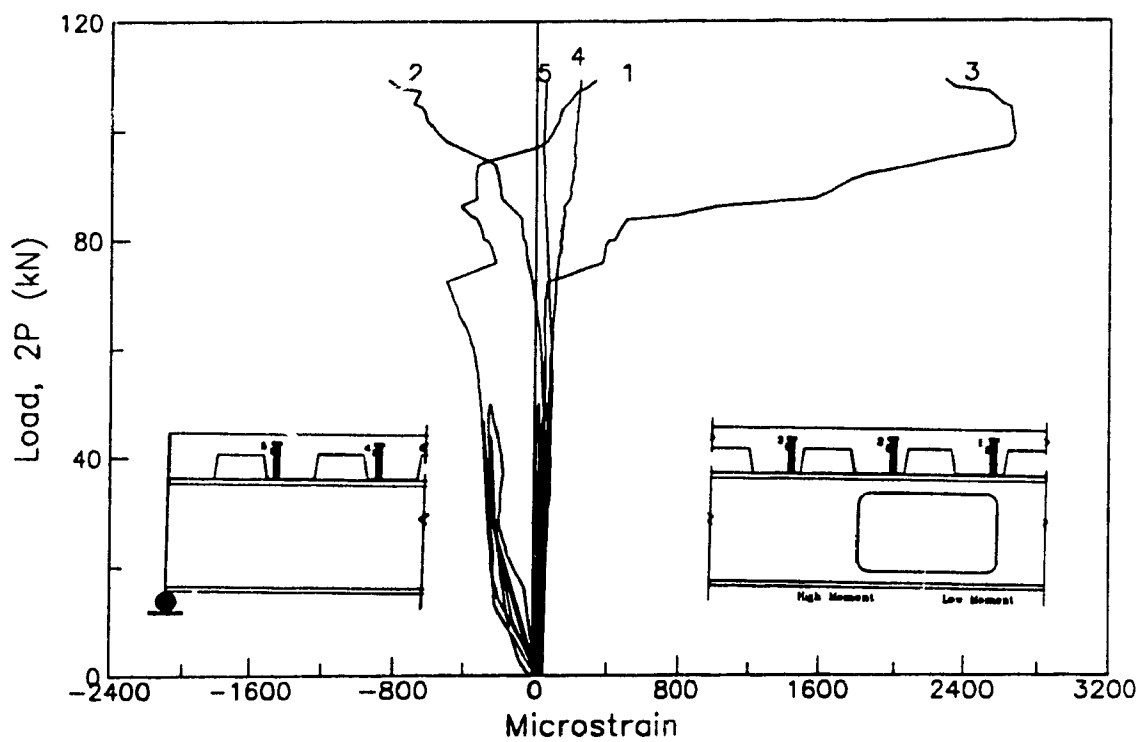
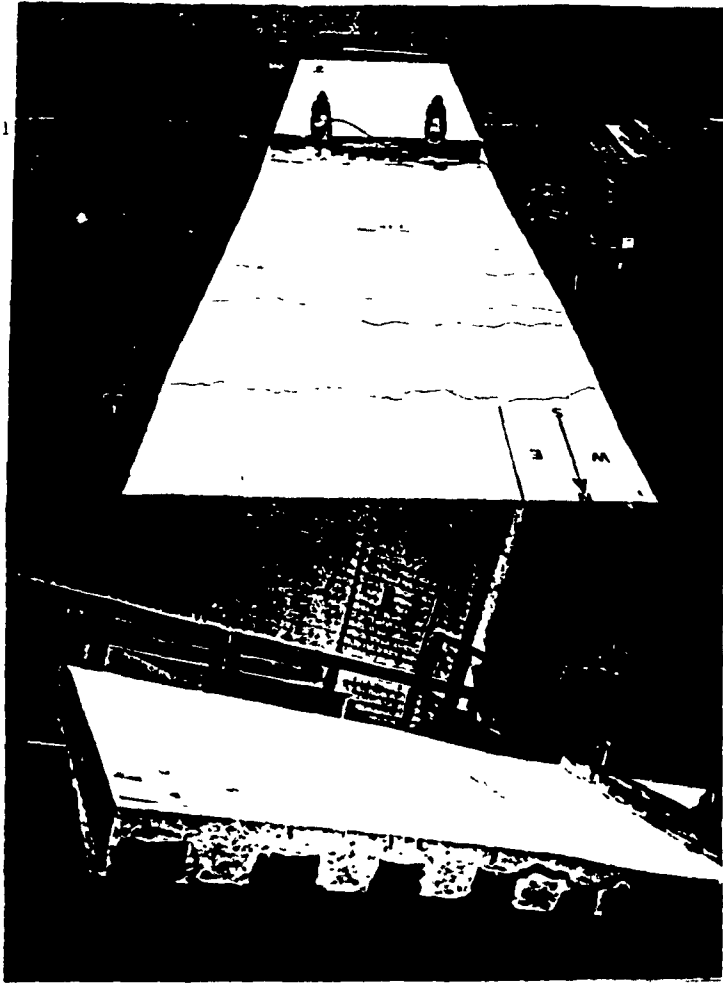


Figure 6.11 Stud Strains Around Hole 2

(a) Hole Deformation



(b) Slab Cracks

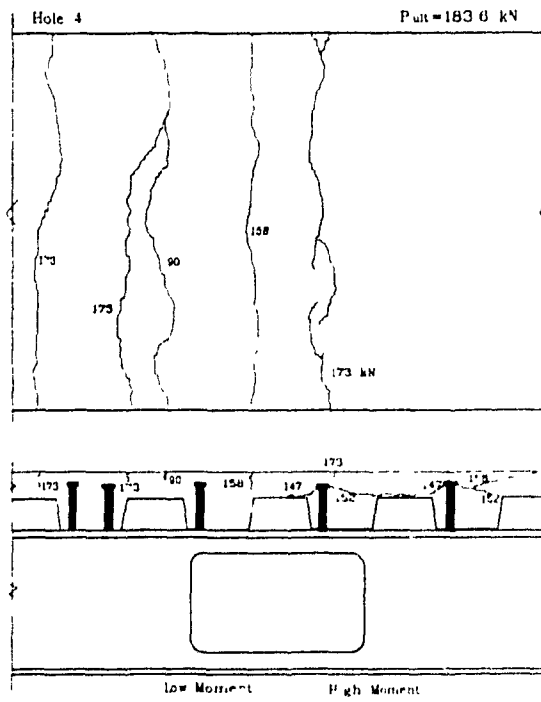
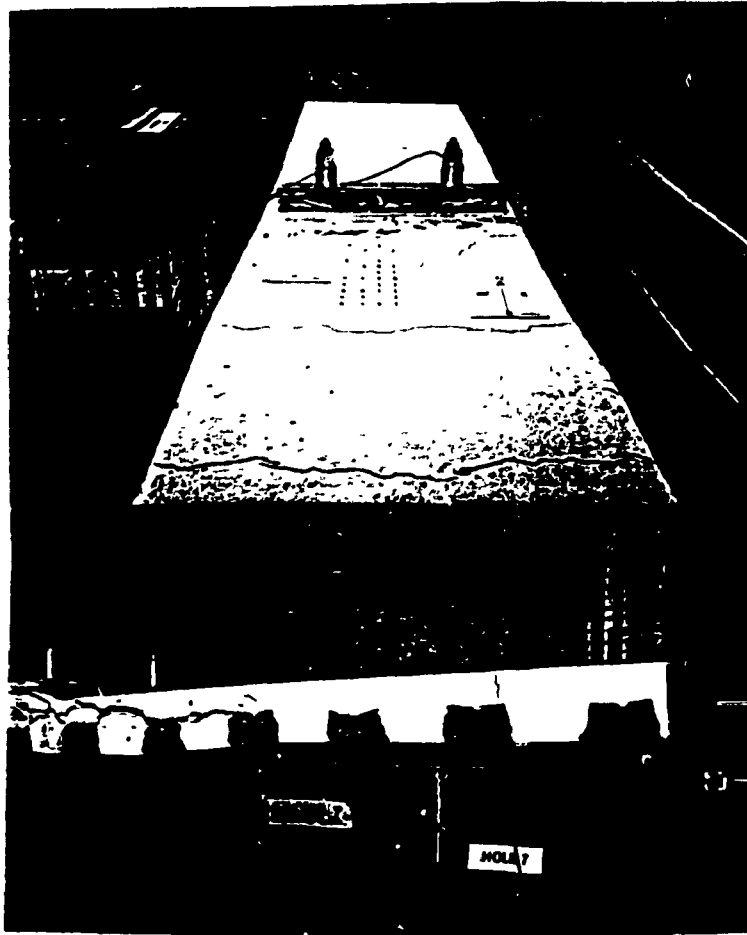


Figure 6.12 Failure of Hole 4

(a) Hole Deformation



(b) Slab Cracks

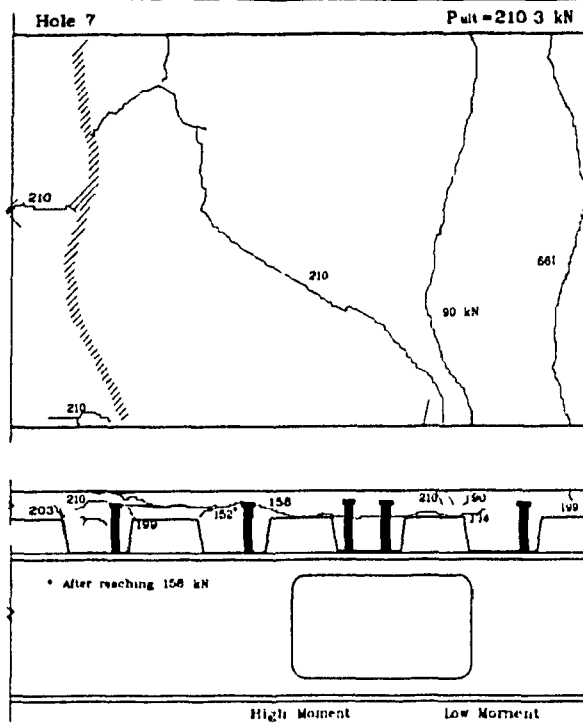


Figure 6.13 Failure of Hole 7

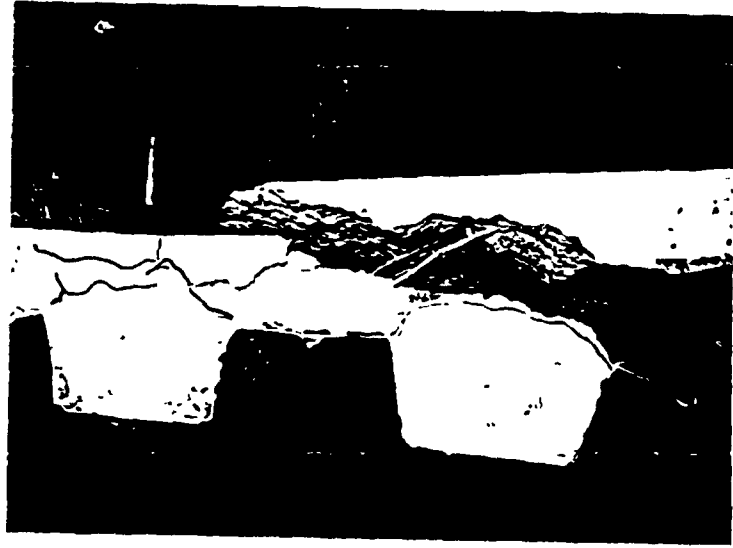


Figure 6.14 Close-up View of Slab After Removing Cracked Concrete

(a) Hole Deformation



(b) Slab Cracks

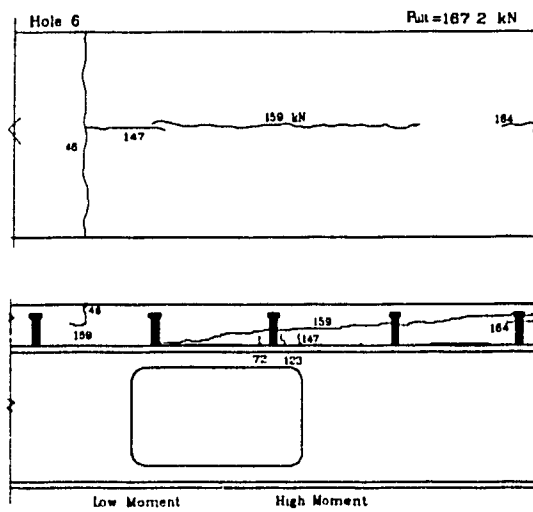
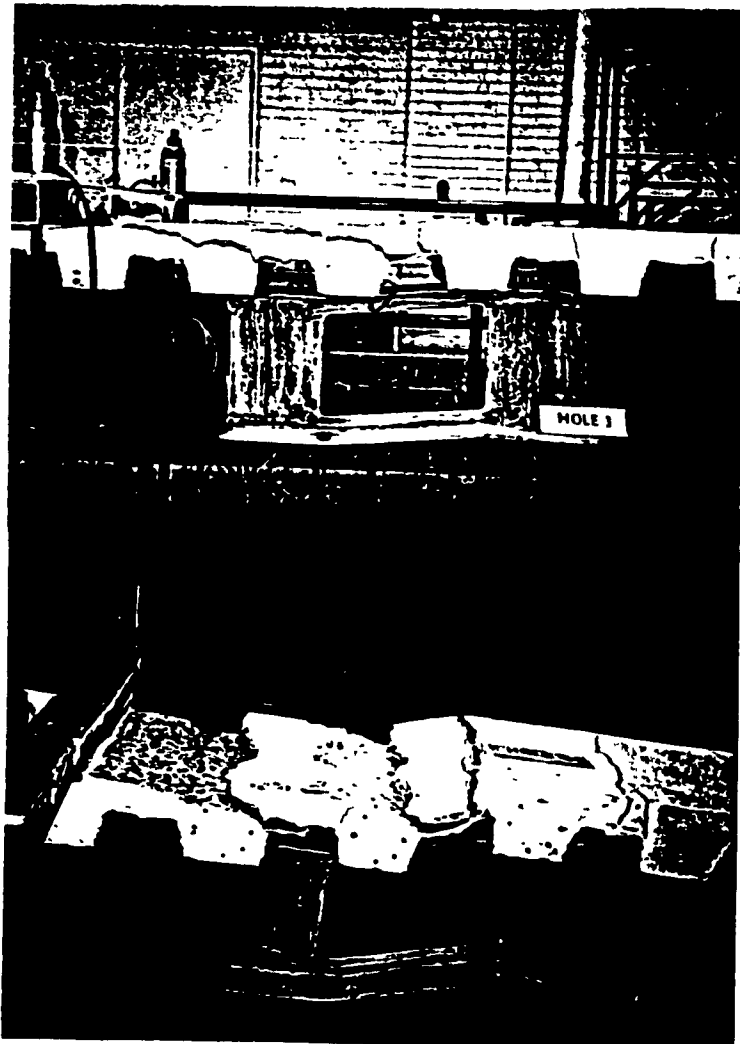


Figure 6.15 Failure of Hole 6



Figure 6.17 Close-up View of Slab Cracking on the Soffit

(a) Hole Deformation



(b) Slab Cracks

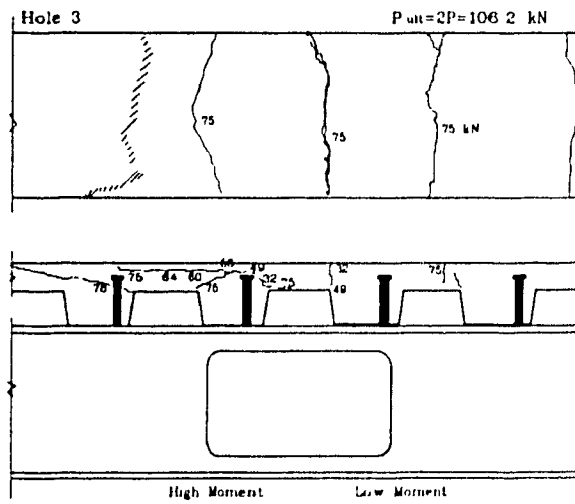


Figure 6.18 Failure of Hole 3

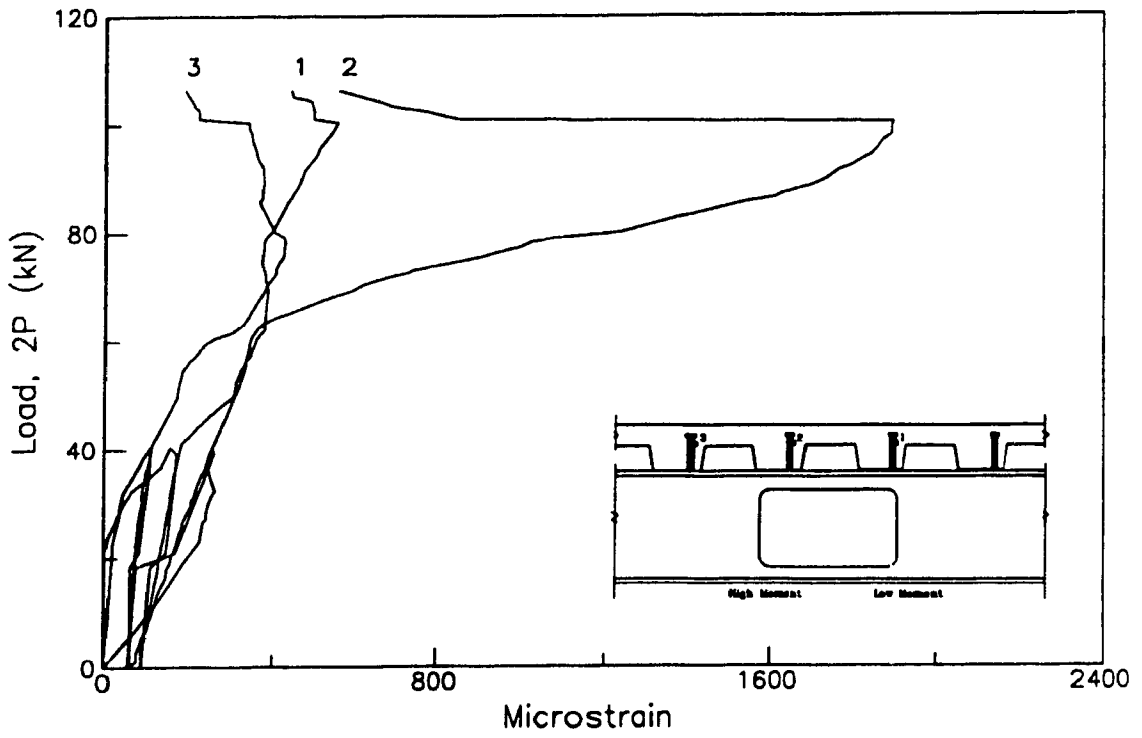
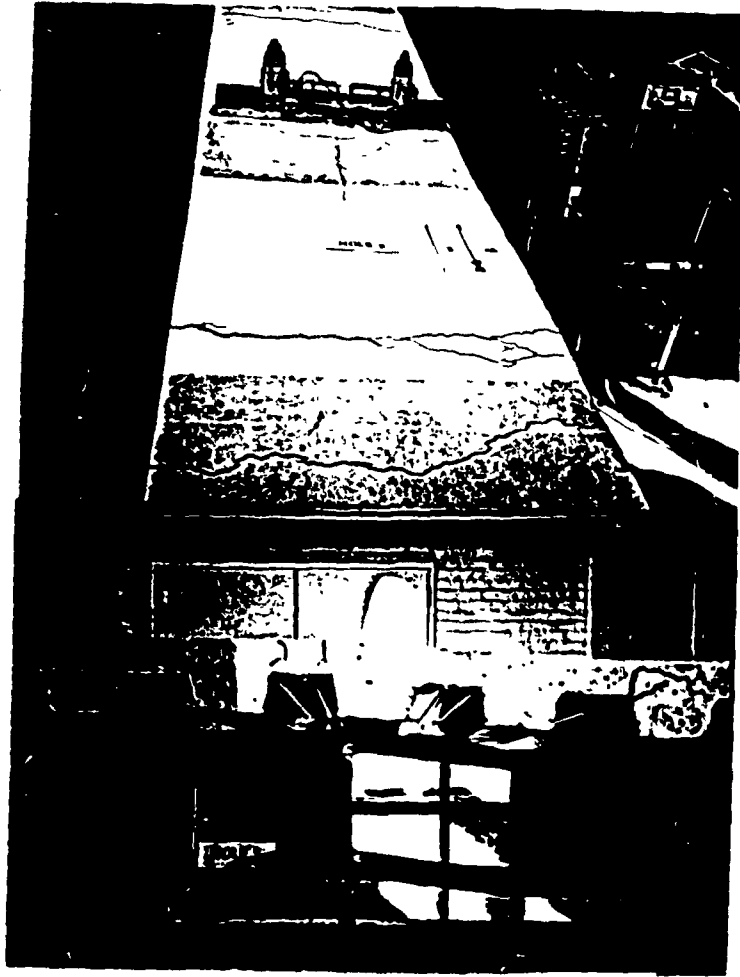


Figure 6.19 Stud Strains Around Hole 3.

(a) Hole Deformation



(b) Slab Cracks

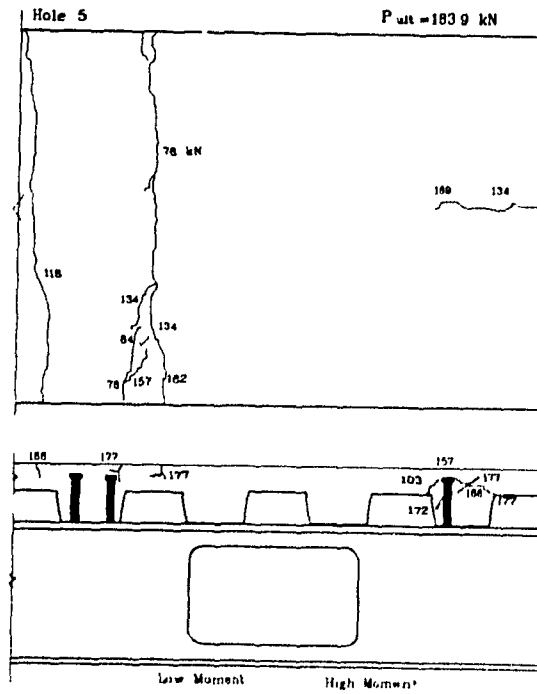
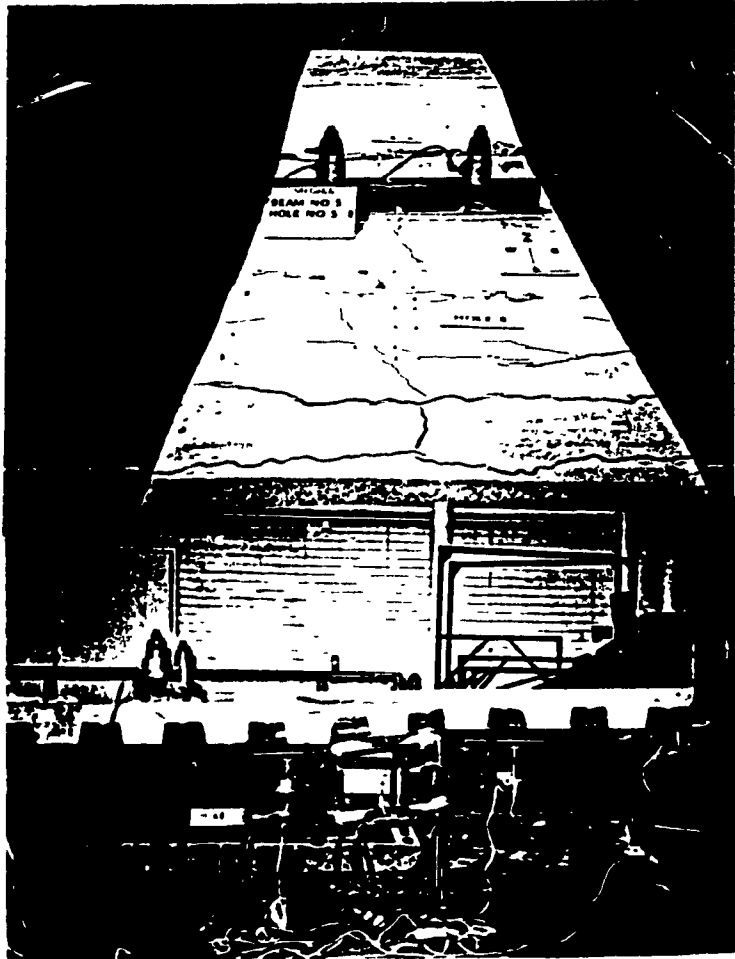


Figure 6.20 Failure of Hole 5

(a) Hole Deformation



(b) Slab Cracks

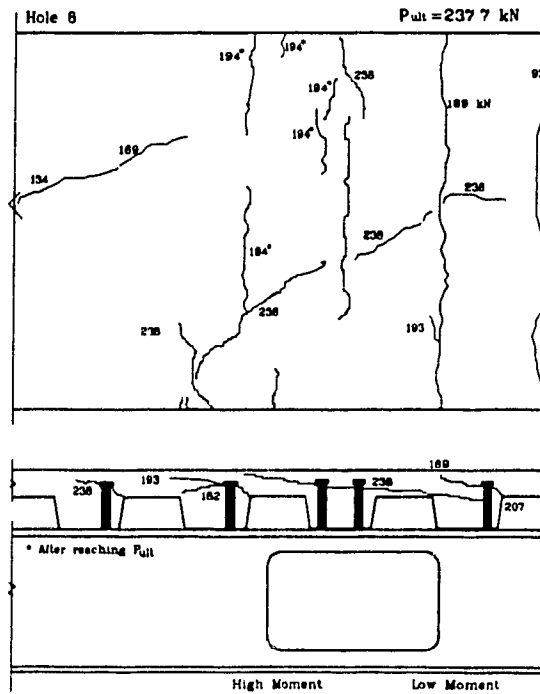


Figure 6.21 Failure of Hole S

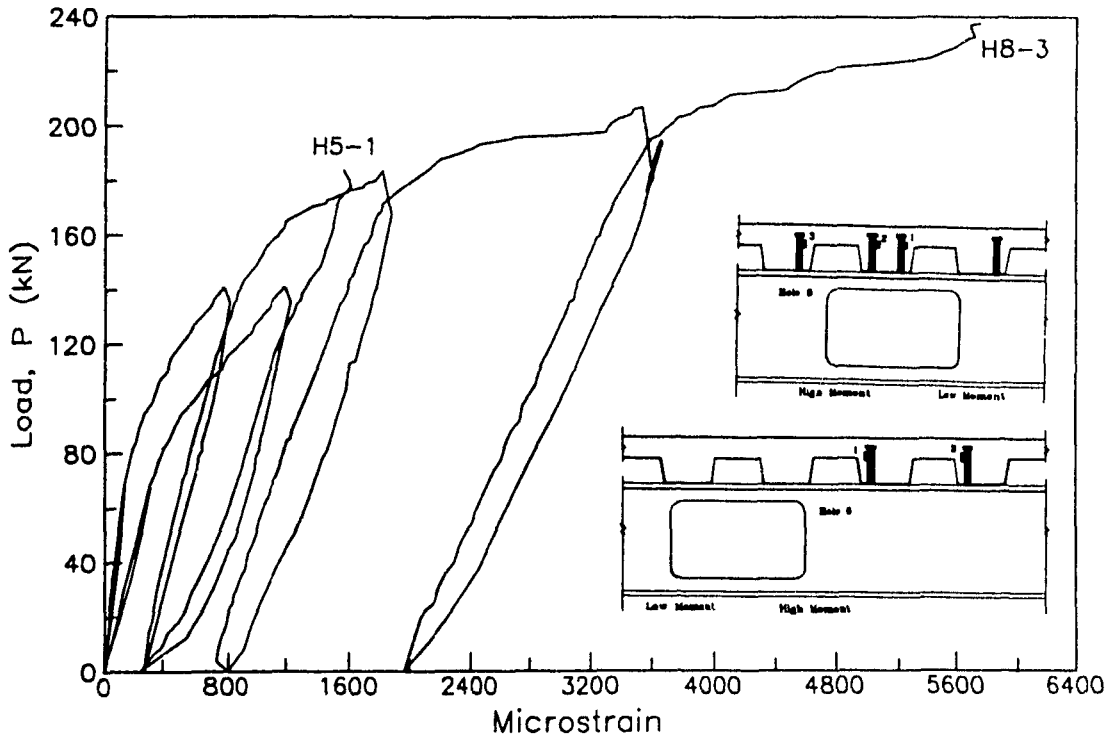


Figure 6.22 Stud Strains Around Holes 5 and 8

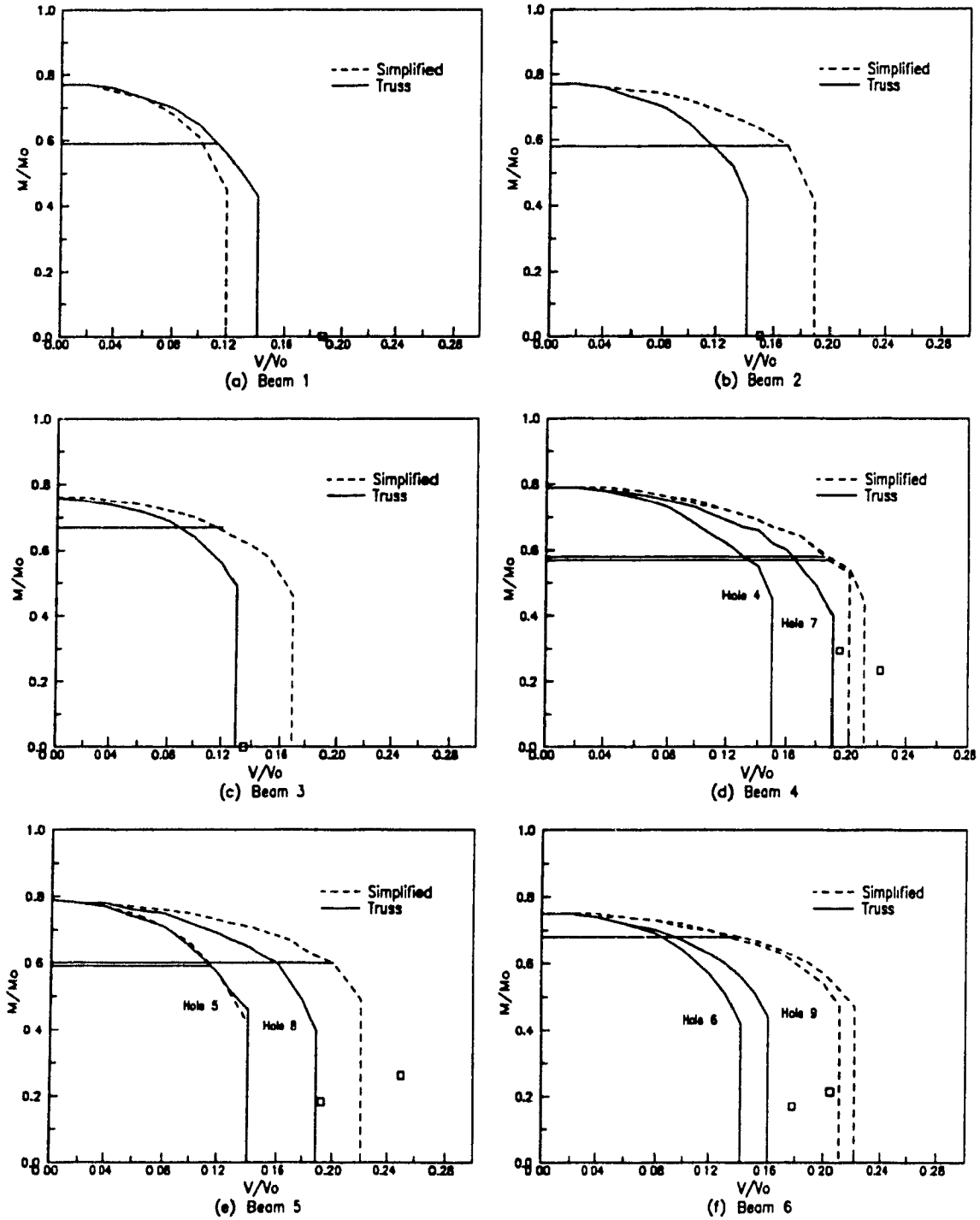


Figure 6.23 Moment-to-Shear Interaction Diagrams

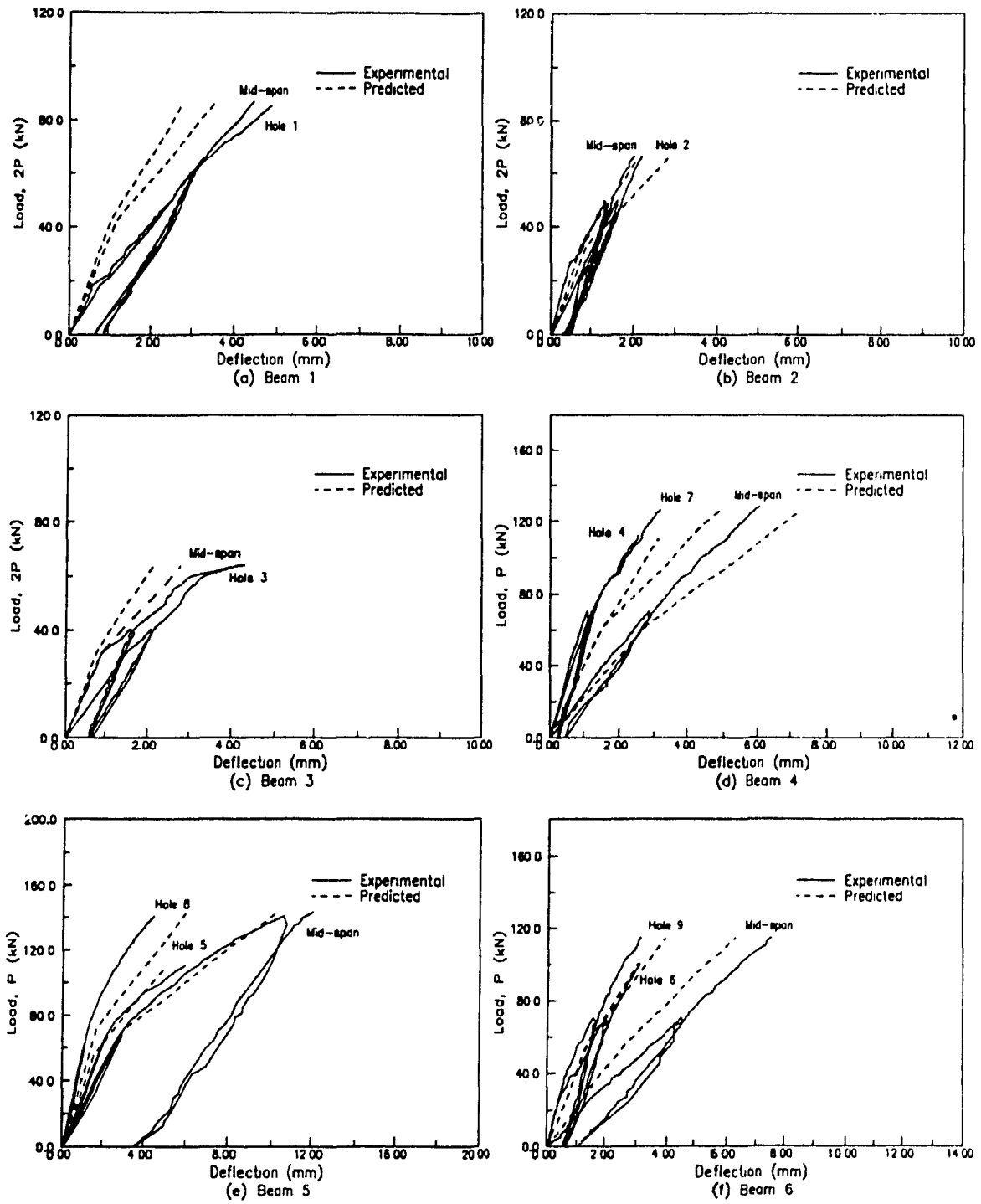


Figure 6.24 Load Versus Deflection Response up to 60% of P_{ult}

Table 6.1 Summary of Test Results.

Beam No	Hole No	Ultimate Load (kN)	Proportional Limit (% of Ult.)	Initial Slab Cracking (% of Ult)			Initial Yielding of Steel (% of Ult)		Ultimate Shear Load (kN)
				*Trans.	Long	Rib Sep	Long.	Shear	
1	1	143.1	42	10	42	22	32 (THM)+	68 (BLM)	95.4
2	2	109.3	44	28	65	76	65 (BLM)	88 (BLM)	72.9
3	3	106.2	30	30	.	30	71 (THM)	75 (THM)	70.8
4	4	183.6	38	49	.	80	60 (BLM)	99 (TLM)	91.8
	7	210.3	38	43	.	75	49 (BLM)	76 (THM)	105.2
5	5	183.9	36	41	73	56	46 (TLM)	71 (TLM)	92.0
	8	237.7	31	39	56	77	58 (THM)	80 (THM)	118.9
6	6	167.2	42	28	88	**74	52 (BLM)	91 (BLM)+	83.6
	9	191.2	46	28	77	**69	56 (BLM)	96 (BHM)	95.8

* Occurred at low moment end of hole

** Crack underneath slab

+ Top tee web at high moment end of hole

Bottom tee web at low moment end of hole

Table 6.2 Theoretical Values Defining Interaction Diagrams.

Beam No.	Hole No.	Moment (kN-m)			Shear (kN)	Simplified Slab Shear Model					θ (degs.)	Truss Model				
		M_0	M_{0h}	M'_{0h}	V_0	V_c	V_{st}	$*V_{sb}$	V_1	M_1		V_c	V_{st}	V'_{st}	V_1	M_1
1	1	492.2	381.4	288.2	506.9	0.0	42.7	18.6	61.3	197.5	12	20.6	30.8	51.4	69.9	176.4
2	2	481.3	372.2	278.0	494.5	0.0	75.4	18.1	93.5	190.4	20	25.5	26.5	52.1	70.2	167.1
3	3	415.0	314.8	280.0	523.7	0.0	67.4	19.1	86.5	187.1	20	24.1	27.1	51.2	70.3	166.7
4	4	510.4	404.2	297.1	473.3	1.8	77.7	17.0	96.4	215.4	20	29.1	26.4	55.5	72.4	177.9
	7	510.4	404.6	288.5	473.3	1.5	78.4	17.3	97.2	215.0	26	44.5	28.4	72.9	89.4	180.7
5	5	498.6	392.4	296.5	476.1	0.0	46.9	17.6	64.5	194.7	10	19.2	30.5	49.7	67.3	167.7
	8	498.6	392.0	298.0	476.1	10.5	78.4	17.3	106.2	215.3	26	44.6	28.3	72.9	90.2	174.0
6	6	414.3	310.9	281.6	470.4	0.2	78.4	17.6	96.6	189.5	14	19.4	27.1	46.5	64.0	169.9
	9	414.3	310.9	281.6	470.4	4.9	78.8	17.6	101.3	188.5	27	30.6	25.1	55.6	73.2	172.0

* Also, applied to Truss Model

Table 6.3 Comparison Between Actual and Predicted Failure Loads.

Beam No	Hole No	Observed Shear (kN)	Predicted Shear (kN)			
			Simplified	Test/Theory	Truss	Test/Theory
1	1	95.4	61.3	1.556	69.9	1.364
2	2	72.9	93.5	0.760	70.2	1.039
3	3	70.8	86.5	0.818	70.3	1.007
4	4	91.8	96.4	0.952	72.4	1.267
	7	105.2	97.2	1.082	89.4	1.177
5	5	92.0	64.5	1.427	67.3	1.367
	8	118.9	106.2	1.120	99.0	1.318
*6	6	83.6	96.6	0.866	64.0 (67.5)**	1.306 (1.238)**
	9	95.8	101.3	0.948	73.2 (83.1)**	1.311 (1.155)**

* Solid Slab

** When T_r is increased up to Q_r

Table 6.4 Horizontal and Vertical Load Carried by Shear Connection.

Beam No	Hole No	Simplified		q_r	Truss			Slab Force at H.M. Truss/Simplified
		q_r (kN per Stud)	q/q_r		T_r (kN per Stud)	q/q_r	T/T_r	
1	1	52.0	1.00	52.0	56.4	0.96	0.18	0.48
2	2	76.1	1.00	76.1	75.6	0.90	0.34	0.45
3	3	70.5	1.00	70.5	76.0	0.91	0.32	0.46
4	4	*73.1	1.00	90.6	72.6	0.86	0.40	0.36
	7	*73.1	1.00	**64.3	**54.4	0.70	0.41	0.41
5	5	*64.3	1.00	+105.0	.	1.00	.	0.41
	8	*86.6	1.00	90.6	.	1.00	.	0.35
6	6	90.5	1.00	90.5	46.3	0.85	0.42	0.34
	9	90.5	1.00	90.5	46.3	0.67	0.66	0.40

* Weighted value considering single and double studs in a rib

** Single stud in a rib

+ Stud having additional reinforcement welded at its head

CHAPTER 7

CONCLUSIONS AND DESIGN RECOMMENDATIONS

7.1 Conclusions

Based on the analytical and experimental investigations carried out in this research program, the following conclusions can be made:

- i) Shear connection provided within the hole length and sufficiently close to the ends of a hole is the only major reason for the large contribution of the concrete slab to shear strength achieved in composite beams at web holes. A corollary to this is that shear connection provided between the low moment end of the hole and the nearest support, which is far apart from the hole region, has a minor influence on the shear capacity of the concrete slab at the hole. The proposed truss analogy directly addresses the vital importance of shear connection provided in a restricted region near the hole.
- ii) Shear connectors with high vertical tensile force capacity near the high moment end of the hole was provided in the tests of Holes 5 and 8, which included additional reinforced bars welded to the heads of the studs. The magnitude of vertical shear in the concrete slab is largely dependent on the tension action in these studs, and the enhanced vertical resistance of shear connectors near the high moment end of

the hole increases the slab shear carrying capacity.

- iii) From test evidence, the width of the concrete slab is not a critical factor affecting the slab shear carrying capacity of ribbed or solid slabs, unless it is insufficient to develop the full tension cones of the studs and horizontal resistance based on dowel action. Much more severe interfacial slips between the concrete slab and steel beam were measured in the hole region compared with those at the ends of the beam.
- iv) In solid slabs, limited evidence indicated that failure of the bearing zone in the bottom part of the slab near the low moment end of the hole initiated a diagonal tension crack through the slab thickness.
- v) Additional longitudinal reinforcement in the slab through the length of the hole will enhance the slab behaviour under high shear, since dowel action was observed in tests.
- vi) The two methods developed for the estimation of ultimate strength at web holes were found to be in satisfactory agreement with previous and present test results. For solid slabs, the simplified slab shear model provides better prediction than the truss model, while both methods are found to be good for ribbed slabs. However, the simplified model also involves highly conservative results in some cases of the stud configurations at the hole, such as when the studs are placed close to the ends of the hole, but just beyond the hole length. Furthermore, concerning ribbed slabs, the truss model provides safer and more realistic prediction than the simplified model, for the reason that the rib separation type of slab failure, which is related to tension action in the studs, is accounted for. As a result, the truss model is more appropriate for ribbed slabs, while the simplified model seems to be more appropriate for solid slabs in which failure of the slab is less related to failure of the studs. However, above all, a major significance of the truss analogy proposed is that it provides an explanation for vertical shear carrying or transfer mechanism

between the concrete slab and shear connectors where the slab carries a lot of vertical shear.

- vii) Using the proposed serviceability analysis that includes flexibility of shear connectors, and truss action as well as transverse cracks in the hole region, deflections at mid-span as well as across the opening can be obtained appropriately. For greater accuracy, more precise information about the horizontal and vertical stiffnesses of shear connectors is necessary.

7.2 Design Recommendations

An explanation of the slab behaviour in composite beams at web holes, and a series of nine tests carried out for the verification of the slab behaviour based on the truss concept, provide useful information about the placement of shear connectors in the hole region.

At least, one and preferably a pair of studs should be placed exactly at, or close to, each end of the hole, thus conforming to the truss concept in which the studs at low and high moment ends of the hole provide bearing and tensile resistance respectively. With this method of stud placement, the concrete slab can carry vertical shear in an efficient manner as was indicated by Solution I of the truss analogy. Of course, placing additional studs near the high moment end is desirable, however, the truss analogy indicates that a low degree of shear connection at the low moment end may also limit the full development of tensile resistance provided at the high moment end.

To estimate the ultimate strength, both the simplified and truss models can be used, however, on ribbed slabs the truss model is preferred

Concerning other considerations related to lateral instability, instability of the compression zone in the top steel tee and web instability, design recommendations made for non-composite beams³⁰ can be used safely, but local web buckling related to web instability might be still of some concern in that if unshored construction is used,

the bare steel state is more critical than the non-composite state. Further research work on this aspect might be necessary.

So far, no research work has been found on composite beams having multiple web holes, and no application of the truss analogy to other areas has been made, such as in composite plate girders (with or without holes), in composite trusses, and possibly also in the link beam of eccentrically braced frames. The truss analogy provides an appropriate tool for analysis of these composite systems.

A number of uncertainties remain for a complete rational application of the truss analogy. These include actual dimensions of diagonal struts, the corresponding anchorages and bearing zones, their failure conditions, the role of tension in the concrete of the truss system, and the role of curved struts in ribbed slabs. Further study of these would have considerable interest, but in view of the available theories, which provide results suitable for design purpose, further studies of these problems may not be justified.

STATEMENT OF ORIGINALITY

The use of the truss concept to identify the slab behaviour in composite beams at web holes was originally made. This enabled full understanding of the structural action between the concrete slab and shear connection, the development of truss idealizations representing the slab forces, and the development of a theory to predict the ultimate strength for composite beams at web holes. Another theory which was extended for the application to solid slabs by limiting horizontal connector resistance was also an original development. Nine full scale experiments were carried out to provide a sound appreciation of the slab behaviour in composite beams at web holes. These provide evidence on truss action in the concrete slab in composite beams at web hole.

REFERENCES

1. Redwood, R. G., 1983. *Design of I-Beams with Web Perforations*, Chapter 4, Beams and Beam Columns: Stability and Strength, R. Narayanan, Ed., Applied Science Publishers, London and New York, pp. 95-133.
2. Porter, D. M., and Cherif, Z. E. A., 1987. *Ultimate Shear Strength of Thin Webbed Steel and Composite Girders*, Proceedings of International Conference on Steel and Aluminium Structures, Univ. College, Cardiff, England, Vol. 3, pp. 55-64.
3. Redwood, R. G., and Poubouras, G., 1984. *Analysis of Composite Beams with Web Openings*, Journal of the Structural Division, ASCE, Vol. 110, No. 9, Sept., pp. 1949-1958.
4. Redwood, R. G., and Cho, S. H., 1987. *Design Tools for Steel Beams with Web Openings*, Proceedings of International Conference on Steel and Aluminium Structures, Univ. College, Cardiff, England, Vol. 3, pp. 55-64.
5. Granade, C. J., 1968. *An Investigation of Composite Beams Having Large Rectangular Openings in Their Webs*, Thesis presented to Univ. of Alabama, in partial fulfillment of the requirements for the degree of Master of Science.
6. Todd, T. M., and Cooper, P. B., 1980. *Strength of Composite Composite Beams with Web Openings*, Journal of the Structural Division, ASCE, Vol. 106, No. 2, Feb., pp. 431-444.
7. Clawson, W. C., and Darwin, D., 1982. *Tests of Composite Beams with Web Openings*, Journal of the Structural Division, ASCE, Vol. 108, No. 1, Jan., pp. 145-162.
8. Clawson, W. C., and Darwin, D., 1982. *Strength of Composite Beams with Web Openings*, Journal of the Structural Division, ASCE, Vol. 108, No. 3, Mar., pp. 623-641.
9. Cho, S. H., 1982. *An Investigation on the Strength of Composite Beams with Web Openings*, Thesis presented to Hanyang Univ., Seoul, Korea, in partial fulfillment of the requirements for the degree of Master of Engineering.
10. Redwood, R. G., and Wong, P. W., 1982. *Web Holes in Composite Beams with Steel Deck*, Proceedings of Eighth Canadian Structural Engineering Conference, Canadian Steel Construction Council, Willowdale, Ont., 41 pp.
11. Redwood, R. G., 1983. *Discussion of Strength of Composite Beams with Web Openings*, Journal of the Structural Division, ASCE, Vol. 109, No. 5, Apr., pp. 1307-1309.
12. Redwood, R. G., and Poubouras, G., 1983. *Tests of Composite Beams with Web Holes*, Canadian Journal of Civil Engineering, Vol. 10, No. 4, pp. 713-721.
13. Redwood, R. G., 1986. *The Design of Composite Beams with Web Openings*, First Pacific Structural Steel Conference, Auckland, New Zealand, Vol. 1, pp. 169-185.
14. Cho, S. H., and Redwood, R. G., 1986. *The Design of Composite Beams with Web Openings*, Structural Engineering Series Report No. 86-2, McGill University, June,

66 pp.

15. Donahey, R. C., and Darwin, D., 1988. *Web Openings in Composite Beams with Ribbed Slabs*, Journal of the Structural Division, ASCE, Vol. 114, No. 3, Mar., pp. 518-534.
16. Darwin, D., and Donahey, R. C., 1988. *LRFD for Composite Beams with Unreinforced Web Openings*, Journal of the Structural Division, ASCE, Vol. 114, No. 3, Mar., pp. 535-552.
17. Cho, S. H., 1989. Discussion of *LRFD for Composite Beams with Web Openings*, Journal of the Structural Division, ASCE, Vol. 109, No. 5, Oct., pp. 1307-1309
18. Canadian Standards Association, 1985. *Steel Structures for Buildings - Limit State Design*, CAN-S16.1-M85 Rexdale, Ontario.
19. Schlaich, J., Schäfer, K., and Jennewein, M., 1987. *Towards a Consistent Design of Structural Concrete*, Journal of the Prestressed Concrete Institute, Vol. 32, No. 3, May/June, pp. 74-150.
20. Brattland, A., and Kennedy, D. J. L., 1986. *Tests of a Full Scale Composite Truss*, Canadian Structural Engineering Conference, Willowdale, Ont., 50 pp
21. Ricles, J. M., and Popov, E. P., 1989. *Composite Action in Eccentrically Braced Frames*, Journal of the Structural Division, ASCE, Vol. 115, No. 8, Aug., pp. 2046-2066.
22. McMakin, P. J., Slutter, R. G., and Fisher, J. W., 1973. *Headed Steel Anchor under Combined Loading*, AISC, Engineering Journal, Second Quarter, pp. 43-52
23. Hawkins, N. H., and Mitchell, D., 1984. *Seismic Response of Composite Shear Connections*, Journal of the Structural Division, ASCE, Vol. 110, No. 9, Sept., pp. 2120-2136.
24. The MacNeal-Schwendler Corp., 1985. *MSC/pal 2 - Version 1.0 (For Educational Use), User's and Reference Manuals*, Los Angeles, California.
25. American Institute of Steel Construction, 1978. *Specification for the Design, Fabrication and Erection of Structural Steel for Buildings*, New York, N.Y., Nov.
26. Redwood, R. G., 1989. *Private Communication with Darwin, D.*
27. Oehlers, D. J., 1989. *Splitting Induced by Shear Connection in Composite Beams*, Journal of the Structural Division, ASCE, Vol. 115, No. 2, Feb., pp. 341-362
28. Johnson, R. P., and May, I. M., 1975. *Partial-interaction Design of Composite Beams*. The Structural Engineer, Vol. 53, No. 8, Aug., pp. 305-311
29. Nelson Stud Welding Company, 1984. *Construction-Design Data - Embedment Properties of Headed Studs*, 50 pp
30. Redwood, R. G., and Shrivastava, S. C., 1980. *Design Recommendations for Steel Beams with Web Holes*, Canadian Journal of Civil Engineering, Vol. 7, No. 4, pp. 642-650.

31. Thompson, P. J., and Ainsworth, I., 1985. *Composite Beams with Web Penetrations*. Grosvenor Place, Sydney, Third Conference on Steel Developments, AISC, Melbourne, Australia, May, 18 pp.

APPENDIX A

Example Calculations

for Ultimate Strength Using Truss Analogy

To illustrate the procedure for estimating the ultimate strength based on the truss concept, two holes having low moment-to-shear ratios and different types of slabs, and which were also referred to Section 3.2.1, are selected.

A.1 Solid Slab

Hole 6⁷ (C-6) in Fig. 3.3 was constructed using a W360×51 section (W14×34 in Imperial units) and 19 mm diameter, 76 mm length headed studs, and tested at the University of Kansas. The M/V ratio at the opening centerline was 0.915m, and the opening height and length were corresponding to 60% and 120% of the steel beam depth respectively.

The locations of the studs and the failure mode of the slab in the hole region are shown in Figs. 3.3 or A.1. Diagonal tension cracks were well developed in the slab, indicating that the concrete slab significantly contributed to the ultimate shear resistance at the hole.

To calculate V_1 and M_1 which correspond to Point 1 on the interaction diagram, we need first to determine the solution category to be used. This requires consideration

of the slab force system associated with the configuration of the studs. From the stud positions used as well as the slab crack pattern observed, Solution I is appropriate if the small length between the location of the bearing studs and the low moment end of the hole is neglected. The final form of the truss model to be used is shown in Fig. A.1.

Then, the following steps are required:

Step 1: Choose a value of q . As first choice, the 60%~80% of q_r is suggested. For example, choose $q = 78 \text{ kN}$ (17.6 kips).

Step 2: Estimate inclination of diagonal struts, θ , from Eq. (3-4).

$$\theta = \tan^{-1} \frac{H_s}{l_{s0}} = \tan^{-1} \frac{76}{203} \cong 21^\circ$$

Step 3: Estimate vertical forces carried by studs from Eq. (3.17).

$V_c = n_t T = n_t q \tan \theta = 2 \times 78 \tan 21 = 58.7 \text{ kN}$. Therefore, the vertical force carried by one connector T is 29.4 kN.

Step 4: Estimate the vertical resistance of a stud, T_r .

Considering double stud action, and using the stud height including the head (H_s), rather than the effective height under the head (L_e), the lateral surface area of the tension cone being considered is given as 51158 mm^2 (see Fig. A.1). Thus, from Eq. (3-19), vertical resistance of one shear connector, $T_r = 0.33 \sqrt{f'_c} A_c = 0.33 \sqrt{27.7} \times 51158 / 2 \cong 44.4 \text{ kN}$.

Step 5: Check failure of stud.

From Eq. (3-18) for studs under combined shear and tension,

$$\left(\frac{q}{q_r}\right)^{1.67} + \left(\frac{T}{T_r}\right)^{1.67} = \left(\frac{78}{118}\right)^{1.67} + \left(\frac{29}{44}\right)^{1.67} \cong 1.00$$

Under this combination of loading, it is considered that the studs in the hole region will reach at their ultimate strengths.

At this step, if the studs are not fully exhausted under given shear and tension loading, a new estimation on q is necessary, and then with this return to Step 1

Step 6: Determine the shearing force carried by the top tee steel web.

From Eq. (3-23),

$$\begin{aligned}\gamma &= 2a/S_t = 407/76 = 5.33 \\ \mu &= \frac{n_t q}{V_{pt}} = \frac{156}{100} = 1.57 \\ V_{st} &= \frac{\mu\gamma + \sqrt{3\gamma^2 - 3\mu^2 + 9}}{(3 + \gamma^2)} V_{pt} = 56.1 \text{ kN}\end{aligned}$$

Then, $V_t = V_c + V_{st} = 114.8 \text{ kN}$.

Step 7: Determine the shearing force carried by the bottom tee steel web.

$$\begin{aligned}\alpha_b &= 0.75S_b^2/a^2 = 0.106 \\ V_{bs} &= V_{pb} \sqrt{\frac{\alpha_b}{1 + \alpha_b}} = 31 \text{ kN}\end{aligned}$$

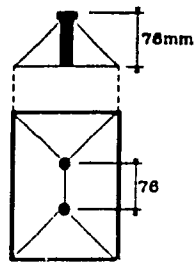
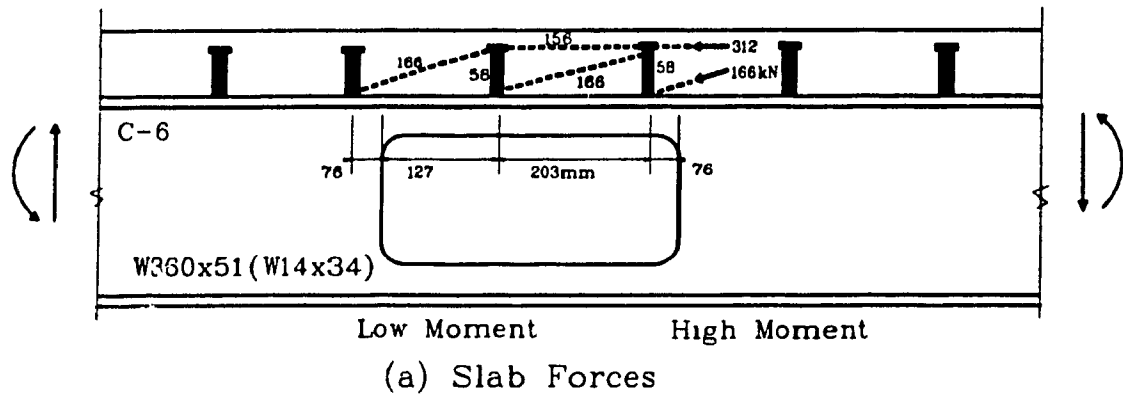
Step 8: Determine V_1 and M_1 from Eqs. (3-25) and (3-26).

$$\begin{aligned}V_1 &= 114.8 + 31 = 146 \text{ kN} \\ M_1 &= dP_{yf}(1 - \beta_b) + 0.5n_t q[(N_v - 1)H_s + l_{s1} \tan\theta - s_t] \\ &= 356 \times 559(1 - 0.294) + 0.5 \times 156[2 \times 76 + 76 \tan 21^\circ - 76] = 146.3 \text{ kN-m}\end{aligned}$$

Step 9: Estimate the failure load at given M/V ratio.

Now, the failure load is predicted as $V_1 = 146 \text{ kN}$, while in test this hole failed at $V = 179.8 \text{ kN}$. Therefore, the ratio of test-to-theory is 1.233

Further, if the tensile resistance of the shear connector (T_r) is increased up to 118 kN (q_r), V_1 corresponds to 150.4 kN .



$d=356$ mm	$T_s=102$
$b=170$	$t_s=102$
$t=12.08$	$b_e=1221$
$w=7.53$	
$a=203$	$n=10$
$H=102$	$n_h=4$
$e=0$	$M/V=916$

(b) Stud Tension Cone

Figure A.1 Truss Model Used for Prediction of Ultimate Strength on Solid Slab

A.2 Ribbed Slab

Details of Hole 1¹⁰ (R-1) are given in Fig. 3.4. This hole was constructed using a W360×51 section (W14×34 in Imperial units) and 19 mm diameter, 114 mm length headed studs, and tested at McGill University. The M/V ratio at the opening was 0.945m, and the opening height and length corresponded to 60% and 120% of the steel beam depth respectively.

Due to the 65 mm thick cover slab supported by the metal deck 76 mm deep and with the fairly low shear connection, rib separation cracks were more apparent than diagonal tension ones. Near the end supports, transverse cracks were also observed in the cover slab (see Figs. 3.4 or A.2). Adopting the solution category I for the reason that the length between the bearing studs and the low moment end of the hole is negligible, the same steps used in solid slabs are required. The truss model representing the slab forces is shown in Fig. A.2.

Step 1: Choose a value of $q = 78$ kN.

Step 2: Estimate inclination of diagonal struts, θ , from Eq. (3-4)

$$\theta = \tan^{-1} \frac{114}{305} \cong 20^\circ$$

Step 3: Estimate vertical forces carried by studs from Eq. (3-17).

$$V_c = n_t T = n_t q \tan \theta = 78 \tan 20 = 29 \text{ kN}, \text{ and } T = 29 \text{ kN}$$

Step 4: Estimate vertical resistance of stud, T_r .

From Fig. A.1, the lateral surface area of the tension cone being considered is given as 46196 mm^2 . Thus, from Eq. (3-19), vertical resistance of one shear connector,

$$T_r = 0.33 \sqrt{f'_c} A_c = 0.33 \sqrt{22} \times 46196 \cong 71.5 \text{ kN}$$

Step 5: Check failure of stud from Eq. (3-18).

$$\left(\frac{q}{q_r}\right)^{1.67} + \left(\frac{T}{T_r}\right)^{1.67} = \left(\frac{78}{91}\right)^{1.67} + \left(\frac{29}{72}\right)^{1.67} \cong 1.00$$

If the studs are not fully exhausted under the given shear and tension loading, return to Step 1 with a new estimation on q .

Step 6: Determine the shearing force carried by the top tee steel web.

From Eq. (3-23),

$$\begin{aligned}\gamma &= 426/71 = 5.97 \\ \mu &= \frac{n_t q}{V_{pt}} = \frac{78}{95} = 0.82 \\ V_{st} &= \frac{\mu\gamma + \sqrt{3\gamma^2 - 3\mu^2 + 9}}{(3 + \gamma^2)} V_{pt} = 38.4 \text{ kN}\end{aligned}$$

Then, $V_t = V_c + V_{st} = 67.4 \text{ kN}$.

Step 7: Determine the shearing force carried by the bottom tee steel web.

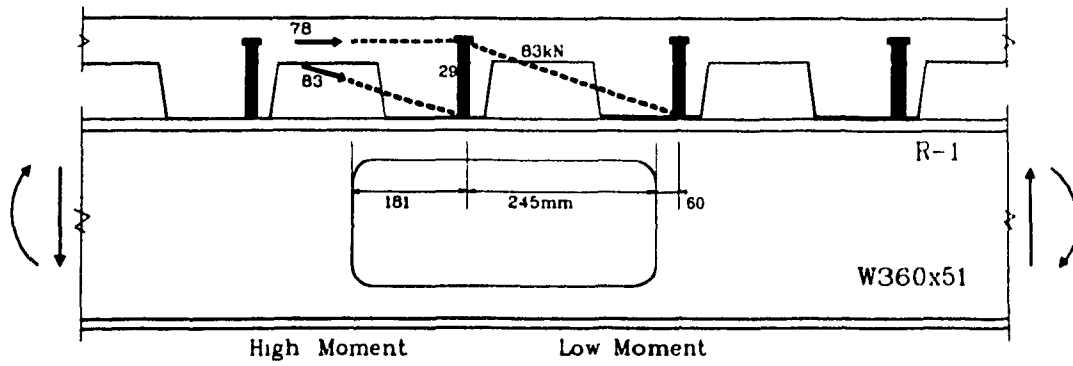
$$\begin{aligned}\alpha_b &= 0.75S_b^2/a^2 = 0.084 \\ V_{bs} &= V_{pb} \sqrt{\frac{\alpha_b}{1 + \alpha_b}} = 26.6 \text{ kN}\end{aligned}$$

Step 8: Determine V_1 and M_1 from Eqs. (3-25) and (3-26).

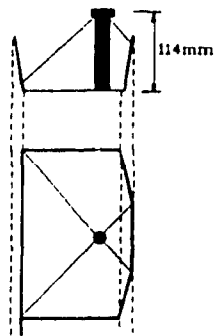
$$\begin{aligned}V_1 &= 67.4 + 26.6 = 94.2 \text{ kN} \\ M_1 &= dP_{yf}(1 - \beta_b) + 0.5n_t q[(N_v - 1)H_s + l_{s1} \tan\theta - s_t] \\ &= 356 \times 549(1 - 0.289) + 0.5 \times 78[76 + 181 \tan 20 - 71] = 143.0 \text{ kN-m}\end{aligned}$$

Step 9: Estimate the failure load at the given M/V ratio.

Now, the predicted failure load is the same as $V_1 = 94.2 \text{ kN}$, while in the test this hole failed at $V = 115.5 \text{ kN}$. Therefore, the ratio of test-to-theory is 1.227.



(a) Slab Forces



$d = 356\text{mm}$	$T_s = 141$
$b = 175$	$t_s = 65$
$t = 11\ 37$	$t_e = 1000$
$w = 7\ 44$	
$a = 213$	$n = 4$
$H = 107$	$n_h = 1$
$e = 0$	$M/V = 9.45$

(b) Stud Tension Cone

Figure A.2 Truss Model Used for Prediction of Ultimate Strength on Ribbed Slab.

APPENDIX B

Prediction of Deflections

B.1 Comments on Analytical Procedure

The frame analogy, which is proposed for the behaviour of composite beams having large web holes at service loads, can be refined with a number of different modelling aspects related to the fundamental assumptions. This includes the effective shear area of the concrete slab, the effective area and location of the diagonal compression strut, and horizontal (k_h) and vertical stiffnesses (k_v) of the shear connectors. Among these, the latter aspect, the stiffnesses of shear connection, will be the most critical factor to determine the local and global behaviour, particularly when dealing with ribbed slabs involving limited shear connection.

For the slab area that can be effective in carrying vertical shear at the serviceability load level, the overall and cover slab areas were considered in solid and ribbed slabs respectively, and furthermore these areas were divided by the shape factor (1.186) that accounts for the non-uniform distribution of shear stresses over a rectangular section.

For the effective area and location of the diagonal compression strut which represents truss action as well as transverse cracks in the hole region, a simple consideration was made which uses half the slab thickness and half the slab width at the correspond-

ing mid-depth of top and bottom half parts of the slab. This might lack justification, but the proposed approach appears to yield safe results after comparison with test results. In addition, for holes with high M/V ratios in which a bending mode of failure governs the hole behaviour, it is noted that no inclination for the compression strut along the hole length is necessary.

Concerning the stiffnesses of shear connectors, the number of previous push-out tests conducted on solid slabs for several diameters of the studs indicated that there is no clear correlation between the size and the horizontal stiffnesses of connectors. A large scatter on the stiffnesses ranging from 100 to 300 kN/mm was reported²⁸. For 19 mm diameter studs, stiffness ranged from 100 to 250 kN/mm

Furthermore, according to recent information provided by the Nelson Stud Co.²⁹, horizontal stiffnesses of shear connectors in solid slabs have been found to be about 173 kN/mm for 19mm × 76mm studs, 120 kN/mm for 16mm×64mm studs, and 70 kN/mm for 13mm×100mm studs. Also, vertical stiffnesses of shear connectors in solid slabs have been found to be about 50 kN/mm for the first two categories of the studs, and 25 kN/mm for the last category. On the other hand, for ribbed slabs, it was possible to obtain horizontal stiffnesses of shear connectors from the companion push out tests of the McGill beam tests. This indicates 79 kN/mm for 19mm×114mm studs. Also, vertical stiffnesses of shear connectors in ribbed slabs was taken as 25 kN/mm without full verification. Further research might be necessary on this aspect which relates to the basic behaviour of shear connectors. Finally, the values described above were incorporated in the analysis for the prediction of elastic deflections in previous tests of composite beams with web holes. The analysis results are given below

At a preliminary stage of the analysis, the sensitivity of results to the stiffnesses of shear connection was checked. The results indicated that for Hole 0 (R-0) having the ribbed slab and 59% shear connection at its high moment end, a 15% of the decreased

deflection was obtained by doubling the horizontal stiffnesses of shear connectors along the whole beam span. This will be more pronounced when there is a lower shear connection used. In solid slabs, no sensitivity was found under the same conditions. It is further indicated that the predictions of deflections are not sensitive to the vertical stiffnesses of shear connectors in either solid or ribbed slabs.

B.2 Analysis Results

Comparisons between predicted and measured deflections at mid-span as well as across the opening were made at 30% and 60% of ultimate load levels for a total of twenty previous tests (see Tables B.1 and B.2). Only the test results published in a usable form were included. The solid slabs tests conducted by Granade⁵ and Cho⁹ were not considered, for the reason that short beam spans were used with relatively large slab depth as well as high degrees of shear connection, thus resulting in an inappropriate evaluation of the proposed analysis due to the smaller deflections involved. In addition, the second holes in recent ribbed slab tests conducted by Donahey and Darwin¹⁶ were excluded, because they were fabricated after completion of the tests on the first holes.

Four tests (C-3, R-3 & 4, and D-3) required horizontal struts along the hole length at 60% of ultimate loads due to the bending related failure. Also, two holes (R-3 & 4) tested at McGill University required the inclusion of additional plates welded on the bottom of the steel flanges. The comparisons indicate that the proposed approach is generally satisfactory for predicting deflections at mid-span as well as across the opening, although there is sizable disagreement found in some cases, particularly relating to relative deflections between the hole ends. It is however noted that in most cases, the present analysis provides safe results and comprises a number of different modelling aspects. Therefore, this can be used for design purposes, or developing a design aid for a limited range of shear connection.

Table B.1 Comparisons of Measured and Predicted Deflections
at 30% of Ultimate Load

Slab Type	Exp. Inves.	Hole No.	At Mid-Span (mm)			Across Opening (mm)		
			Measured	Predicted	Pre./Mea.	Measured	Predicted	Pre./Mea.
Solid Slab	Clawson and Darwin	C-1	8.722	8.245	0.945	1.246	0.949	0.762
		C-2	7.258	9.818	1.353	1.722	1.988	1.154
		C-3	7.498	9.381	1.251	0.741	1.001	1.351
		C-5	4.486	5.444	1.214	1.424	1.606	1.128
		C-6	3.164	3.908	1.235	1.256	1.371	1.092
Ribbed Slab	Redwood, Wong and Pombouras	R-0	3.689	4.367	1.184	0.930	1.124	1.209
		R-1	2.344	2.442	1.042	1.031	1.138	1.104
		R-2	5.500	6.080	1.105	1.060	1.078	1.017
		R-3	6.800	7.067	1.039	0.400	0.431	1.078
		R-4	8.000	8.078	1.010	0.600	0.519	0.865
		R-5	2.500	2.605	1.042	1.000	1.026	1.026
		R-6	1.637	1.943	1.187	1.802	0.979	0.543
	R-7	2.346	2.781	1.185	1.190	1.044	0.877	
	Donahey and Darwin	D-1	2.950	3.397	1.152	1.653	1.556	0.941
		D-2	3.484	3.624	1.040	1.526	1.381	0.905
		D-3	5.366	5.742	1.070	1.322	0.568	0.430
		D-5A	2.823	3.494	1.238	1.322	1.247	0.943
		D-6A	1.221	1.155	0.946	1.195	1.123	0.940
		D-8A	1.577	1.379	0.874	0.839	0.635	0.757
		D-9A	1.450	2.251	1.552	1.400	1.558	1.113
		Mean			1.133		0.962	
		Std. Dev.			0.157		0.220	
		Coeff. of Var. (%)			23.8		22.9	

Table B.2 Comparisons of Measured and Predicted Deflections
at 60% of Ultimate Load

Slab Type	Exp. Inves.	Hole No.	At Mid-Span (mm)			Across Opening (mm)		
			Measured	Predicted	Pre./Mea.	Measured	Predicted	Pre./Mea.
Solid Slab	Clawson and Darwin	C-1	23.472	17.377	0.740	1.221	0.966	0.791
		C-2	17.099	20.940	1.225	4.065	4.473	1.100
	Darwin	C-3	17.954	20.339	1.133	1.895	1.486	0.784
		C-5	11.028	11.705	1.061	3.804	3.825	1.006
		C-6	7.146	7.840	1.097	3.001	3.550	1.183
Ribbed Slab	Redwood, Wong and Poubouras	R-0	6.505	9.793	1.505	1.589	3.078	1.937
		R-1	4.500	5.739	1.275	2.760	2.886	1.046
		R-2	10.000	13.384	1.338	2.200	2.474	1.125
		R-3	12.000	14.718	1.227	0.600	1.338	2.230
		R-4	16.000	16.748	1.047	2.100	1.291	0.615
		R-5	5.200	6.122	1.177	2.500	2.511	1.004
		R-6	4.180	5.314	1.271	4.133	2.260	0.547
	Donahey and Darwin	R-7	9.650	7.606	0.788	4.154	2.872	0.691
		D-1	6.510	7.630	1.172	4.323	3.981	0.921
		D-2	7.756	8.167	1.053	4.094	3.465	0.846
		D-3	11.367	12.828	1.129	2.238	1.802	0.805
		D-5A	6.205	7.720	1.244	5.442	2.960	0.544
		D-6A	2.721	2.716	0.998	3.789	3.020	0.797
		D-8A	4.043	2.994	0.741	2.289	1.671	0.730
		D-9A	3.865	6.227	1.611	4.425	5.694	1.287
		Mean					1.142	0.999
Std. Dev.					0.223	0.427		
Coeff. of Var. (%)					19.5	42.7		

APPENDIX C

Summary of Previous Tests

A total of eleven solid slab tests conducted by Granade⁵, Clawson and Darwin⁷, and Cho⁹, and a total of twenty four ribbed slab tests conducted by Redwood, Wong¹⁰ and Poubouras¹², and Donahey and Darwin¹⁵ form a database for the ultimate strength and serviceability analyses in the present study. Geometric and material properties of all these tests are summarized in Tables C.1 and C.2.

Additionally two holes with reinforcement around the hole and tested by Cho were not included because they are not matching with the fundamental purpose of this research project. Another test conducted by Thompson and Ainsworth³¹ in Australia was also excluded because of not being continued up to collapse.

Table C.1 Geometric Properties for Previous Tests

Slab Type	Exp. Inves.	Hole No.	Steel Beam Dimensions (mm)				Hole Dimensions (mm)			Slab Dimensions (mm)			
			d	b	t	w	a	H	e	be	ts	ts	
Solid Slab	Granade	G-1	203.4	165.3	11.13	7.95	91	61	0.0	610	89	89	
		G-2	203.4	165.3	11.13	7.95	91	61	0.0	610	89	89	
	Clawson and Darwin	C-1	356.0	171.7	11.52	7.30	203	102	0.0	1221	102	102	
		C-2	454.6	190.7	12.08	9.05	275	138	0.0	1221	102	102	
		C-3	454.6	190.7	12.08	9.05	275	138	0.0	1221	102	102	
		C-4	454.6	190.7	12.33	8.72	275	138	0.0	1221	102	102	
		C-5	460.9	152.6	15.84	9.66	275	138	0.0	1221	102	102	
		C-6	356.0	170.1	12.08	7.53	203	102	0.0	1221	102	102	
	Cho	CH-1	194.0	150.0	9.00	6.00	90	60	0.0	550	130	130	
		CH-2	300.0	150.0	9.00	6.50	135	90	0.0	600	130	130	
		CH-3	300.0	150.0	9.00	6.50	135	90	0.0	600	130	130	
	Ribbed Slab	Redwood, Wong and Pombouras	R-0	253.6	102.0	6.49	5.80	150	75	0.0	1000	141	65
			R-1	355.8	174.5	11.37	7.44	213	107	0.0	1000	141	65
			R-2	356.8	171.3	11.20	7.85	213	107	0.0	1200	141	65
			R-3	356.4	171.3	11.28	7.94	213	107	0.0	1200	141	65
R-4			356.5	174.2	11.09	7.94	213	107	0.0	1200	141	65	
R-5			355.8	174.5	11.37	7.44	213	107	35.5	1000	141	65	
R-6			357.0	171.5	11.10	7.75	213	107	0.0	1000	141	65	
R-7			357.0	171.5	11.10	7.75	213	107	0.0	1000	141	65	
Donahey and Darwin		D-1	524.6	165.6	11.06	9.10	315	157	0.0	1221	127	51	
		D-2	524.6	165.6	11.14	9.08	315	157	0.0	1221	127	51	
		D-3	524.6	167.1	10.91	9.10	315	157	0.0	1221	127	51	
		*D-4A	524.6	166.3	11.14	9.08	315	157	0.0	1221	127	51	
		D-4B	524.6	166.3	11.14	9.08	315	157	0.0	1221	127	51	
		D-5A	524.6	165.6	11.06	9.10	315	157	0.0	1221	127	51	
		D-5B	524.6	165.6	11.06	9.10	315	157	-25.4	1221	127	51	
		D-6A	524.6	167.3	11.09	9.08	315	157	0.0	1221	127	51	
		+D-6B	524.6	167.3	11.09	9.08	315	157	0.0	1221	127	51	
		**D-7A	524.6	168.6	10.45	9.15	315	157	0.0	1221	127	89	
		**D-7B	524.6	168.6	10.45	9.15	315	157	0.0	1221	127	89	
		D-8A	257.6	101.7	6.97	5.87	150	76	0.0	915	140	64	
		D-8B	257.6	101.7	6.97	5.87	237	81	-3.8	915	140	64	
		D-9A	524.6	168.9	10.86	9.28	315	188	0.0	1221	178	102	
		D-9B	524.6	168.9	10.86	9.38	188	188	-3.3	1221	178	102	

* Puddle weld used over the opening

** Longitudinally ribbed slab

+ Deck pan used

Table C.2 Material Properties for Previous Tests

Slab Type	Exp. Inves.	Hole No.	F _{yf} (Mpa)	F _{yw}	f'c (Mpa)	q _r (kN)	nh	n	
Solid Slab	Granade	G-1	302.0	330.3	27.4	81.6	2	8	
		G-2	302.0	330.3	27.4	81.6	2	14	
	Clawson and Darwin	C-1	243.9	245.3	48.3	117.9	4	14	
		C-2	268.4	279.8	29.0	117.9	2	16	
		C-3	268.4	279.8	34.0	117.9	2	16	
		C-4	295.2	335.9	30.8	117.9	4	10	
		C-5	285.4	272.1	32.3	117.9	4	16	
		C-6	272.4	301.7	27.7	117.9	4	10	
	Cho	CH-1	302.0	350.1	21.6	47.1	4	12	
		CH-2	360.9	445.2	21.6	47.1	4	18	
		CH-3	360.9	445.2	21.6	47.1	4	20	
	Ribbed Slab	Redwood, Wong and Pombouras	R-0	348.6	386.8	26.4	93.4	1	4
			R-1	276.6	311.2	22.0	91.2	1	4
R-2			301.8	326.2	19.5	59.8	2	18	
R-3			291.3	325.5	29.6	81.8	4	22	
R-4			301.1	331.7	27.3	107.1	0	5	
R-5			276.6	311.2	22.0	91.2	1	4	
R-6			301.5	325.4	18.0	64.6	0	4	
R-7			301.5	325.4	18.0	64.6	4	8	
R-8		303.8	303.2	17.1	62.2	4	8		
Donahey and Darwin		D-1	349.2	357.2	30.8	76.6	4	10	
		D-2	337.9	349.6	33.4	73.2	4	22	
		D-3	345.4	347.5	37.2	79.8	4	20	
		D-4A	345.4	349.6	32.7	113.1	0	5	
		D-4B	345.4	349.6	36.4	73.2	0	18	
		D-5A	344.4	344.7	32.7	79.8	2	7	
		D-5B	344.4	344.7	35.1	79.8	4	16	
		D-6A	346.5	346.1	27.7	70.8	4	12	
		D-6B	346.5	346.1	29.7	74.4	8	20	
		D-7A	265.1	267.5	28.9	73.0	10	22	
		D-7B	265.1	267.5	29.7	74.4	6	22	
		D-8A	310.6	328.9	27.2	65.5	2	8	
		D-8B	310.6	328.9	34.4	69.8	2	6	
		D-9A	265.1	267.5	28.8	121.3	4	10	
	D-9B	265.1	267.5	30.1	125.4	2	8		